Holtec Licensing Report HI-2043162 Rev. 1 (Non-proprietary)

SPENT FUEL STORAGE EXPANSION

at

DIABLO CANYON POWER PLANT

for

PACIFIC GAS AND ELECTRIC CO.

HOLTEC PROJECT NO. 1368

HOLTEC REPORT HI-2043162

REPORT CATEGORY: A

REPORT CLASS: SAFETY RELATED

HOLTEC INTERNATIONAL

DOCUMENT NUMBER: ___HI-2043162____ PROJECT NUMBER: ___1368____

DOCUMENT ISSUANCE AND REVISION STATUS

DOCUMENT NAME: __Spent Fuel Storage Expansion_____
__at Diablo Canyon Power Plant_____

DOCUMENT CATEGORY: ☐ GENERIC ☒ PROJECT SPECIFIC

No.	Document Portion††	REVISION No. ___0____			REVISION No. ___1____			REVISION No. _____		
		Author's Initials	Date Approved	VIR #	Author's Initials	Date Approved	VIR #	Author's Initials	Date Approved	VIR #
1.	CHAP01	SP	10/15/04	806077	CWB	10/27/04	542637			
2.	CHAP02	SP	10/15/04	314657	CWB	10/27/04	343808			
3.	CHAP03	SP	10/15/04	139839	CWB	10/27/04	680474			
4.	CHAP04	SPA	10/15/04	320072	---	---	---			
5.	CHAP05	ER	10/15/04	393867	---	---	---			
6.	CHAP06	SP	10/15/04	814221	---	---	---			
7.	CHAP07	SP	10/15/04	730005	CWB	10/27/04	721102			
8.	CHAP08	SP	10/15/04	534945	---	---	---			
9.	CHAP09	VJB	10/15/04	313258	---	---	---			
10.	CHAP10	SP	10/15/04	157764	---	---	---			
11.	CHAP11	SP	10/15/04	758318	---	---	---			
12.										

†† Chapter or section number.

HOLTEC INTERNATIONAL

DOCUMENT NUMBER: ___HI-2043162___ PROJECT NUMBER: ___1368___

DOCUMENT CATEGORIZATION

In accordance with the Holtec Quality Assurance Manual and associated Holtec Quality Procedures (HQPs), this document is categorized as a:

☐ Calculation Package[3] (Per HQP 3.2) ☒ Technical Report (Per HQP 3.2)(Such as a Licensing Report)

☐ Design Criterion Document (Per HQP 3.4) ☐ Design Specification (Per HQP 3.4)

☐ Other (Specify):

DOCUMENT FORMATTING

The formatting of the contents of this document is in accordance with the instructions of HQP 3.2 or 3.4 except as noted below:

DECLARATION OF PROPRIETARY STATUS

☐ Nonproprietary ☒ Holtec Proprietary ☐ Privileged Intellectual Property (PIP)

Documents labeled Privileged Intellectual Property contain extremely valuable intellectual/commercial property of Holtec International. They cannot be released to external organizations or entities without explicit approval of a company corporate officer. The recipient of Holtec's proprietary or Top Secret document bears full and undivided responsibility to safeguard it against loss or duplication.

Notes:

1. This document has been subjected to review, verification and approval process set forth in the Holtec Quality Assurance Procedures Manual. Password controlled signatures of Holtec personnel who participated in the preparation, review, and QA validation of this document are saved in the N-drive of the company's network. The Validation Identifier Record (VIR) number is a random number that is generated by the computer after the specific revision of this document has undergone the required review and approval process, and the appropriate Holtec personnel have recorded their password-controlled electronic concurrence to the document.

2. A revision to this document will be ordered by the Project Manager and carried out if any of its contents is materially affected during evolution of this project. The determination as to the need for revision will be made by the Project Manager with input from others, as deemed necessary by him.

3. Revisions to this document may be made by adding supplements to the document and replacing the "Table of Contents", this page and the "Revision Log".

SUMMARY OF REVISIONS

Revision 1 contains the following pages:	
COVER PAGE	1 page
DOCUMENT ISSUANCE AND REVISION STATUS	2 page
SUMMARY OF REVISIONS	1 page
TABLE OF CONTENTS	8 pages
1.0 INTRODUCTION	8 pages
2.0 CASK PIT STORAGE RACKS AND SUPPORT PLATFORMS	27 pages
3.0 MATERIAL AND HEAVY LOADS CONSIDERATIONS	14 pages
4.0 CRITICALITY SAFETY ANALYSES	26 pages
-- APPENDIX 4A	26 pages
5.0 THERMAL-HYDRAULIC CONSIDERATIONS	26 pages
6.0 STRUCTURAL/SEISMIC CONSIDERATIONS	43 pages
7.0 FUEL HANDLING AND CONSTRUCTION ACCIDENTS	19 pages
8.0 FUEL POOL STRUCTURE INTEGRITY CONSIDERATIONS	10 pages
9.0 RADIOLOGICAL EVALUATION	8 pages
10.0 INSTALLATION	8 pages
11.0 ENVIRONMENTAL COST/BENEFIT ASSESSMENT	5 pages
TOTAL	232 pages

Revision 0 Initial issue.

Revision 1 Minor editorial changes made on pages R1, 1-3, 2-1, 2-2, 2-14, 3-5, 3-7, and 7-8.

TABLE OF CONTENTS

TABLE OF CONTENTS

TABLE OF CONTENTS

TABLE OF CONTENTS

Tables

Figures

1.0 INTRODUCTION

The Diablo Canyon Nuclear Plant (DCPP) is operated by the Pacific Gas and Electric Company (PG&E). The plant is located on the central California coast in San Luis Obispo County, approximately 12 miles west-southwest of the city of San Luis Obispo. The plant consists of two Westinghouse pressurized water reactors (PWR) nuclear units. Unit 1 has been in commercial operation since 1985 and Unit 2 since 1986.

Each unit utilizes a spent fuel pool (SFP) for the storage of irradiated and un-irradiated nuclear fuel in order to maintain a sub-critical array, remove decay heat and provide radiation shielding. The DCPP SFPs are designed as mirror images of one another and have identical storage capabilities. Each SFP is currently licensed for 1,324 fuel assembly storage locations, arranged in 16 distinct rack modules.

Until 2002, the DCPP SFP racks were licensed for storage utilizing a two-region configuration with one region utilizing Boraflex as a neutron absorber. In 2002, a License Amendment was approved which allowed for credit of soluble boron in the SFP and resulted in a single region rack configuration without relying on the use of Boraflex.

PG&E is currently undertaking a project to license and construct an Independent Spent Fuel Storage Installation (ISFSI) at DCPP. It is planned for the ISFSI facility to be in operation by early 2007 to maintain a Full Core Offload Capability (FCOC) for both Units at DCPP. However, to avoid the potential for the loss of FCOC due to unforeseen design, permitting or construction delays with the ISFSI Project, PG&E intends to temporarily expand the spent fuel storage capacity by adding a new fuel storage rack within the Cask Pit of each Unit. Based on the current inventory of fuel assemblies stored in the spent fuel pools and the anticipated future discharges of spent fuel, Unit 1 will lose full core reserve capacity in 2007 and Unit 2 will lose full core reserve capacity in 2008. The addition of the new racks will provide a two cycle extension to the loss of full core offload capability.

PG&E intends to expand spent fuel storage capacity by adding one new 13 by 12 rack (154 total cells due to the elimination of two corner cells in each rack) Region II style rack within the Cask Pit of the SFP in Unit 1 by May 2007 and in Unit 2 by February 2008. Details of the Region II rack design are discussed in Section 2.6.1. This modification would temporarily increase the licensed storage capacity in each Unit from the current 1,324 storage cells to 1,478 storage cells. However, other that an unexpected event requiring a full core offload, the only times when the actual inventory of fuel in the pools would exceed the current licensing basis of 1324 would be during the short duration when the core is offloaded during the 14th and 15th refueling outages on each Unit.

In order to simplify the design and licensing of the cask pit racks, the following general design considerations are employed:

- From a criticality standpoint, the cask pit racks are designed for use as a "single zone" rack and will not rely on defined loading patterns within the rack.

- Storage of fuel assemblies with only relatively low initial enrichments and/or high burnups will be licensed for storage within the racks. New, "unirradiated" fuel will not be stored within the racks.

- The cask pit racks will not be used for general fuel storage operations. The racks are to be fully loaded once, freeing up storage locations in the existing SFP racks, and unloaded and removed from the cask pit when the dry cask storage facility (ISFSI) is implemented. This minimizes fuel movements associated with the addition of the racks.

- The cask pit racks are only to be used for storage of fuel with relatively long decay times (>10 years) and low thermal output.

This report provides the design basis, analysis methodology, and results for the proposed temporary cask pit storage racks at Diablo Canyon to support the licensing process.

The physical description of the cask pit racks is provided in Section 2 of this report. The functional fuel storage capabilities and safety margins are discussed in Section 4 of this report. The proposed fuel storage rack arrays for Units 1 and 2 are shown in the plan views provided by Figures 1.0.1 and 1.0.2, respectively. Note that two corner cells in each rack are eliminated to avoid interference with the cask restraint system.

The new storage racks are similar in construction to other racks previously licensed by the NRC and installed at numerous plants. The racks are not seismically braced at the top, but do have seismic restraints at the base pedestal connections to the supporting platform, as discussed in Section 6 of this report. The principal construction materials for the cask pit racks are ASME SA-240 Type 304L stainless steel sheet and plate stock, and ASME SA564-630, Condition H1100 (precipitation hardened stainless steel) for the adjustable support spindles. The only non-stainless material utilized in the rack is the neutron absorber material, which is a boron carbide and aluminum-composite available under the patented product name Metamic™.

The racks are designed to the stress limits of, and analyzed in accordance with, Section III, Division 1, Subsection NF of the ASME Boiler and Pressure Vessel (B&PV) Code [1]. The material procurement, analysis, fabrication, and installation of the rack modules conform to 10CFR50 Appendix B requirements.

The rack design and analysis methodologies employed are a direct evolution of previous license applications. This report documents the design and analyses performed to demonstrate that the racks meet all governing requirements of the applicable codes and standards, in particular, "OT Position for Review and Acceptance of Spent Fuel Storage and Handling Applications", USNRC (1978) and 1979 Addendum thereto [2].

Sections 2 and 3 of this report provide an abstract of the design and material information on the racks.

Section 4 provides a summary of the methods and results of the criticality evaluations performed for the cask pit racks. The criticality safety analysis requires that the effective neutron multiplication factor (k_{eff}) is less than or equal to 0.95 with the storage racks fully loaded with fuel of the highest permissible reactivity and the pool flooded with borated water at a temperature corresponding to the highest reactivity. In addition, it is demonstrated that k_{eff} is less than 1.0 under the assumed accident of the loss of soluble boron in the pool water, i.e. assuming unborated water in the spent fuel pool. The maximum calculated reactivities include a margin for uncertainty in reactivity calculations, including manufacturing tolerances, and are calculated with a 95% probability at a 95% confidence level. The criticality safety analysis sets the requirements on the neutron absorber length and the amount of B^{10} per unit area (i.e., loading density) of the neutron absorber panel for the cask pit racks.

Thermal-hydraulic considerations require that local boiling will not occur in the cask pit racks, and that the pool bulk temperature will remain within the licensing basis described in the DCPP FSAR Update to satisfy the pool structural strength, operational, and regulatory requirements.

The rack module structural analysis requires that the primary stresses in the rack module structure will remain below the ASME B&PV Code (Subsection NF) [1] allowables. Demonstrations of seismic and structural adequacy are presented in Section 6. The structural qualification also requires that the subcriticality of the stored fuel will be maintained under all postulated accident scenarios. The structural consequences of these postulated accidents are evaluated and presented in Section 7 of this report.

Section 8 discusses the evaluation of the cask pit area of the SFP structure to withstand the new rack loads. The radiological considerations are documented in Section 9. Section 10 discusses installation of the cask pit racks. Section 11 discusses a cost/benefit and environmental assessment to establish the acceptability of the wet storage expansion option.

All computer programs utilized to perform the analyses documented in this report are benchmarked and verified. Holtec International has utilized these programs in numerous license applications over the past decade.

The analyses presented herein clearly demonstrate that the cask pit racks possess wide margins of safety with respect to all design considerations specified in the OT Position Paper [2], namely, nuclear subcriticality, thermal-hydraulic safety, seismic and structural adequacy, radiological compliance, and mechanical integrity.

1.1 References

[1] American Society of Mechanical Engineers (ASME), Boiler & Pressure Vessel Code, Section III, 1989 Edition, Subsection NF, and Appendices.

[2] USNRC, "OT Position for Review and Acceptance of Spent Fuel Storage and Handling Applications, April 14, 1978, and Addendum dated January 18, 1979.

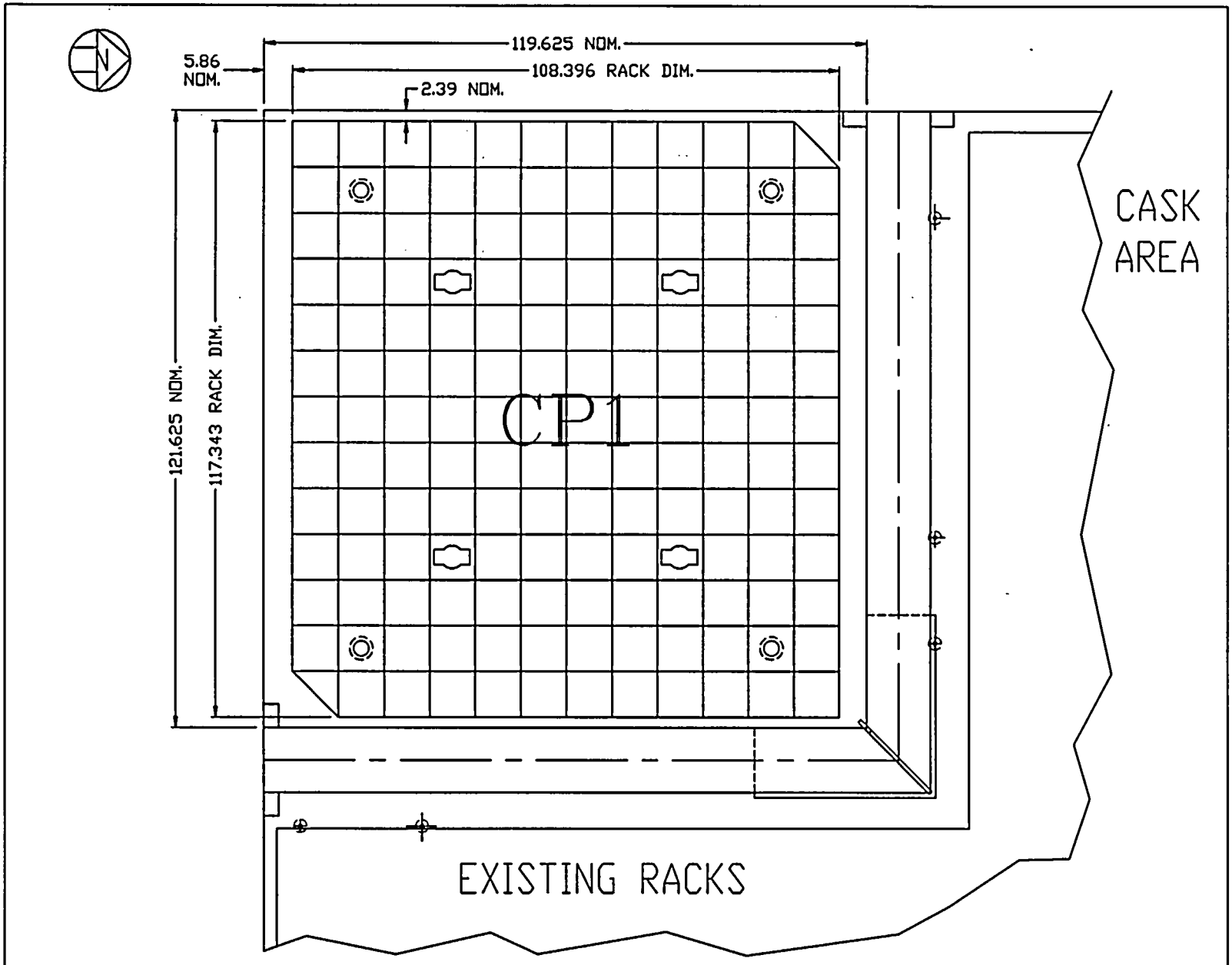

FIGURE 1.0.1 CASK PIT LAYOUT FOR DIABLO CANYON POWER PLANT UNIT 1.

H1368

HI-2043162

G\DRAWINGS\0-FIGURES\1368\FIG1_0_1

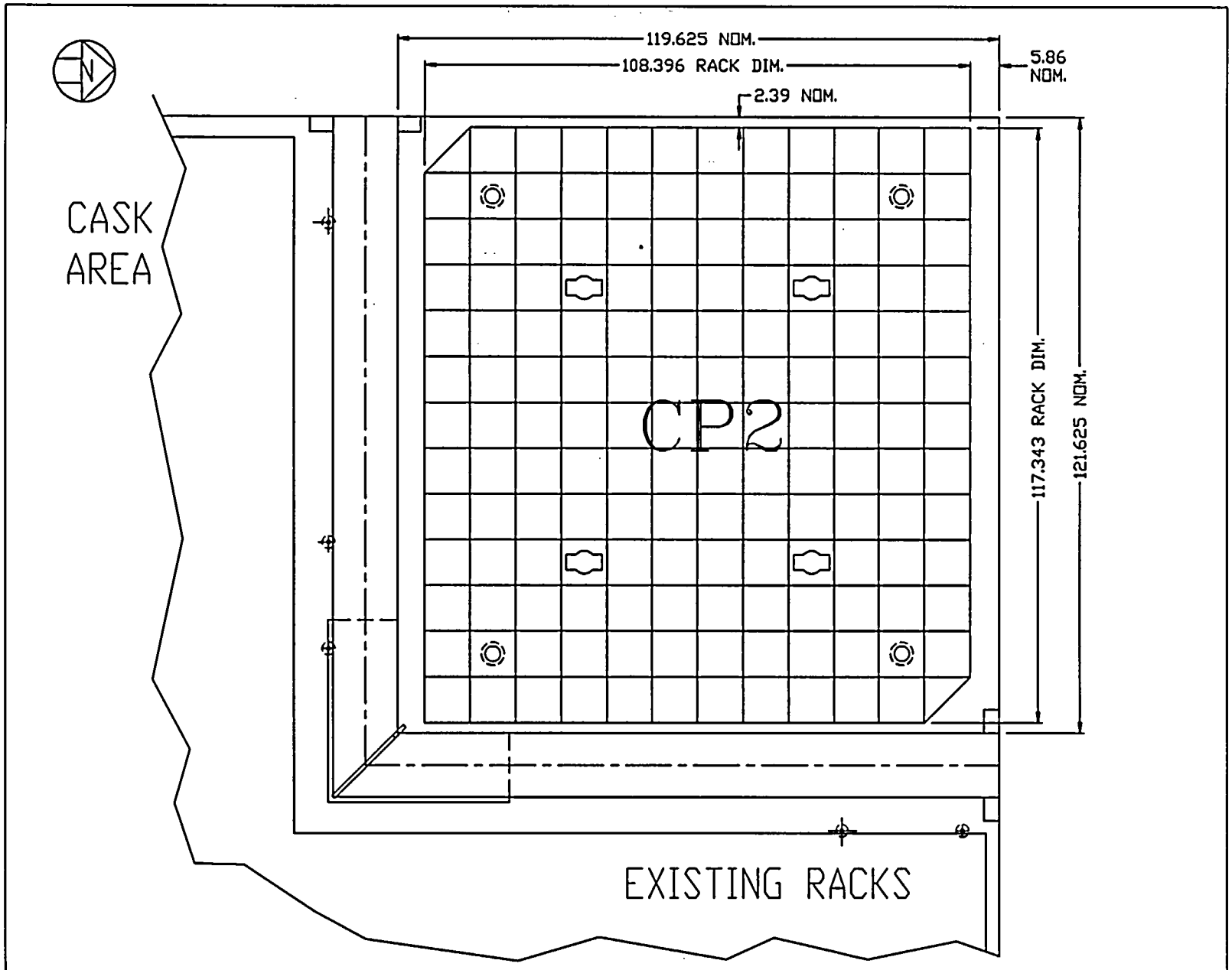

FIGURE 1.0.2 CASK PIT LAYOUT FOR DIABLO CANYON POWER PLANT UNIT 2.

2.0 CASK PIT STORAGE RACKS AND SUPPORT PLATFORMS

2.1 Introduction

The Diablo Canyon Power Plant (DCPP) cask pit fuel storage racks will each be 13 x 12 cell Region II style racks with a storage capacity of 154 assemblies, after the elimination of two corner cells as noted in Table 2.1.1. Each rack will be made primarily from Type 304L austenitic stainless steel containing honeycomb storage cells interconnected through longitudinal welds. Neutron absorber panels containing a high areal loading of the boron-10 (B-10) isotope provide appropriate neutron attenuation between adjacent storage cells.

Figure 2.1.1 provides an isometric schematic of a typical Region II storage rack module. The cask pit rack modules for Units 1 and 2 are designed and constructed to have identical configurations. Data on the cross sectional dimensions, weight and cell count for the two rack modules are presented in Table 2.1.1.

The baseplates on both cask pit rack modules extend approximately ¼" beyond the rack module periphery wall such that the contiguous edges of the plates establish a geometric separation between the rack and the surrounding racks or wall. The rack module support pedestals are engineered to accommodate minor level adjustments. Each rack is supported by four threaded pedestals, which are remotely height-adjustable. Thus, the racks can be made plumb and the top of the racks can easily be made co-planar with the racks in the adjacent Spent Fuel Pool (SFP).

Each of the two pools at the DCPP site will be equipped with a cask pit platform (CPP) in the cask pit cavity. The CPP, custom engineered to ASME Section III Subsection NF, provides the staging and mounting surface for the cask pit rack. The CPP is an all-stainless steel weldment of rectangular cross-section manufactured from SA240-304 plate and bar stock. A gridwork of plates in both orthogonal directions provides the required level of in-plane load resistance capacity to the platform. An isometric of the CPP is provided in Figure 2.1.2 and detailed cross-section and cut-away isometric views of the rack pedestal mating and attachment to the CPP are provided in Figures 2.1.3 and 2.1.4. Figure 2.1.5 provides an isometric of the connector link that provides the seismic restraint that holds the rack down onto the platform. Figure 2.1.6 provides

a view of the baseplate and upper (female) portion of the rack pedestal that will receive the connector link.

The platform serves five major operational functions pertaining to the use of the cask pit as a fuel storage and fuel loading space:

i. The baseplate structure of the fuel rack is fastened to the CPP through eight "connector links" that are configured to be installed and removed remotely. The connector links provide a robust connectivity between the CPP and the fuel rack structure, allowing for a minimal side sway of the rack under seismic conditions.

ii. With the aid of lateral wedges (to be installed between the recess on the periphery of the CPP shown in Figure 2.1.2 and the liner), the platform is rendered essentially immovable in the horizontal direction, which eliminates the potential of platform-to-cask pit wall impacts during a seismic event. The relatively modest state of stress condition that may develop in the platform from an elevated pool bulk temperature (discussed in Chapter 5) is accounted for in the stress analysis of the CPP structure. (The structural analysis of the CPP entails the consideration of the combined effect of thermal and seismic (inertial) loads.)

iii. The design of the CPP/fuel rack interface ensures that the rack structure will not be subject to "restraint-of-free end expansion" under the most severe thermal conditions that may obtain in the cask pit region.

iv. While the CPP is structurally unconstrained to lift off in the vertical direction, the considerable nominal dead weight of the platform (22,825 lbs) and the location of the above-mentioned "wedges" (a total of 16 in number) and kinematic coupling of the CPP with the fuel rack through the connector links, collectively help ensure that the platform will not lift off during any of the applicable earthquakes for the DCPP pool. Thus, the incidence of uplift of the fuel rack and the resulting vertical impact load are completely eliminated.

v. The CPP is designed to stage a transfer cask, if necessary, to faciliate the transfer of the plant's used fuel in dry storage, or off-site transport, if required. The CPP is designed to be physically compatible with the HI-TRAC transfer cask (reference Docket No. 72-1014). Thus, while the CPP is intended to be installed as a permanent appurtenance in the cask pit, it is nevertheless equipped with lifting and handling facilities to enable convenient and ALARA installation into and removal from the cask pit.

Structural attributes of the cask pit platform are further discussed in Section 6.2.

The overall design of the rack modules is similar to those presently in service in the spent fuel pools at many other nuclear plants, such as Davis-Besse, Callaway, Byron and Braidwood. Altogether, Holtec International has provided over fifty thousand storage cells of this design to various nuclear plants around the world.

2.2 Summary of Principal Rack Design Criteria

The key design criteria for the cask pit racks are set forth in the USNRC memorandum entitled "OT Position for Review and Acceptance of Spent Fuel Storage and Handling Applications", dated April 14, 1978 as modified by amendment dated January 18, 1979. The individual sections of this report address the specific design bases derived from the above-mentioned "OT Position Paper". The design bases for the new racks are summarized in the following:

a. Disposition: Both cask pit rack modules are designed without bracing to the wall at the top of the rack. The base pedestals are restrained from lateral and vertical movement by connections to the supporting platform, as discussed later in this section and in greater detail in section 6.

b. Kinematic Stability: Each module must be kinematically stable (against tipping or overturning) if a seismic event is imposed.

c. Structural Compliance: All primary stresses in the rack modules must satisfy the limits postulated in Section III subsection NF of the ASME B & PV Code.

d. Thermal-Hydraulic Compliance: With forced cooling available (i.e., Spent Fuel Pool Cooling System operating) the maximum SFP bulk temperature for a partial core offload must not exceed 140°F, the maximum SFP bulk temperature for a full core offload must not exceed 174°F (the current licensing basis value) and the maximum temperature for an emergency core offload must be less than 212°F. These temperature limits are consistent with the DCPP FSAR.

e. Criticality Compliance: The cask pit racks must be able to store spent fuel of 4.1 weight percent (w/o) maximum enrichment while maintaining the reactivity (K_{eff}) less than 0.95 with the storage racks fully loaded with fuel of the highest permissible reactivity and the pool flooded with borated water at a temperature corresponding to the highest reactivity. In addition, it is demonstrated that k_{eff} is less than 1.0 under the assumed accident of the loss of soluble boron in the pool water, i.e. assuming unborated water in the spent fuel pool. The maximum calculated reactivities include a margin for uncertainty in reactivity calculations, including manufacturing tolerances, and are calculated with a 95% probability at a 95% confidence level.

f. Accident Events: In the event of postulated drop events (uncontrolled lowering of a fuel assembly, for instance), it is necessary to demonstrate that the subcritical geometry of the rack structure is not compromised. Credit for borated water is allowed under accident scenarios.

The foregoing design bases are further articulated in Sections 4 through 7 of this licensing report.

2.3 Applicable Codes and Standards

The following codes, standards and practices are used as applicable for the design, construction, and assembly of the fuel storage racks. Additional specific references related to detailed analyses are given in each section.

a. Design Codes

(1) American Institute of Steel Construction (AISC) Manual of Steel Construction, 1969 Edition.

(2) American National Standards Institute/ American Nuclear Society ANSI/ANS- 57.2-1983, "Design Requirements for Light Water Reactor Spent Fuel Storage Facilities at Nuclear Power Plants" (contains guidelines for fuel rack design).

(3) American Society of Mechanical Engineers (ASME), Boiler and Pressure Vessel (BP&V) Code, Section III, 1988 Edition through 2000 Addenda.

(4) American Society for Nondestructive Testing SNT-TC-1A, 2001, Personnel Qualifications and Certification in Non-destructive Testing.

(5) American Concrete Institute Building Code Requirements for Reinforced Concrete (ACI 318-63).

(6) Code Requirements for Nuclear Safety Related Concrete Structures, ACI 349-80/ACI 349R-80.

(7) ASME Y14.5M, Dimensioning and Tolerancing for Engineering Drawings and Related Documentation Practices

(8) ASME B&PV Code, Section II, Parts A and C, 1989 Edition.

(9) ASME B&PV Code NCA3800 - Metallic Material Organization's Quality System Program.

b. Standards of American Society for Testing and Materials (ASTM)

(1) ASTM E165 - Standard Test Method for Liquid Penetrant Examination.

(2) ASTM A240 - Standard Specification for Heat-Resisting Chromium and Chromium-Nickel Stainless Steel Plate, Sheet and Strip for Pressure Vessels.

(3) ASTM A262 - Standard Practices for Detecting Susceptibility to Intergranular Attack in Austenitic Stainless Steel.

(4) ASTM A276 - Standard Specification for Stainless Steel Bars and Shapes.

(5) ASTM A479 - Standard Specification for Stainless Steel Bars and Shapes for use in Boilers and other Pressure Vessels.

(6) ASTM A564 - Standard Specification for Hot-Rolled and Cold-Finished Age-Hardening Stainless Steel Bars and Shapes.

(7) ASTM C750 - Standard Specification for Nuclear-Grade Boron Carbide Powder.

(8) ASTM A380 - Standard Practice for Cleaning, Descaling, and Passivation of Stainless Steel Parts, Equipment and Systems.

(9) ASTM C992 - Standard Specification for Boron-Based Neutron Absorbing Material Systems for Use in Nuclear Spent Fuel Storage Racks.

(10) ASTM E3 - Standard Practice for Preparation of Metallographic Specimens.

(11) ASTM E190 - Standard Test Method for Guided Bend Test for Ductility of Welds.

c. Welding Code:

(1) ASME B&PV Code, Section IX - Welding and Brazing Qualifications, 1989.

d. Quality Assurance, Cleanliness, Packaging, Shipping, Receiving, Storage, and Handling

(1) ANSI N45.2.1 - Cleaning of Fluid Systems and Associated Components during Construction Phase of Nuclear Power Plants - 1973 (R.G. 1.37).

(2) ANSI N45.2.2 - Packaging, Shipping, Receiving, Storage and Handling of Items for Nuclear Power Plants - 1972 (R.G. 1.38).

(3) ANSI N45.2.6 - Qualifications of Inspection, Examination, and Testing Personnel for the Construction Phase of Nuclear Power Plants - 1978. (R.G. 1.58).

(4) ANSI N45.2.8 - Supplementary Quality Assurance Requirements for Installation, Inspection and Testing of Mechanical Equipment and Systems for the Construction Phase of Nuclear Plants - 1975 (R.G. 1.116).

(5) ANSI N45.2.11 - Quality Assurance Requirements for the Design of Nuclear Power Plants - 1974 (R.G. 1.64).

(6) ANSI N45.2.12 - Requirements for Auditing of Quality Assurance Programs for Nuclear Power Plants - 1977 (R.G. 1.144).

(7) ANSI N45.2.13 - Quality Assurance Requirements for Control of Procurement of Items and Services for Nuclear Power Plants - 1976 (R. G. 1.123).

(8) ANSI N45.2.23 - Qualification of Quality Assurance Program Audit Personnel for Nuclear Power Plants - 1978 (R.G. 1.146).

(9) ASME B&PV Code, Section V, Nondestructive Examination, 2001 Edition.

(10) ANSI N16.9-75 - Validation of Calculation Methods for Nuclear Criticality Safety.

e. USNRC Documents

(1) "OT Position for Review and Acceptance of Spent Fuel Storage and Handling Applications," dated April 14, 1978 and the modifications to this document by USNRC letter dated January 18, 1979.

(2) NUREG 0612, "Control of Heavy Loads at Nuclear Power Plants", USNRC, Washington, D.C., July 1980.

f. Other ANSI Standards (not listed in the preceding)

(1) ANSI/ANS 8.1 - Nuclear Criticality Safety in Operations with Fissionable Materials Outside Reactors.

(2) ANSI/ANS 8.17 - Criticality Safety Criteria for the Handling, Storage, and Transportation of LWR Fuel Outside Reactors.

(3) ANSI N45.2 - Quality Assurance Program Requirements for Nuclear Power Facilities - 1971.

(4) ANSI N45.2.9 - Requirements for Collection, Storage and Maintenance of Quality Assurance Records for Nuclear Power Plants - 1974.

(5) ANSI N45.2.10 - Quality Assurance Terms and Definitions - 1973.

(6) ANSI N14.6 - American National Standard for Special Lifting Devices for Shipping Containers Weighing 10,000 pounds (4500 kg) or more for Nuclear Materials - 1993.

(7) ANSI/ASME N626-3 - Qualification and Duties of Personnel Engaged in ASME Boiler and Pressure Vessel Code Section III, Div. 1, Certifying Activities.

(8) ANSI/ANS- 57.3 – Design Requirements for New Fuel Storage Facilities at Light Water Reactor Plants.

g. Code-of-Federal Regulations (CFR)

(1) 10CFR20 - Standards for Protection Against Radiation.

(2) 10CFR21 - Reporting of Defects and Non-compliance.

(3) 10CFR50 Appendix A - General Design Criteria for Nuclear Power Plants.

(4) 10CFR50 Appendix B - Quality Assurance Criteria for Nuclear Power Plants and Fuel Reprocessing Plants

(5) 10CFR50.68 - Criticality Accident Requirements

h. Regulatory Guides (RG)

(1) RG 1.13 - Spent Fuel Storage Facility Design Basis (Proposed Revision 2, dated 12/81).

(2) RG 1.25 - Assumptions Used for Evaluating the Potential Radiological Consequences of a Fuel Handling Accident in the Fuel Handling and Storage Facility for Boiling and Pressurized Water Reactors, Rev. 0 - March 1972.

(3) RG 1.28 - Quality Assurance Program Requirements - Design and Construction, Rev. 2 - February, 1979 (endorses ANSI N45.2).

(4) RG 1.33 - Quality Assurance Program Requirements.

(5) RG 1.29 - Seismic Design Classification, Rev. 3 - September 1978.

(6) RG 1.31 - Control of Ferrite Content in Stainless Steel Weld Metal, Rev. 3 - April 1978.

(7) RG 1.38 - Quality Assurance Requirements for Packaging, Shipping, Receiving, Storage and Handling of Items for Water-Cooled Nuclear Power Plants, Rev. 2 - May 1977 (endorses ANSI N45.2.2).

(8) RG 1.44 - Control of the Use of Sensitized Stainless Steel, Rev. 1 - 1973.

(9) RG 1.58 - Qualification of Nuclear Power Plant Inspection, Examination, and Testing Personnel, Rev. 1 - September 1980 (endorses ANSI N45.2.6).

(10) RG 1.61 - Damping Values for Seismic Design of Nuclear Power Plants, Rev. 0 - 1973.

(11) RG 1.64 - Quality Assurance Requirements for the Design of Nuclear Power Plants, Rev. 2 - June 1976 (endorses ANSI N45.2.11).

(12) RG 1.71 - Welder Qualifications for Areas of Limited Accessibility.

(13) RG 1.74 - Quality Assurance Terms and Definitions, Rev. 2 - February 1974 (endorses ANSI N45.2.10).

(14) RG 1.84 - Design and Fabrication Code Case Acceptability

(15) RG 1.85 - Materials Code Case Acceptability - ASME Section III, Division 1.

(16) RG 1.88 - Collection, Storage and Maintenance of Nuclear Power Plant Quality Assurance Records, Rev. 2 - October 1976 (endorses ANSI N45.2.9).

(17) RG 1.92 - Combining Modal Responses and Spatial Components in Seismic Response Analysis, Rev. 1 - February 1976.

(18) RG 1.116 - Quality Assurance Requirements for Installation, Inspection and Testing of Mechanical Equipment and Systems, Rev. 0-R - May 1977 (endorses ANSI N45.2.8-1975)

(19) RG 1.123 - Quality Assurance Requirements for Control of Procurement of Items and Services for Nuclear Power Plants, Rev. 1 - July 1977 (endorses ANSI N45.2.13).

(20) RG 1.124 - Service Limits and Loading Combinations for Class 1 Linear-Type Component Supports, Rev. 1 - January 1978.

(21) RG 1.144 - Auditing of Quality Assurance Programs for Nuclear Power Plants, January 1979 revision (endorses ANSI N45.2.12-1977)

(22) RG 3.4 - Nuclear Criticality Safety in Operations with Fissionable Materials at Fuels and Materials Facilities.

(23) RG 8.8 - Information Relative to Ensuring that Occupational Radiation Exposures at Nuclear Power Stations will be as Low as Reasonably Achievable (ALARA).

(24) IE Information Notice 83-29 - Fuel Binding Caused by Fuel Rack Deformation.

(25) RG 8.38 - Control of Access to High and Very High Radiation Areas in Nuclear Power Plants, June, 1993.

i. Branch Technical Position

(1) CPB 9.1-1 - Criticality in Fuel Storage Facilities.

j. American Welding Society (AWS) Standards

(1) AWS D1.1 - Structural Welding Code - Steel.

(2) AWS D1.3 - Structure Welding Code - Sheet Steel.

(3) AWS D9.1 - Sheet Metal Welding Code.

(4) AWS A2.4 - Standard Symbols for Welding, Brazing and Nondestructive Examination.

(5) AWS A3.0 - Standard Welding Terms and Definitions.

(6) AWS A5.12 - Specification for Tungsten and Tungsten Alloy Electrodes for Arc-Welding and Cutting

(7) AWS QC1 - Standard and Guides for Qualification and Certification of Welding Inspectors.

(8) AWS 5.4 – Specification for Stainless Steel Electrodes for Shielded Metal Arc Welding.

(9) AWS 5.9 – Specification for Bare Stainless Steel Welding Electrodes and Rods.

2.4 Quality Assurance Program

The governing quality assurance requirements for design and fabrication of the spent fuel racks are stated in 10CFR50 Appendix B. Holtec's Nuclear Quality Assurance program complies with this regulation and is designed to provide a system for the design, analysis and licensing of customized components in accordance with various codes, specifications, and regulatory requirements.

The manufacturing of the racks will be carried out by Holtec's designated manufacturer, U.S. Tool & Die, Inc. (UST&D). The Quality Assurance system enforced on the manufacturer's shop floor shall provide for all controls necessary to fulfill all quality assurance requirements. UST&D has manufactured high-density racks for over 60 nuclear plants around the world. UST&D has been audited by the nuclear industry group Nuclear Procurement Issues Committee (NUPIC), and the Quality Assurance branch of the USNRC Office of Nuclear Material Safety and Safeguards (NMSS) with satisfactory results.

The Quality Assurance system that will be used by Holtec to install the racks is also controlled by the Holtec Nuclear Quality Assurance Manual and by the Diablo Canyon site-specific requirements.

2.5 Mechanical Design

The DCPP cask pit rack modules are designed as cellular structures such that each fuel assembly has a square opening with conforming lateral support and a flat horizontal-bearing surface. All of the storage locations are constructed with multiple cooling flow holes to ensure that redundant flow paths for the coolant are available. The basic characteristics of the cask pit racks are summarized in Table 2.5.1.

A central objective in the design of the new rack modules is to maximize structural strength while minimizing inertial mass and dynamic response. Accordingly, the rack modules have been designed to simulate multi-flange beam structures resulting in excellent de-tuning characteristics with respect to the applicable seismic events. The next subsection presents an item-by-item description of the cask pit rack modules in the context of the fabrication methodology.

2.6 Rack Fabrication

The object of this section is to provide a brief description of the rack module construction activities, which enable an independent appraisal of the adequacy of design. The pertinent methods used in manufacturing the cask pit racks may be stated as follows:

1. The rack modules are fabricated in such a manner that the storage cell surfaces, which would come in contact with the fuel assembly, will be free of harmful chemicals and projections (e.g., weld splatter).

2. The component connection sequence and welding processes are selected to reduce fabrication distortions.

3. The fabrication process involves operational sequences that permit immediate accessibility for verification by the inspection staff.

4. The racks are fabricated per the UST&D Appendix B Quality Assurance program, which ensures, and documents, that the fabricated rack modules meet all of the requirements of the design and fabrication documents.

5. The corners of these storage cells are connected to each other using austenitic stainless steel connector elements, which lead to a honeycomb lattice construction. The extent of welding is selected to "detune" the racks from the seismic input motion

2.6.1 Region II Rack Module

As stated in Section 2.1 the DCPP cask pit racks are Region II style racks. As such the cask pit racks are comprised of five significant components: (a) the composite box subassembly, (b) the baseplate, (c) the neutron absorber material, (d) the sheathing, and (e) the support pedestals. Fabrication details for each of these components is discussed below.

a. Composite box subassembly: The rack module manufacturing begins with fabrication of the "box." The boxes are fabricated from two precision formed channels by seam welding in a machine equipped with copper chill bars and pneumatic clamps to minimize distortion due to welding heat input. The minimum weld penetration is 80% of the box metal gage. The nominal inside dimension of the fabricated box (or cell) is 8.75 inches. This process results in a square box as shown in Figure 2.6.1. Metal sheathing is then attached to select sides of each box, and the poison material is installed in the sheathing cavities.

The square cross section box with neutron absorber panels affixed to its external surfaces is referred to as the "composite box assembly." Each composite box has 1-inch diameter holes punched near its bottom edge to provide auxiliary flow. Region II storage cells have two holes at the base aligned in one direction.

The composite boxes are arranged in a checkerboard array and welded edge-to-edge to form an assemblage of storage cell locations as shown in Figure 2.6.2. Filler panels and corner angles are welded to the edges of boxes at the outside boundary of the rack to complete the formation of the peripheral cells. Some of the cell inside dimension at these locations are larger by the thickness of the adjacent cell walls (approximately 0.09") to become 8.85", because the filler panels and corner angles are welded to the outside of the adjacent fabricated cell walls, as seen in Figure 2.6.2. The inter-box welding and pitch adjustment are accomplished by small longitudinal connectors. The connectors are sized and placed to ensure that the inside cell dimension for developed boxes is maintained after inclusion of any reductions from the sheathing. This assemblage of composite boxes results in a honeycomb structure with axial, flexural and torsional rigidity, which depend on the extent of inter-cell welding. Figures 2.6.2 shows that all four corners of each interior box are connected to the adjacent boxes, which creates a well-defined path for "shear flow."

As stated in Section 1.0, two corner cells are eliminated from the rectangular cell array. Figure 2.6.2 indicates a typical array, but has been adjusted to indicate the manner in which these two corner cells are to be eliminated. In the instance shown in the upper left of the figure, a normally placed corner angle will be eliminated. In the lower right, the missing cell will be eliminated through the use of a larger corner angle fabricated to enclose two cells instead of the usual one cell. The baseplate will be cut at a 45-degree angle at the corner beneath the area of the eliminated cells.

A typical elevation view of Region II storage cells is shown in Figure 2.6.3.

b. Baseplate: A 1-inch thick baseplate provides a continuous horizontal surface for supporting the fuel assemblies. The baseplate has 5-1/4 inch diameter holes at each cell location, except at lift locations. At the four lift locations, a 5-1/2 inch by 2-5/8 inch rectangular cut-out is centered over a 3-13/16 inch circular flow hole to allow insertion and engagement of the lifting rig. The location of all baseplate holes coincides with the cell centerlines. The baseplate is attached to the base of the cell assemblage by fillet welds and extends horizontally beyond the periphery of the rack cells (refer to Figure 2.6.3).

c. Neutron absorber material: For the DCPP cask pit racks, every interior cell wall and boundary wall are equipped with one integral neutron absorber panel. The neutron absorber material is a boron carbide and aluminum-composite available under the patented product name Metamic™. A further discussion of the neutron absorber material is provided in Section 3.

d. Sheathing: As described earlier, metal sheathing is fastened to all four sides of each box wall. The design objective calls for attaching the neutron absorber material tightly on the box surface. This is accomplished by die forming the internal and external sheathing to provide end flares with smooth edges, as shown in Figure 2.6.1. The flanges of the sheathing are welded to the box using skip welds and spot welds. The sheathing serves to locate and position the poison sheet accurately and to preclude its movement under seismic conditions. The sheathing also provides a vented enclosure for the neutron absorber material.

e. Support pedestals: All support pedestals are the adjustable type as shown in Figure 2.6.4. The top (female threaded) portion is made of austenitic stainless steel. The bottom (male threaded) portion is made of SA564-630 stainless steel. Each support pedestal is equipped with a readily accessible socket to enable remote leveling of the rack after its placement in the cask pit. The support pedestals are located at the centerlines of cells to ensure accessibility of the leveling tool through the 5-1/4 inch diameter flow hole in the baseplate. A vertical hole is drilled in the bottom portion of the support pedestals to allow for cooling flow.

The assembly of the rack modules is carried out by welding the composite boxes in a vertical fixture with the precision fabricated baseplate serving as the bottom positioner.

Appropriate NDE (nondestructive examination) occurs on all welds including visual examination of sheathing welds, box longitudinal seam welds, box-to-baseplate welds, and box-to-box connection welds; and liquid penetrant examination of support pedestal welds, in accordance with the design drawings.

Table 2.1.1
Geometric and Physical Data for Cask Pit Storage Racks

UNIT	RACK I.D.	RACK TYPE	CELL-TO-CELL PITCH		NO. OF CELLS		MODULE ENVELOPE SIZE		DRY WEIGHT (lb)	NO. OF CELLS PER RACK†
			N-S (in)	E-W (in)	N-S Direction	E-W Direction	N-S (in)	E-W (in)		
1	CP1	Region II	8.946	8.946	12	13	108.4	117.3	26,000	154
2	CP2	Region II	8.946	8.946	12	13	108.4	117.3	26,000	154

† Two corner cells are eliminated from each rack, as shown in Figure 1.0.1, 1.0.2 and 2.6.2, to avoid interference with the cask restraint system.

Table 2.5.1

MODULE DATA FOR REGION II CASK PIT RACKS †

Storage cell inside nominal dimension	8.75 in ††
Cell pitch (North-South)	8.964 in
Cell pitch (East-West)	8.964 in
Storage cell height (above the baseplate)	169 in
Baseplate hole size ††† (except for lift locations and two tie-down restraint locations on each pedestal)	5.25 in
Baseplate thickness	1.0 in
Female support pedestal height	4.0 in +/- 1/16 in.
Male support pedestal height (protrusion below female pedestal)	3.0 in +/- 1/2 in.
Support pedestal type	Remotely adjustable pedestals w/ vertical and horizontal seismic restraints
Number of support pedestals per rack	4
Number of cell walls containing 1-inch diameter flow holes at base of cell wall	2 (aligned in one direction)
Remote lifting and handling provisions	Yes
Poison length	150 in
Poison width	7.5 in (7.0 inches wide at all boundary wall locations)

† All dimensions indicate nominal values

†† As discussed in section 2.6.1(a), cells formed by corner angles and filler panels will have dimensions enlarged by the thickness of the adjacent cell walls to 8.85".

††† There are two examples of exceptions to the standard baseplate hole diameter. The rack is lifted at four points using irregular shaped holes placed at the centerline of specific cells in lieu of the standard baseplate hole. The lifting holes are sized with approximately the same area as the standard holes. The second exception is the two baseplate holes that align with the pedestal vertical seismic restraint (hold-down) connector links, shown in Figure 6.2.3. These holes are 7.25 inches in diameter and the lower portion is a rectangular opening sized 6.5 by 3.25 inches.

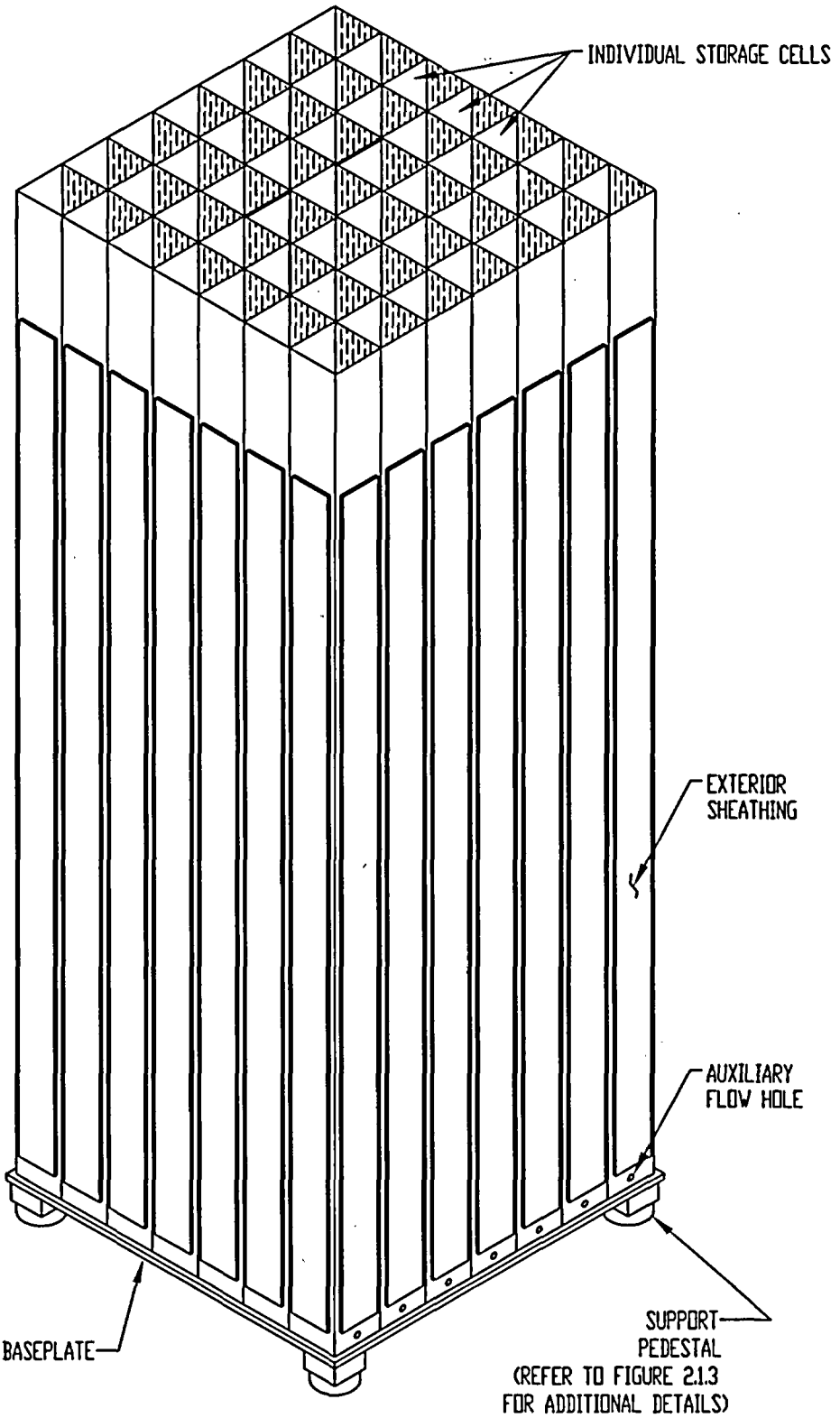

FIGURE 2.1.1; PICTORIAL VIEW OF A TYPICAL REGION II RACK MODULE

NOTE: THE NUMBER OF CELLS SHOWN IS NOT INTENDED TO DEPICT ACTUAL RACK SIZES

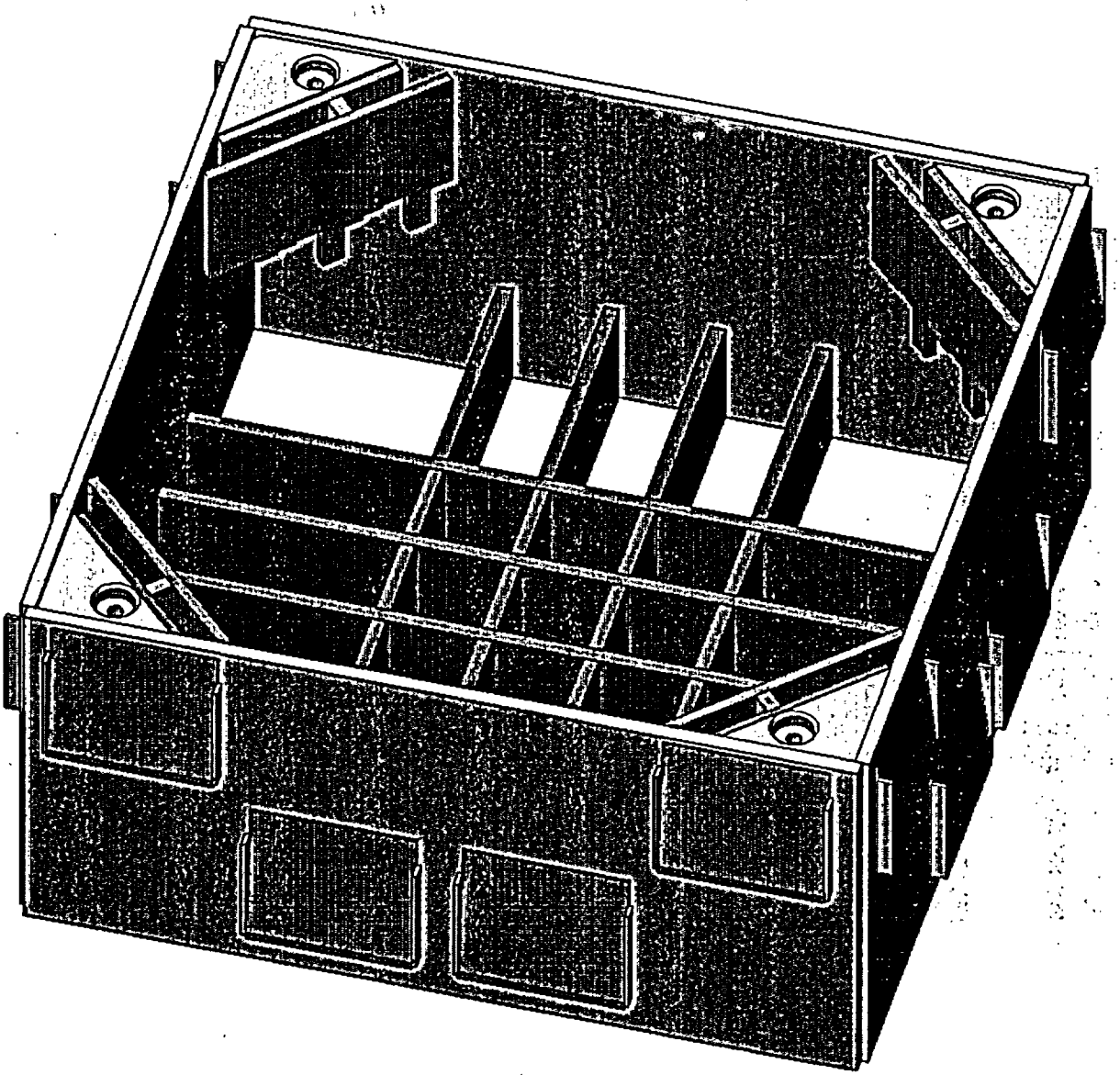

FIGURE 2.1.2 - Rack Platform in Isometric View

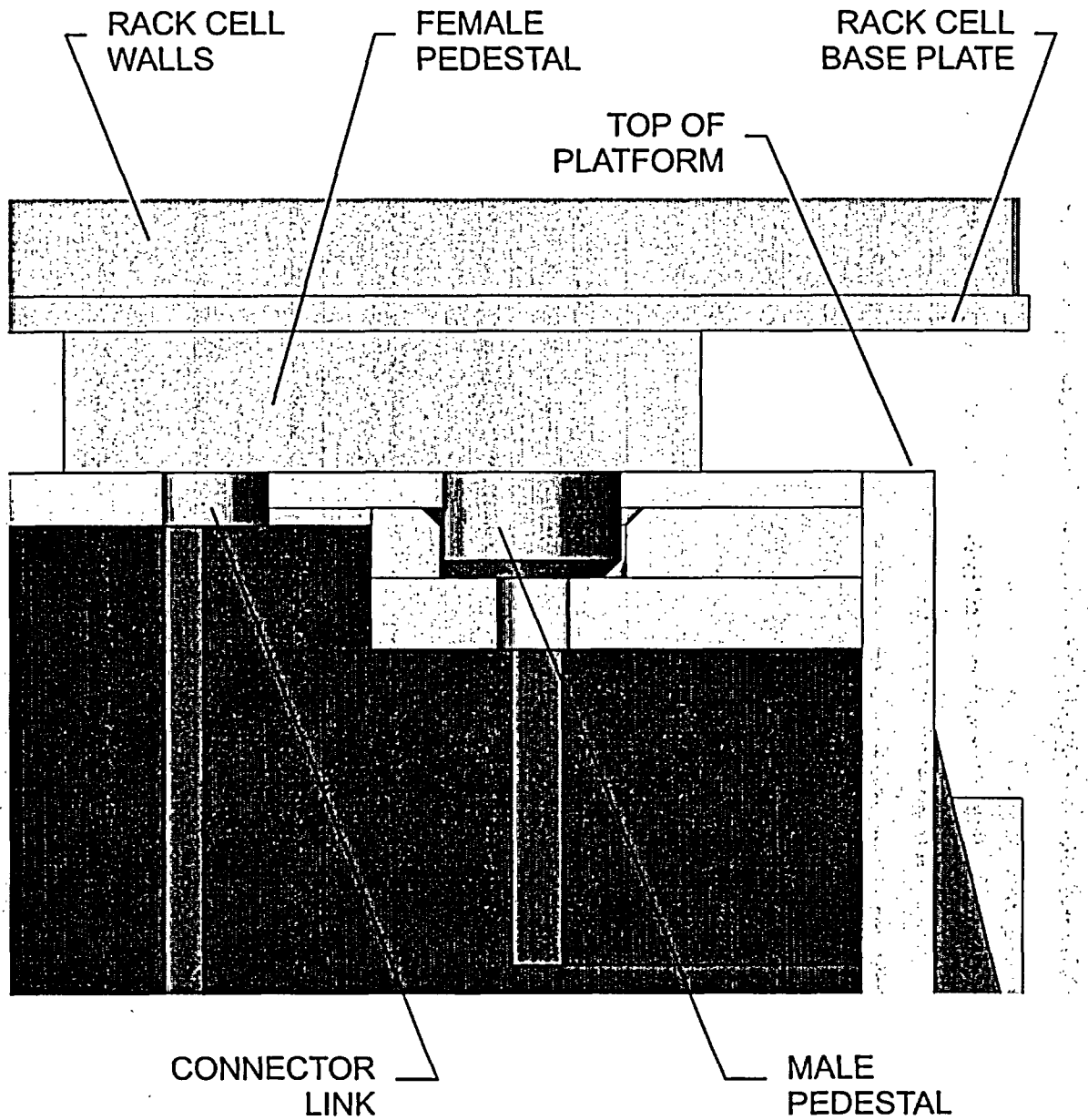

FIGURE 2.1.3 - Recess configuration in the "Cask Pit Platform" for confining the Rack Support Pedestal

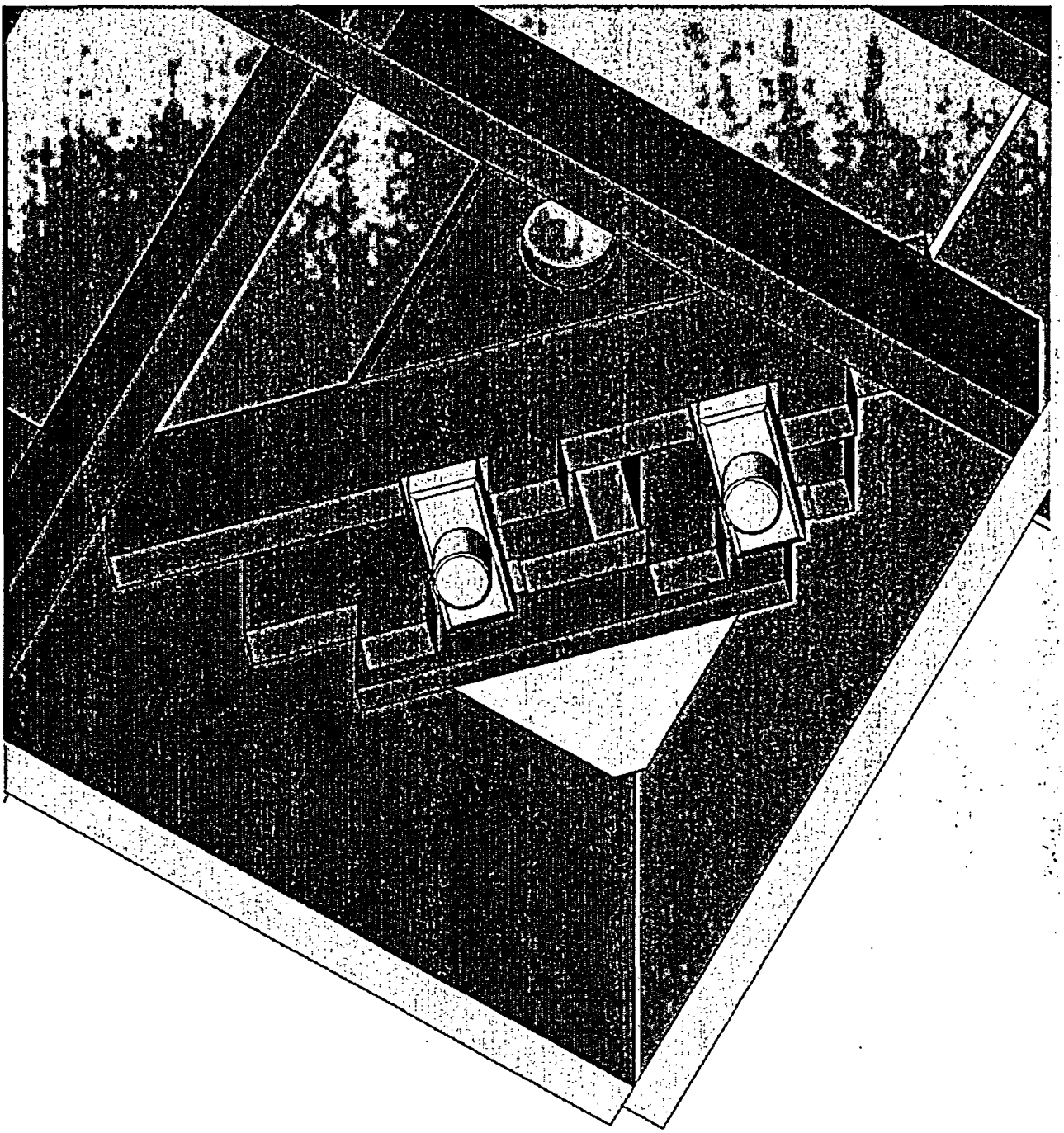

FIGURE 2.1.4 - Rack to Platform Connection in Isometric

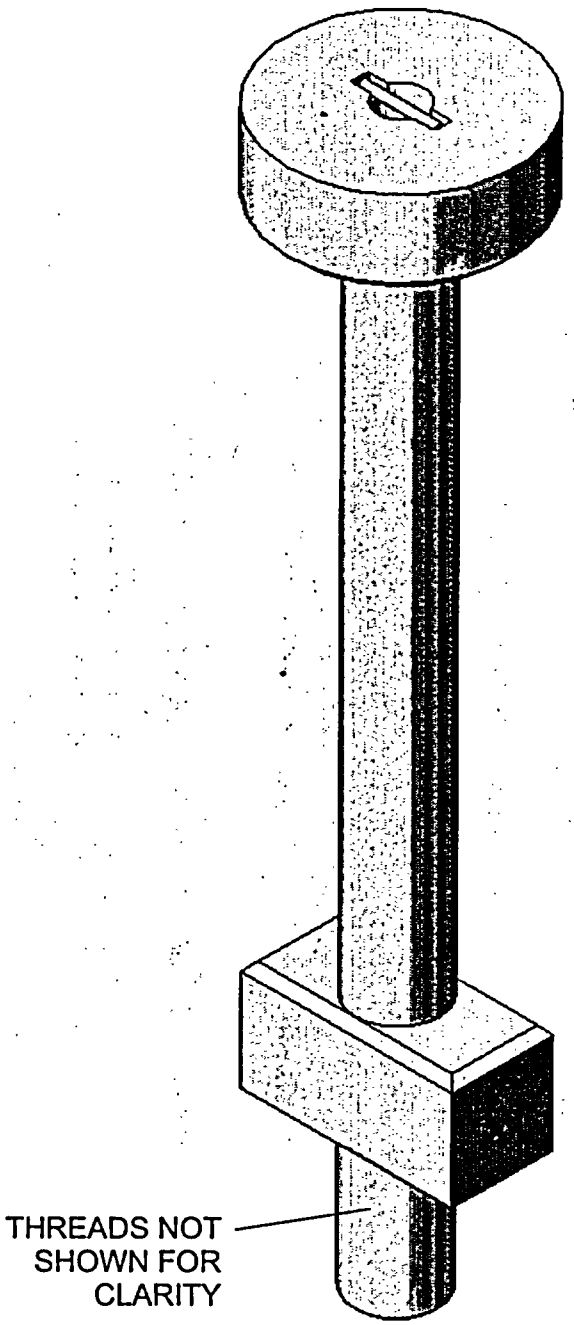

FIGURE 2.1.5 - Rack to Platform "Connector Link"

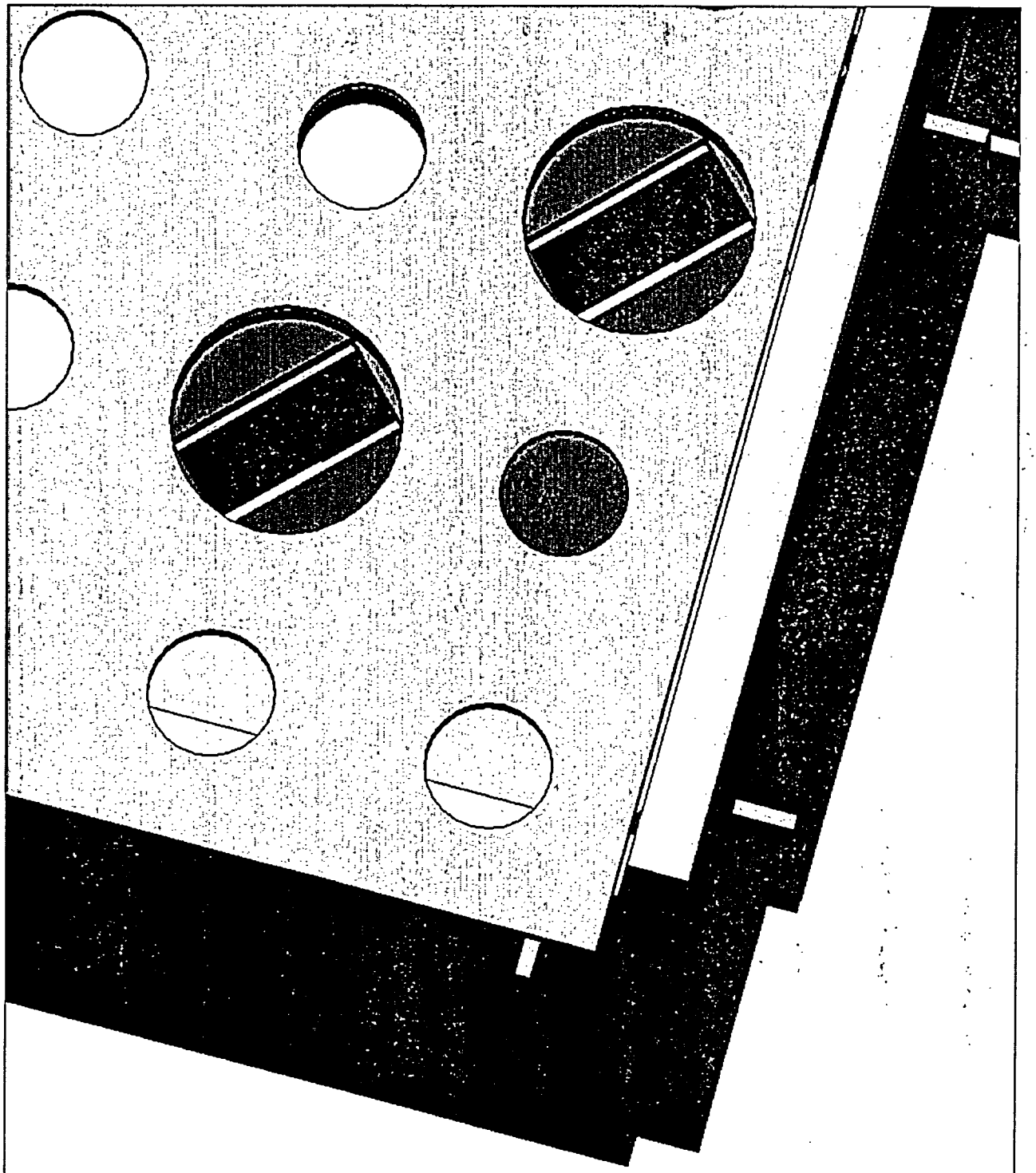

FIGURE 2.1.6 - Base Plate with Pedestal

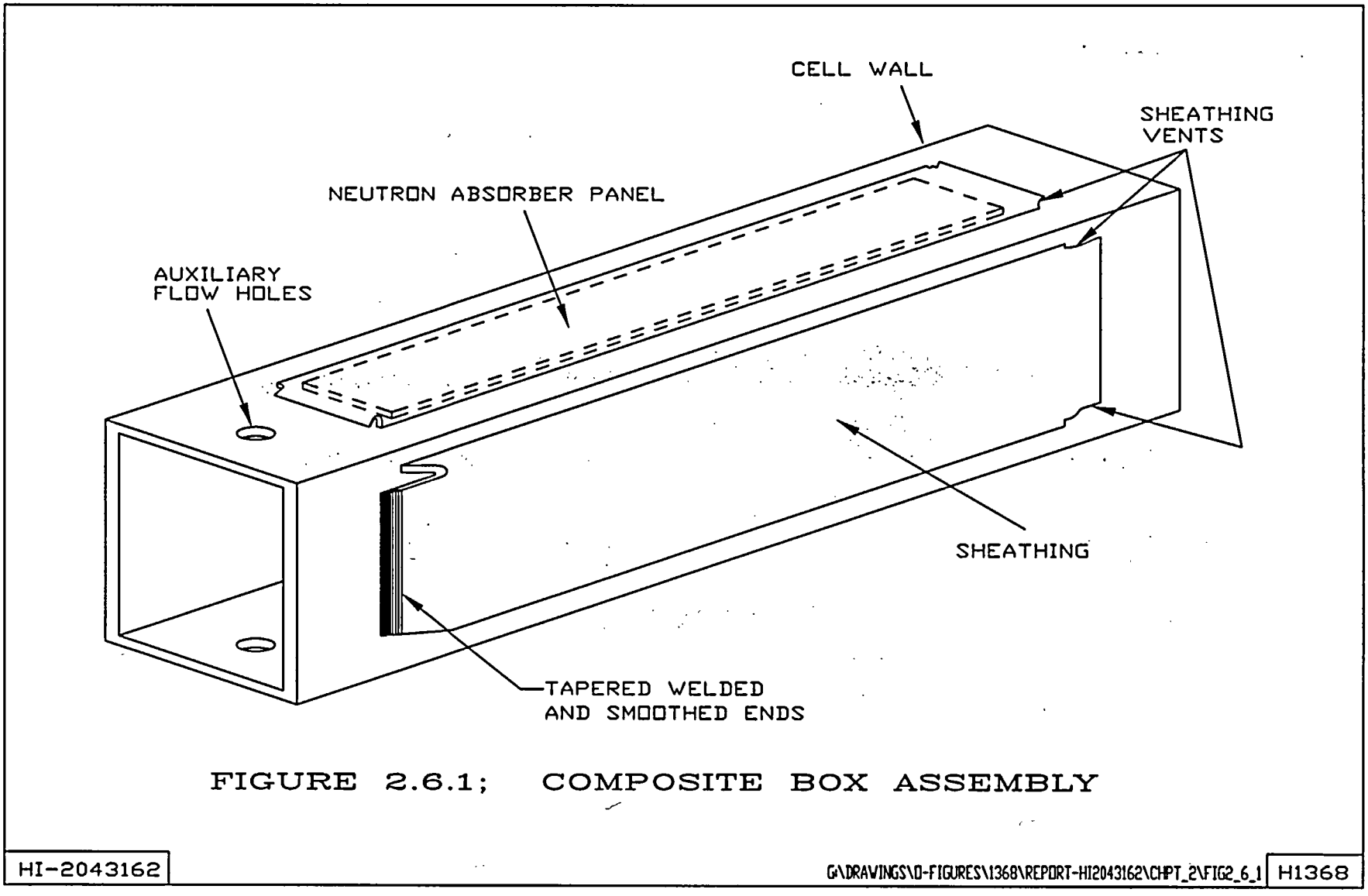

FIGURE 2.6.1; COMPOSITE BOX ASSEMBLY

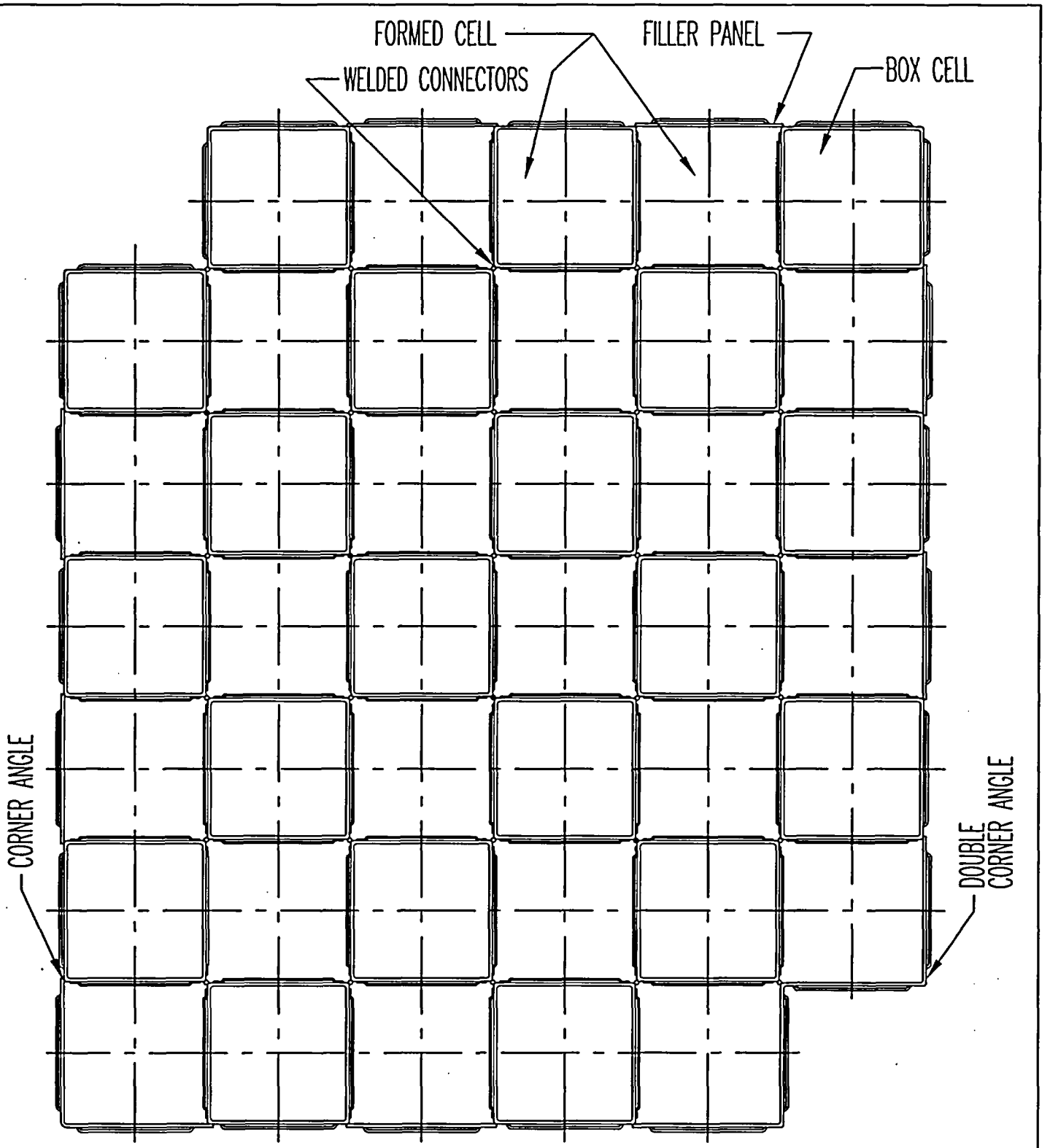

FIGURE 2.6.2; TYPICAL ARRAY OF STORAGE CELLS (NON-FLUX TRAP CONSTRUCTION)

H1368

NOTE: THIS FIGURE IS INTENDED TO INDICATE THE TYPICAL COMPONENTS OF THE RACK AND IS NOT INTENDED TO ACCURATELY REFLECT THE NUMBER OF CELLS OR SPECIFY LOCATIONS OF FABRICATED VS FORMED CELLS.

HI-20243162

G:\DRAWINGS\0-FIGURES\1368\REPORT-HI-2043162\FIGURES2.6.2

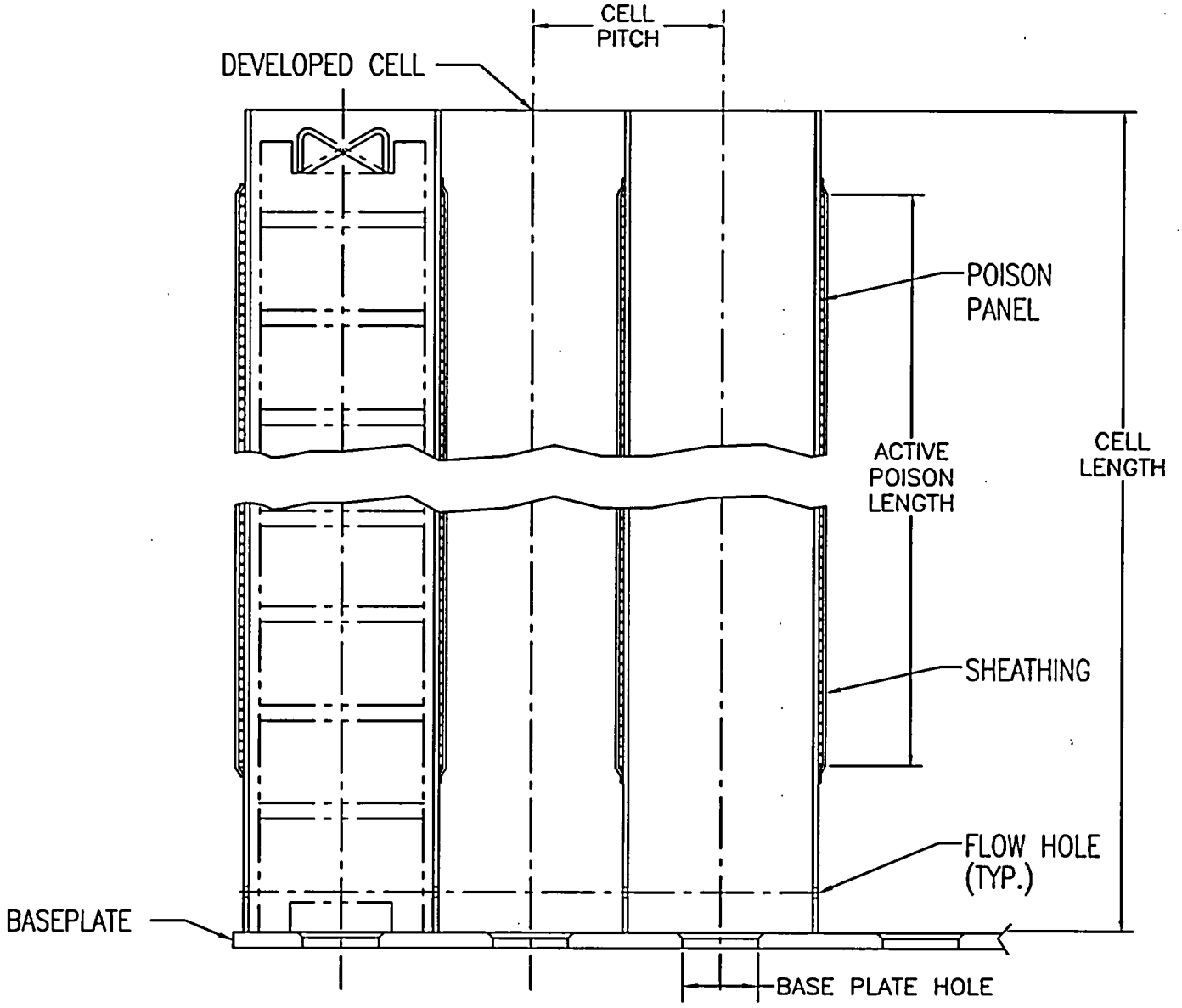

FIGURE 2.6.3; ELEVATION VIEW OF STORAGE RACK MODULE

NOTE: DEPICTION OF STORED FUEL ASSEMBLY IS NOT INTENDED TO BE ACCURATE.

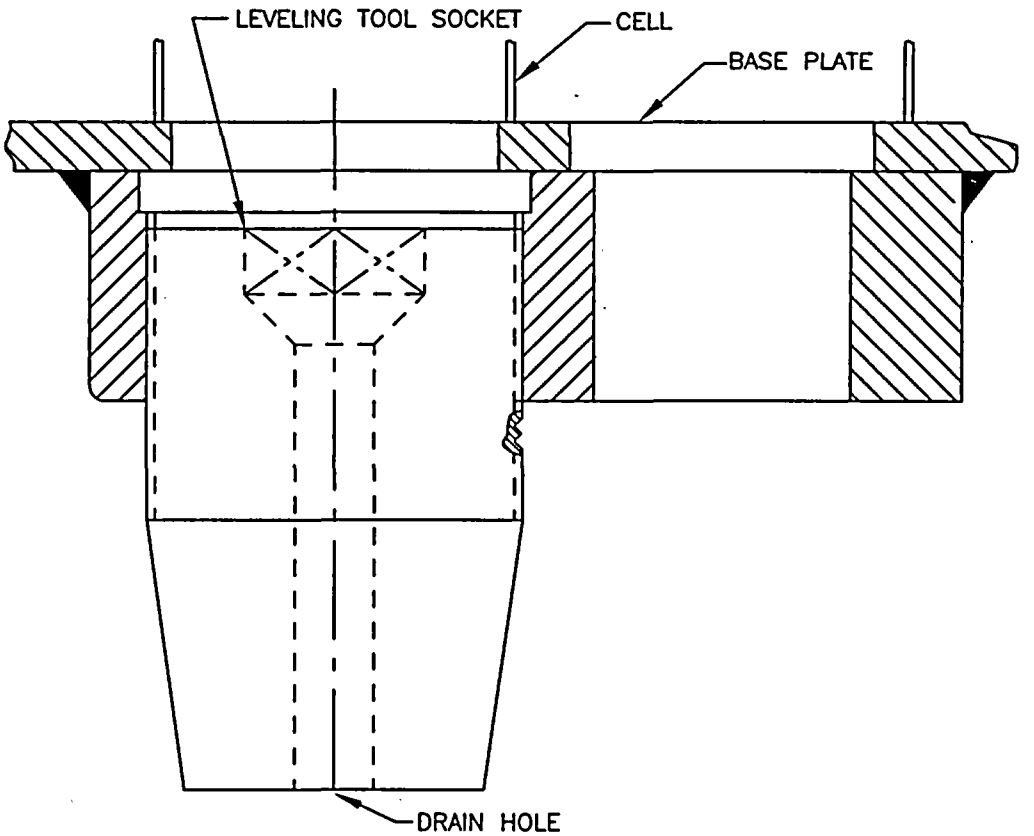

TYPICAL ELEVATION VIEW

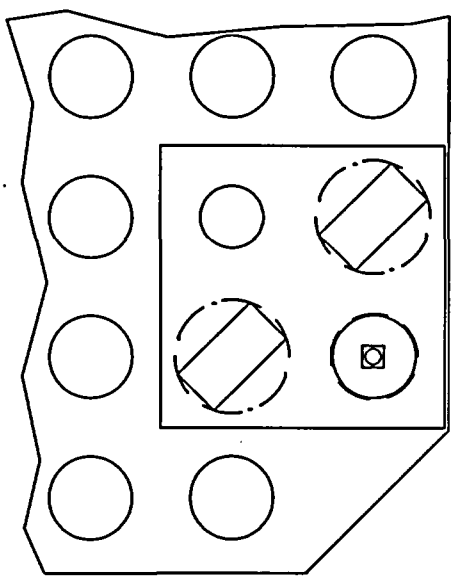

TYPICAL BOTTOM VIEWS OF RACK BASEPLATE CORNER

FIGURE 2.6.4; SUPPORT PEDESTALS FOR DCPP CASK PIT RACKS

3.0 MATERIAL AND HEAVY LOAD CONSIDERATIONS

3.1 Introduction

Safe storage of nuclear fuel in the SFP requires that the materials utilized in the rack fabrication be of proven durability and compatible with the pool water environment. This section provides a synopsis of the considerations with regard to long-term design service life of 40 years.

3.2 Structural Materials

The following structural materials will be utilized in the fabrication of the DCPP cask pit racks and associated support platforms:

a. ASME SA240 Type 304L for all sheet metal stock and baseplate

b. Internally threaded support legs: ASME SA240 Type 304L

c. Externally threaded support spindle: ASME SA564-630, Condition H1100 (precipitation hardened stainless steel)

d. Weld material – austenitic stainless steel

3.3 Neutron Absorbing Material

3.3.1 Characteristics of Metamic™

3.4 Compatibility with Environment

All materials used in the construction of the Holtec racks have been determined to be compatible with the DCPP SFP, including the cask pit area. Austenitic stainless steel (Type 304L) is a widely used stainless alloy in nuclear power plants and has a proven in-service performance as the liner material for many fuel pools in the U.S. and abroad. The materials used in Metamic, boron carbide and aluminum, are chemically compatible and ideally suited for long-term use in the radiation, thermal and chemical environment of a spent fuel pool.

3.5 Heavy Load Considerations for the Proposed Rack Installations

The Fuel Handling Building (FHB) Crane will be used to install the cask pit racks and associated support platforms in both units. The Fuel Building Crane is designed as Seismic Category I equipment. The capacity of the main hook is 125 tons. The FHB Crane is designed for spent fuel cask handling operations. More specifically, it is used to place casks within the cask pit area for removal of spent fuel from the plant.

Safe handling of heavy loads by the FHB Crane will be ensured by following the defense in depth approach guidelines of NUREG 0612:

- Defined safe load paths in accordance with the Plant Staff Review Committee approved procedures
- Supervision of heavy load lifts by designated qualified individuals
- Crane operator training and qualification that satisfies the requirements of ANSI/ASME B30.2-1976 [3.5.2]
- Use of lifting devices (slings) that are selected, inspected and maintained in accordance with ANSI B30.9-1971 [3.5.3]
- Inspection, testing and maintenance of cranes in accordance with ANSI/ASME B30.2-1976, as supplemented by CALOSHA requirements.
- Ensuring the design of the FHB Crane meets the intent of requirements of CMAA-70 [3.5.4] and ANSI/ASME B30.2-1976
- Reliability of special lifting devices by application of design safety margins, and periodic inspection and examinations using approved procedures, in accordance with ANSI N14.6

The salient features of the lifting rigs and associated procedures are described as follows:

a. Safe Load Paths and Procedures

Safe load paths will be defined for moving the new racks and platforms into and within the Fuel Handling Building. All movements of the racks and platforms within the FHB will be performed using the FHB Crane. During the receipt, inspection and placement of the platforms and racks into the cask pit area, heavy loads will not be carried over any portions of the existing storage racks containing active fuel assemblies. All phases of rack installation activities will be conducted in accordance with written procedures, which will be reviewed and approved by the owner.

b. Supervision of Lifts

Procedures used during the installation of the racks require supervision of heavy load lifts by a designated qualified individual who is responsible for ensuring procedural compliance and safe lifting practices. Holtec personnel experienced in similar rack installations will oversee the installation of the racks and support platforms.

c. Crane Operator Training

All crew members involved in the use of the lifting and upending equipment will be given training by Holtec International using a videotape-aided instruction course which has been utilized in previous rack installation operations. Crane operators will also be trained and qualified in accordance with PG&E's training program.

d. Lifting Devices Design and Reliability

The FHB Crane can access the truck bay, the adjacent laydown area, and the cask pit area of both SFPs. The FHB Crane has sufficient capacity to handle all lifts during the reracking process. The FHB crane is anticipated to be upgraded to single failure proof capability before the rack and support platform installation commences.

The following table determines the maximum lift weight during the installation of the cask pit racks.

Item	Weight (lb)
Rack	26,000 (max.)
Lift Rig	1,800
Rigging	500
Total Lift	28,300

The following table determines the maximum lift weight during the installation of the rack platforms.

Item	Weight (lb)
Platform	22,825 (max.)
Lift Rig	2,300
Rigging	500
Total Lift	25,625

It is clear, based on the heaviest rack or platform weight to be lifted, that the heaviest load will be well below the 125-ton rating of the FHB Crane Main Hook.

Remotely engaging lift rigs, meeting all requirements of NUREG-0612, will be used to lift the racks and support platforms. The rack and platform lift rigs consist of four independently loaded traction rods in a lift configuration. The individual lift rods have a safety factor of greater than 10. If one of the rods

break, the load will still be supported by at least two rods, which will have a safety factor of more than 5 against ultimate strength. Therefore, the lift rigs comply with the duality feature called for in Section 5.1.6 (3) of NUREG 0612.

The lift rigs have the following attributes:

- The traction rod is designed to prevent loss of its engagement with the rig in the locked position. Moreover, the locked configuration can be directly verified from above the pool water without the aid of an underwater camera.

- A stress analysis of each of the rigs is carried out and the primary stress limits postulated in ANSI N14.6 [3.5.5] are met.

- The rigs are load tested with 300% of the maximum weight to be lifted. The test weight is maintained in the air for 10 minutes. All critical weld joints are liquid penetrant examined to establish the soundness of all critical joints.

e. Crane Maintenance

The FHB Crane is maintained functional per the DCPP preventive maintenance procedures.

The proposed heavy load lifts will comply with the guidelines of NUREG-0612, which calls for measures to "provide an adequate defense-in-depth for handling of heavy loads near spent fuel...". The NUREG-0612 guidelines cite four major causes of load handling accidents, namely

i. operator errors
ii. rigging failure
iii. lack of adequate inspection
iv. inadequate procedures

The rack installation ensures maximum emphasis on mitigating the potential load drop accidents by implementing measures to eliminate shortcomings in all aspects of the operation including the four aforementioned areas. A summary of the measures specifically planned to deal with the major causes is provided below.

Operator errors: As mentioned above, comprehensive training will be provided to the installation crew. All training shall be in compliance with ANSI B30.2.

Rigging failure: The lifting rigs designed for handling and installing the new racks and support platforms have redundancies in the lift legs and lift eyes such that there are four independent load members in the new rack lift rig. Failure of any one load bearing member would not lead to uncontrolled lowering of the load. The rig complies with all provisions of ANSI N14.6-1993, including compliance with the primary stress criteria, load testing at 300% of maximum lift load, and dye examination of critical welds.

The rig designs are similar to the rigs used in the initial racking or the rerack of numerous other plants, such as Hope Creek, Millstone Unit 1, Indian Point Unit 2, Ulchin 2, Laguna Verde, J.A. FitzPatrick, and Three Mile Island Unit 1.

Lack of adequate inspection: The designer of the racks has developed a set of inspection points that have been proven to produce high quality installations in numerous prior rerack projects. Surveys and measurements are performed on the storage racks prior to and subsequent to placement into the pool to ensure that the as-built dimensions and installed locations are acceptable. Measurements of the pool and floor elevations are also performed to determine actual pool configuration and to allow height adjustments of the platforms prior to rack installation. These inspections minimize rack manipulation during placement into the pool. Preoperational crane testing will verify proper function of crane interlocks prior to rack movement.

Inadequate procedures: Procedures will be developed to address operations pertaining to the rack installation effort, including, but not limited to, mobilization, rack handling, upending, lifting, installation, verticality, alignment, dummy gage testing, site safety, and ALARA compliance. The procedures will be the successors of the procedures successfully implemented in previous projects.

Table 3.5.1 provides a synopsis of the requirements delineated in NUREG-0612, and its intended compliance.

3.6 References

[3.3.7] "Safety Evaluation by the Office of Nuclear Reactor Regulation Related to Holtec International Report HI-2022871 Regarding Use of Metamic in Fuel Pool Applications," Facility Operating License Nos. DPR-51 and NPF-6, Entergy Operations, Inc., Docket No. 50-313 and 50-368, USNRC, June 2003.

[3.3.8] USNRC Docket No. 72-1004, NRC's Safety Evaluation Report on NUHOMS 61BT (2002).

[3.3.9] "METAMIC 6061 + 40% boron Carbide Metal Matrix Composite Test Program for NAC International, Inc.", California Consolidated Technology, Inc. (2001).

[3.3.10] "METAMIC" Qualification Program for Nuclear Fuel Storage Applications, Final Test Results", Report NET 152-03, Prepared for Reynolds Metal Company, Inc. by Northeast Technology Corporation.

[3.3.11] "Use of METAMIC® in Fuel Pool Applications," Holtec Information Report No. HI-2022871, Revision 1 (2002).

[3.3.12] "Sourcebook for Metamic™ Performance Assessment" by Dr. Stanley Turner, Holtec Report No. HI-2043215 (2004).

[3.5.1] DCPP Final Safety Analysis Report Update (FSAR).

[3.5.2] ANSI/ASME B30.2, "Overhead and Gantry Cranes, (Top Running Bridge, Single or Multiple Girder, Top Running Trolley Hoist)," American Society of Mechanical Engineers, 1976.

[3.5.3] ANSI B30.9, "Safety Standards for Slings," 1971.

[3.5.4] CMMA Specification 70, "Electrical Overhead Traveling Cranes," Crane Manufacturers Association of America, Inc., 2000.

[3.5.5] ANSI N14.6-1993, Standard for Special Lifting Devices for Shipping Containers Weighing 10000 Pounds or more for Nuclear Materials," American National Standard Institute, Inc., 1978.

[3.5.6] ANSI/ASME B30.20, "Below-the-Hook Lifting Devices," American Society of Mechanical Engineers, 1993.

Table 3.5.1

HEAVY LOAD HANDLING COMPLIANCE MATRIX (NUREG-0612)

	Criterion	Compliance
1.	Are safe load paths defined for the movement of heavy loads to minimize the potential of impact, if dropped, on irradiated fuel?	Yes
2.	Will procedures be developed to cover: identification of required equipment, inspection and acceptance criteria required before movement of load, steps and proper sequence for handling the load, defining the safe load paths, and special precautions?	Yes
3.	Will crane operators be trained and qualified?	Yes
4.	Will special lifting devices meet the guidelines of ANSI 14.6-1993?	Yes
5.	Will non-custom lifting devices be installed and used in accordance with ANSI B30.20 [3.5.6], latest edition?	Yes
6.	Will the crane be inspected and tested prior to use in rack installation?	Yes
7.	Does the crane meet the requirements of ANSI B30.2-1976 and CMMA-70?	Yes

4.0 CRITICALITY SAFETY ANALYSES

4.1 Introduction and Summary

Overview

This section documents the criticality safety evaluation for the storage of PWR spent nuclear fuel in Holtec Region 2 style spent fuel storage racks at the Diablo Canyon Power Plant (DCPP), Unit 1 and 2. These racks are designed to be placed into the cask pits of the spent fuel pools of the units. The racks for the two units are identical in all characteristics relevant to criticality control. Therefore, no distinction needs to be made between the racks for the two units in this section, and all results apply to both units. The scope of the analysis is limited to fuel assemblies with an initial enrichment of no more than 4.1 wt% ^{235}U from cycles 1 through 7 of each unit.

The objective of this analysis is to ensure that the effective neutron multiplication factor (k_{eff}) is less than or equal to 0.95 with the storage racks fully loaded with fuel of the highest permissible reactivity and the pool flooded with borated water at a temperature corresponding to the highest reactivity. In addition, it is demonstrated that k_{eff} is less than 1.0 under the assumed accident of the loss of soluble boron in the pool water, i.e. assuming unborated water in the spent fuel pool. The maximum calculated reactivities include a margin for uncertainty in reactivity calculations, including manufacturing tolerances, and are calculated with a 95% probability at a 95% confidence level [4.1].

A curve for the minimum required fuel burnup as a function of the initial fuel enrichment is developed, that ensures that the requirements stated above are met.

Reactivity effects of abnormal and accident conditions are also been evaluated to assure that under all credible conditions, the reactivity will not exceed the regulatory limit of 0.95, considering the presence of soluble boron.

Summary of Results

The analysis demonstrates that for the defined acceptance criteria that are summarized below, the effective neutron multiplication factor (k_{eff}) is less than 1.00 with unborated water and less than 0.95 with 500 ppm of soluble boron, at a 95% probability with a 95% confidence level. Further, the reactivity effects of abnormal and accident conditions have been evaluated. To assure that under credible abnormal and accident conditions the reactivity will not exceed 0.95 at a 95% probability with a 95% confidence level, a soluble boron level of 800 ppm must be maintained.

Calculations have been performed to qualify the racks for storage of burned fuel assemblies with a maximum nominal enrichment of 4.1 wt% ^{235}U and a minimum burnup of 28.53 GWd/mtU, from cycles 1 through 7 from DCPP Unit 1 and Unit 2. Results for this condition are summarized in Table 4.1.1 and Table 4.1.2 for unborated and borated water, respectively. For other enrichments, the minimum burnup can be determined with the function

$$BU = A + B^* E + C * E^2$$

with

BU	Minimum Burnup in GWd/mtU
E	Initial Enrichment in wt% ^{235}U (2.0 through 4.1 wt%)
A	Coefficient, = -40.627
B	Coefficient, = 24.903
C	Coefficient, = -1.960

This function is also shown as a graph in Figure 4.1.1.

4.2 Acceptance Criteria

The objective of this analysis is to ensure that the effective neutron multiplication factor (k_{eff}) is less than or equal to 0.95 with the storage racks fully loaded with fuel of the highest permissible reactivity and the pool flooded with borated water at a temperature corresponding to the highest reactivity. In addition, it is demonstrated that k_{eff} is less than 1.0 under the assumed accident of the loss of soluble boron in the pool water, i.e. assuming unborated water in the spent fuel pool. The maximum calculated reactivities include a margin for uncertainty in reactivity calculations, including manufacturing tolerances, and are calculated with a 95% probability at a 95% confidence level [4.1].

Applicable codes, standard, and regulations or pertinent sections thereof, include the following:

- Code of Federal Regulations, Title 10, Part 50, Appendix A, General Design Criterion 62, "Prevention of Criticality in Fuel Storage and Handling."

- USNRC Standard Review Plan, NUREG-0800, Section 9.1.2, Spent Fuel Storage, Rev. 3 - July 1981.

- USNRC letter of April 14, 1978, to all Power Reactor Licensees - OT Position for Review and Acceptance of Spent Fuel Storage and Handling Applications, including modification letter dated January 18, 1979.

- L. Kopp, "Guidance on the Regulatory Requirements for Criticality Analysis of Fuel Storage at Light-Water Reactor Power Plants," NRC Memorandum from L. Kopp to T. Collins, August 19, 1998.

- USNRC Regulatory Guide 1.13, Spent Fuel Storage Facility Design Basis, Rev. 2 (proposed), December 1981.

- ANSI ANS-8.17-1984, Criticality Safety Criteria for the Handling, Storage and Transportation of LWR Fuel Outside Reactors.

- Code of Federal Regulation 10CFR50.68, Criticality Accident Requirements (for soluble boron)

4.3 Assumptions

To assure the true reactivity will always be less than the calculated reactivity, the following conservative design criteria and assumptions were employed:

1) Moderator is borated or unborated water at a temperature that results in the highest reactivity, as determined by the analyses.

2) Neutron absorption in minor structural members is neglected, i.e., spacer grids are replaced by water.

3) The effective multiplication factor of an infinite radial array of fuel assemblies is calculated in the analyses.

4) As cooling time increases, decay of Pu-241 and build-up of Am-241 and Gd-155 result in a continuous decrease in reactivity, which provides an increasing subcriticality margin with time. No credit is taken for this decrease in reactivity, i.e. calculations are performed for 0 cooling time. This is a significant conservatism, since the assemblies qualified for the cask pit rack (discharged in cycles 1 through 7) have already cooling times between 8 and 18 years by mid 2004.

5) The presence of burnable poison rod assemblies (BPRAs) during fuel depletion potentially increases the k_{eff} of an assembly [4.11]. Therefore, depletion calculations with and without BPRAs were performed to determine the most reactive condition. Two major assumptions were made when performing calculations with BPRAs: a) All assemblies are assumed to contain a burnable poison rod assembly (BPRA) during depletion; and b) all BPRAs are assumed to contain the maximum number of poison rods. Both assumptions represent a major conservatism, since in reality a) only a small fraction of fuel assemblies were exposed to a BPRA; and b) most BPRAs contain less than the maximum number of poison rods.

6) No credit is taken for the potential presence of BPRAs in fuel assemblies when the assemblies are in the spent fuel racks.

7) Higher soluble boron concentrations during fuel depletion result in a higher reactivity of the assemblies due to spectrum hardening. Therefore, the highest cycle average soluble boron concentration of all applicable cycles is used in the depletion analyses.

8) To bound the reactivity effect associated with the axial burnup distribution in a fuel assembly, calculations with an axial burnup profile and calculations with an axially constant burnup were performed in the design basis calculations, and the higher of the two resulting reactivities is used for each case.

9) The moderator temperature during depletion has a significant impact on reactivity, with higher temperatures resulting in higher k_{eff} values. Conservatively, the core average exit temperature is used as the moderator temperature in the depletion calculations.

10) For power density and fuel temperature, average values from cycles 1 through 7 are used in the depletion calculations. This is acceptable, since these values have a comparably small effect on reactivity. The potential effect due to variations in these parameters is more than compensated

by the effect of the other conservative assumptions, including neglecting cooling time and assuming there are BPRAs with the maximum number of rods in all assemblies during depletion.

Additionally, there are a small number of modeling assumptions, as listed below. These assumptions have a negligible effect on the calculated reactivities.

1) The single instrument tube in each fuel assembly is modeled with the same dimensions as the 24 guide tubes in the assembly.
2) Some minor variations of guide tube dimensions in some assemblies from the values used in the analyses are neglected.
3) All zirconium alloys are modeled as pure zirconium.
4) The majority of the rack cells have a cell ID of 8.75 Inches, while a few cells on the rack periphery have an ID of 8.85 Inches. In the calculations, all rack cells are modeled with a cell ID of 8.75 Inches

4.4 Design and Input Data

4.4.1 Fuel Assembly and Fuel Insert Specification

The design specifications for the fuel assemblies, which were used for this analysis, are given in Table 4.4.1. The assembly types listed in this table, i.e. STD (LOPAR) and OFA (Vantage 5), are the only types analyzed. Therefore, these are the only assembly types allowed to be stored in the cask pit racks.

The operating parameters used in the depletion analysis are given in Table 4.4.2. The data is applicable to cycles 1 through 7 for both units. For data that differ slightly between the two units, the higher, i.e. more conservative data is listed in Table 4.4.2 and used in the analysis. For the soluble boron level, the highest cycle average value for any of the cycles 1 through 7 in both units is used.

Specification of Burnable Poison Rod Assemblies (BPRAs) assumed in the assemblies during depletion are listed in Table 4.4.3. For the BPRAs, only nominal specifications are used, since these devices are only used in the depletion calculations to establish a bounding approach to represent the conservative effect of poison inserts. Any effect of the tolerances or small variations of these specifications would be small, and would be bounded by the effect of assuming a poison insert with the maximum number of poison rods in every assembly during depletion.

4.4.2 Cask Area Storage Rack Specification

The storage cell characteristics which are used in the criticality evaluations are summarized in Table 4.4.4.

4.5 Methodology

The principal method for the criticality analysis of the high-density storage racks is the three-dimensional Monte Carlo code MCNP4a [4.2]. MCNP4a is a continuous energy three-dimensional Monte Carlo code developed at the Los Alamos National Laboratory. MCNP4a was selected because it has been previously used and benchmarked for criticality analyses and has all of the necessary features for this analysis. The critical benchmark experiments considered the effects of varying fuel enrichment, boron-10 loading, lattice spacing, fuel pellet diameter, and soluble boron concentration. The experimental data are sufficiently diverse to establish that the method bias and uncertainty will apply to the DCPP temporary rack conditions. MCNP4a calculations used continuous energy cross-section data based on ENDF/B-V and ENDF/B-VI, as distributed with the code [4.2]. Exceptions are two lumped fission products and one individual fission product calculated by the CASMO-4 depletion code (see below), that do not have corresponding cross sections in MCNP. For these isotopes, the CASMO-4 cross sections are used in MCNP. This approach has been validated by showing that the cross sections result in the same reactivity

effect in both CASMO-4 and MCNP. Independent verification calculations were performed with KENOV.a [4.8], which is a three-dimensional multigroup Monte Carlo code developed at the Oak Ridge National Laboratory. The KENOV.a calculations used the 238-group cross-section library, which is based on ENDF/B-V data and is distributed as part of the SCALE-4.3 package [4.9], in association with the NITAWL-II program [4.10], which adjusts the uranium-238 cross sections to compensate for resonance self-shielding effects.

Benchmark calculations, presented in Appendix A, indicate a bias of 0.0030 with an uncertainty of ± 0.0012 for KENOV.a and 0.0009 ± 0.0011 for MCNP4a, both evaluated with a 95% probability at the 95% confidence level [4.1]. The calculations for this analysis utilize the same computer platform and cross-section libraries used for the benchmark calculations discussed in Appendix A.

The convergence of a Monte Carlo criticality problem is sensitive to the following parameters: (1) number of histories per cycle, (2) the number of cycles skipped before averaging, (3) the total number of cycles and (4) the initial source distribution. The MCNP4a criticality output contains a great deal of useful information that may be used to determine the acceptability of the problem convergence. This information has been used in parametric studies to develop appropriate values for the aforementioned criticality parameters to be used in storage rack criticality calculations. Based on these studies, a minimum of 10,000 histories were simulated per cycle, a minimum of 20 cycles were skipped before averaging, a minimum of 100 cycles were accumulated, and the initial source was specified as uniform over the fueled regions (assemblies). Further, the output was reviewed to ensure that each calculation achieved acceptable convergence. These parameters represent an acceptable compromise between calculational precision and computational time.

Fuel depletion analyses during core operation were performed with CASMO-4 (using the 70-group cross-section library), a two-dimensional multigroup transport theory code based on capture probabilities [4.3-4.5]. CASMO-4 is used to determine the isotopic composition of the spent fuel. In addition, the CASMO-4 calculations are restarted in the storage rack geometry yielding the two-

dimensional infinite multiplication factor (k_{inf}) for the storage rack to determine the reactivity effect of fuel and rack tolerances, and to perform various studies. For all calculations in the spent fuel pool racks, the Xe-135 concentration in the fuel is conservatively set to zero.

The following equation was used to perform the k_{eff} calculations:

$$k_{eff} = k_{calc} + \Delta k_{bias} + \Delta k_{temp} + \Delta k_{uncert}$$

where

k_{calc}	=	k_{eff} under nominal conditions
Δk_{bias}	=	bias determined from benchmark calculations
Δk_{temp}	=	temperature bias
Δk_{uncert}	=	statistical summation of tolerance and uncertainty components
	=	$[tol1^2 + tol2^2 + \ldots + uncert1^2 + uncert2^2 + \ldots]^{1/2}$

As allowed in [4.6], the methodology employed to calculate the tolerance effects combine both the worst-case bounding value and sensitivity study approaches. For each individual parameter associated with a tolerance, the full tolerance value is utilized to determine the maximum reactivity effect. All of the Δk values from the various tolerances are then statistically combined to determine the final reactivity allowance for manufacturing tolerances.

In the geometric models used for the calculations, each fuel rod and its cladding were described explicitly and reflecting boundary conditions were used in the radial direction which has the effect of creating an infinite radial array of storage cells.

4.6 Analysis

This section describes the calculations that were used to determine the acceptable storage criteria for the racks and summarizes the results. In addition, this section discusses the possible abnormal and accident conditions.

Unless otherwise stated, all calculations assumed nominal characteristics for the fuel and the fuel storage cells. The effect of the manufacturing tolerances is accounted for with a reactivity adjustment as discussed below.

4.6.1 Bounding Fuel Assemblies

To determine the bounding assembly, calculations are performed for both assembly types listed in Table 4.4.1 and for assemblies with and without BPRAs during depletion. Calculations are performed for three enrichments, 2.0 wt%, 3.0 wt% and 4.1 wt%, and a representative burnup for each enrichment. The results show that the LOPAR assemblies with a BPRA has the highest reactivity. This assembly type is therefore used in all subsequent calculations, and all depletion calculations are performed assuming the presence of a BPRA during the initial fuel burnup.

4.6.2 Moderator Temperature Effect

For the depletion calculations, the core exit temperature is used as the moderator temperature (see Table 4.4.2). However, the residual fuel assembly reactivity that would be stored in the rack is dominated by the area slightly below the top of the active fuel region, where the moderator temperature in the core is lower. Since the calculated residual reactivity increases significantly with increasing moderator temperature, the assumption used in the depletion calculations is conservative.

4.6.3 Pool Water Temperature Effects

Pool water temperature effects on reactivity have been calculated with CASMO-4. The results demonstrate that the spent fuel pool temperature coefficient of reactivity is negative, i.e. a lower temperature results in a higher reactivity. Consequently, all CASMO-4 calculations are evaluated at 38 °F, which is well below the actual minimum SFP water temperature.

In MCNP4a, the Doppler treatment and cross-sections are valid only at 300K (80.6 °F). Therefore, a Δk is determined in CASMO-4 from 80.6 °F to 38 °F, and is included in the final k_{eff} calculation as a bias.

4.6.4 Uncertainties Due to Manufacturing Tolerances

In the calculation of the final k_{inf}, the effect of manufacturing tolerances on reactivity must be included. CASMO-4 was used to perform these calculations. As allowed in [4.6], the methodology employed to calculate the tolerance effects combine both the worst-case bounding value and sensitivity study approaches. The evaluations include tolerances of the rack dimensions (see Table 4.4.4) and tolerances of the fuel dimensions (see Table 4.4.1). In addition to the tolerances specified in these tables, an enrichment tolerance of 0.05 wt% is analyzed. As for the bounding assembly, calculations are performed for different enrichments and burnups. The reference condition is the condition with nominal dimensions and properties. To determine the Δk associated with a specific manufacturing tolerance, the k_{inf} calculated for the reference condition is compared to the k_{inf} from a calculation with the tolerance included. Note that for the individual parameters associated with a tolerance, no statistical approach is utilized. Instead, the full tolerance value is utilized to determine the maximum reactivity effect. All of the Δk values from the various tolerances are statistically combined (square root of the sum of the squares) to determine the final reactivity allowance for manufacturing tolerances.

Calculations are performed for three enrichments, 2.0 wt%, 3.0 wt% and 4.1 wt%, and a representative burnup for each enrichment. The maximum of the statistically combined values are used in the final k_{eff} calculations (see Tables 4.1.1. and 4.1.2).

4.6.5 Uncertainty in Depletion Calculations

CASMO-4 was used to perform the depletion calculations. Since critical experiment data with spent fuel is not available for determining the uncertainty in burnup-dependent reactivity calculations, an allowance for uncertainty in reactivity was assigned based upon other considerations. Assuming the uncertainty in depletion calculations is less than 5% of the total reactivity decrement, a burnup dependent uncertainty in reactivity for burnup calculations may be assigned. This uncertainty is statistically combined with the other reactivity allowances in the determination of the maximum k_{eff}.

4.6.6 Isotopic Compositions

To perform the criticality evaluation for spent fuel in MCNP, the isotopic composition of the fuel is calculated with the depletion code CASMO-4 and then specified as input data in the MCNP4A run.

The CASMO-4 calculations to obtain the isotopic compositions for MCNP4Awere performed generically, with one calculation for each enrichment, and burnups in increments of 2.5 GWD/MTU or less. The isotopic composition for any given burnup is then determined by linear interpolation.

4.6.7 Eccentric Fuel Assembly Positioning

The fuel assembly is assumed to be normally located in the center of the storage rack cell. Nevertheless, MCNP4a calculations were made with the fuel assemblies assumed to be in the corner of the storage rack cell (four-assembly cluster at closest approach). These calculations indicated that eccentric fuel positioning results in a decrease in reactivity.

4.6.8 Reactivity Effect of Axial Burnup Distribution

Generic analytic results of axial burnup effects have been provided by Turner [4.7] based upon calculated and measured axial burnup distributions. These analyses confirm a minor and generally negative reactivity effect of the axially distributed burnup, becoming positive at burnups greater than about 30 GWD/MTU. The required burnup for all enrichments analyzed here is less than 30 GWD/MTU. Therefore, a positive reactivity effect of the axially distributed burnup would not be expected. However, for additional assurance, all design basis calculations are performed with an axial burnup distribution and with an axially constant burnup, and the higher of the two resulting reactivities is used.

4.6.9 Burnup Versus Enrichment Curve

To establish a burnup versus enrichment curve (loading curve), calculations were performed at selected enrichments between 2.0 wt% and 4.1 wt%, and for burnup values slightly above and below the expected loading curve. Points on the proposed loading curve are then calculated by linear interpolation for each enrichment, based on an appropriate target value for the reactivity. The loading curve is then determined by a curve fit to these calculated burnup values. The curve fit results in the following equation:

$$BU = A + B^* E + C * E^2$$

with

BU	Minimum Burnup in GWd/mtU
E	Initial Enrichment in wt% ^{235}U
A	Coefficient, = -40.627
B	Coefficient, = 24.903
C	Coefficient, = -1.960

The loading curve is also shown graphically in Figure 4.1.1.

To confirm the validity of this curve for all enrichments, calculations are performed for a total of seven enrichment values between 2.0 wt% and 4.1 wt%, and the corresponding burnups determined from the loading curve. Results of these calculations demonstrate that the maximum k_{eff} including all applicable biases and uncertainties is well below the regulatory limit of 1.0 for the entire enrichment range. The results for 4.1 wt% initial enrichment (corresponding burnup is 28.53 GWd/mtU) are listed in Table 4.1.1.

4.6.10 Interfaces

The cask area racks face the pool wall on two sides, and face existing Region 2 racks on the other two sides. To evaluate whether there is the possibility of any neutronic coupling between the new cask area racks and the existing Region 2 racks, the following needs to be noted:

- The distance between the racks is more than 12 inches, and there is an existing structure in the pool which precludes the racks from being closer than 12 inches. The mean free path of neutrons in steel or water, as determined in the MCNP4A calculations, is about 1 inch or less. The separation of more than 12 inches, i.e. more than 12 times the mean free path, is therefore already sufficient to preclude any neutronic interaction.

- In addition, the existing Region 2 racks are designed as non-poisoned racks, with a distance between individual cells of about 2 inches. These racks are analyzed as infinite arrays of cells. A fuel assembly would have to be placed closer than two inches on the outside of these racks in order to have an impact on the reactivity. However, the minimum possible distance is about 12 inches, as discussed above. Therefore, the placement of the cask area racks has no effect on the reactivity of the existing racks in the spent fuel pool.

- The new cask area racks contain poison panels on all four sides of the racks, and are conservatively analyzed as infinite cell arrays. Even the inadvertent mis-placement of an individual fuel assemblies placed directly on the outside of a rack would not affect the calculated reactivity. The existing racks are at least 12 inches away from the new cask area racks and do not affect the reactivity of the cask area racks. Therefore, there is no need to consider the existing racks in the criticality calculations presented here.

In summary, the new and existing racks are sufficiently separated to preclude any neutronic interaction, and no specific criticality calculations of any interface configuration are required.

4.6.11 Soluble Boron Concentration for Maximum k_{eff} of 0.95

The calculations crediting soluble boron in the spent fuel pool to ensure that the reactivity does not exceed 0.95 are performed for several enrichments at a soluble boron level of 500 ppm. In all cases, the maximum k_{eff} including all applicable biases and uncertainties is well below the regulatory limit of 0.95. The results for 4.1 wt% initial enrichment (corresponding burnup is 28.53 GWd/mtU) are also listed in Table 4.1.2.

4.6.12 Abnormal and Accident Conditions

The effects on reactivity of credible abnormal and accident conditions are examined in this section. None of the abnormal or accident conditions that have been identified as credible cause the reactivity of the storage racks to exceed the limiting reactivity value of $k_{eff} = 0.95$, considering the presence of soluble boron. The double contingency principle of ANSI N16.1-1975 (and the USNRC letter of April 1978) specifies that it shall require at least two unlikely independent and concurrent events to produce a criticality accident. This principle precludes the necessity of considering the simultaneous occurrence of multiple accident conditions.

4.6.12.1 Temperature and Water Density Effects

Temperature effects on reactivity have been calculated with CASMO-4. The results show that the spent fuel pool temperature coefficient of reactivity is negative, and that introducing voids in the water internal to the storage cell (to simulate boiling) further decreased reactivity. Using the lowest temperature (38°F) in the analysis, therefore, assures that the true reactivity will always be lower than the calculated value regardless of temperature.

4.6.12.2 Dropped Assembly - Horizontal

For the case in which a fuel assembly is assumed to be dropped on top of a rack, the fuel assembly will come to rest horizontally on top of the rack with a minimum separation distance from the active fuel region of more than 12 inches, which is sufficient to preclude neutron coupling (i.e., an effectively infinite separation as discussed in section 4.6.10). Maximum expected deformation under seismic or accident conditions will not reduce the minimum spacing to less than 12 inches. Consequently, the horizontal fuel assembly drop accident will not result in a significant increase in reactivity.

4.6.12.3 Dropped Assembly - Vertical

It is also possible to vertically drop an assembly into a location that might be occupied by another assembly or that might be empty. Such a vertical impact would at most cause a small compression of the stored assembly, if present, or result in a small deformation of the baseplate for an empty cell. These deformations could potentially increase reactivity. However, the reactivity increase would be small compared to the reactivity increase created by the misloading of a fresh assembly discussed in the following section. The vertical drop is therefore bounded by this misloading accident and no separate calculation is performed for the drop accident.

4.6.12.4 Abnormal Location of a Fuel Assembly

4.6.12.4.1 Misloaded Fresh Fuel Assembly

The misplacement of a fresh unburned fuel assembly could, in the absence of soluble poison, result in exceeding the regulatory limit (k_{eff} of 0.95). This could possibly occur if a fresh fuel assembly of the highest permissible enrichment (5.0 wt%) were to be inadvertently misloaded into a storage cell intended for spent fuel. The reactivity consequence of this situation was investigated. The corresponding calculational model consists of a 5x5 array of cells with a fresh assembly in the center cell. The model is surrounded by periodic boundary conditions, which generates an infinite arrangement of 5x5 arrays with a misloaded assembly. Calculations are performed with 500 ppm and 1000 ppm soluble boron, and the minimum allowable soluble boron concentration is determined by linear interpolation. As the target values for k_{eff}, the maximum value from the design basis calculations is used. To assure that the regulatory limit is not exceeded under this condition, a soluble boron concentration of at least 800 ppm in the spent fuel pool is required.

4.6.12.4.2 Mislocated Fresh Fuel Assembly

The mislocation of a fresh unburned fuel assembly, i.e. the accidental placement of an assembly outside of a storage rack adjacent to other fuel assemblies, has also been considered. There are two locations at opposite corners of the racks where a single assembly could be placed on the outside of the racks. The racks have been designed to prevent this event. Nevertheless, this event was conservatively evaluated. The assemblies would still be separated from the assemblies inside the rack by a neutron absorber panel, since all peripheral walls of the racks are equipped with such panels, although with a slightly smaller panel width than on the walls inside the racks. Further, the assemblies in these locations would still be more than 12 inches away from the existing Region 2 racks, which precludes any significant neutron interaction (see also Section 4.6.10, first item in bulleted list). The effect of the slightly smaller panel width (7 inches instead 7.5 inches) would be more than compensated by the increased neutron leakage on the periphery of the racks, which is not credited in the design basis calculations. In summary, the mislocation of an assembly would not result in any significant increase in reactivity, compared to placement of the same assembly inside the racks. The mislocation accident of a fresh assembly is therefore bounded by the misloading accident discussed in the previous section, and no specific calculations were performed for this mislocation accident.

4.6.13 Code Comparison

A comparison between MCNP4A and KENOV.A is performed for fresh fuel at 2.0 wt% enrichment. The comparison shows a good agreement between the two codes, with a difference in reactivity (including Bias) of only 0.0013 Δk. Of the two codes, MCNP shows the higher value.

4.7 References

4.1 M.G. Natrella, Experimental Statistics, National Bureau of Standards, Handbook 91, August 1963.

4.2 J.F. Briesmeister, Editor, "MCNP - A General Monte Carlo N-Particle Transport Code, Version 4A," LA-12625, Los Alamos National Laboratory (1993).

4.3 M. Edenius, K. Ekberg, B.H. Forssén, and D. Knott, "CASMO-4 A Fuel Assembly Burnup Program User's Manual," Studsvik/SOA-95/1, Studsvik of America, Inc. and Studsvik Core Analysis AB (proprietary).

4.4 D. Knott, "CASMO-4 Benchmark Against Critical Experiments", SOA-94/13, Studsvik of America, Inc., (proprietary).

4.5 D. Knott, "CASMO-4 Benchmark Against MCNP," SOA-94/12, Studsvik of America, Inc., (proprietary).

4.6 L.I. Kopp, "Guidance on the Regulatory Requirements for Criticality Analysis of Fuel Storage at Light-Water Reactor Power Plants," NRC Memorandum from L. Kopp to T. Collins, August 19, 1998.

4.7 S.E. Turner, "Uncertainty Analysis - Burnup Distributions", presented at the DOE/SANDIA Technical Meeting on Fuel Burnup Credit, Special Session, ANS/ENS Conference, Washington, D.C., November 2, 1988.

4.8 L.M. Petrie and N.F. Landers, "KENO Va - An Improved Monte Carlo Criticality Program with Supergrouping," Volume 2, Section F11 from "SCALE: A Modular System for Performing Standardized Computer Analysis for Licensing Evaluation" NUREG/CR-0200, Rev. 4, January 1990.

4.9 "SCALE 4.3: A Modular System for Performing Standardized Computer Analysis for Licensing Evaluations," NUREG-CR-0200, Rev. 5, Oak Ridge National Laboratory (1995).

4.10 N.M. Greene, L.M. Petrie and R.M. Westfall, "NITAWL-II: Scale System Module for Performing Shielding and Working Library Production," Volume 1, Section F1 from "SCALE: A Modular System for Performing Standardized Computer Analysis for Licensing Evaluation" NUREG/CR-0200, Rev. 4, January 1990.

4.11 "Parametric Study of the Effect of Burnable Poison Rods for PWR Burnup Credit", NUREG/CR-6761, ORNL/TM-2000/373, March 2002

Table 4.1.1
Summary of the Criticality Safety Analyses for Holtec Cask Area Rack without Soluble Boron

Design Basis Burnup at 4.1 wt% ^{235}U		28.53 GWd/mtU
Soluble Boron Concentration		0 ppm
Uncertainties and Tolerances		
Bias Uncertainty (95%/95%)		± 0.0011
Calculational Statistics (95%/95%, 2.0×σ)		± 0.0014
Depletion Uncertainty		± 0.0105
Fuel Eccentricity		negative
Fuel Tolerances		
Fuel Density	+0.0021	
Enrichment	+0.0068	
Rod Pitch	±0.0014	
Clad-OD	±0.0008	
Minimum Clad Thickness	+0.0006	
Fuel Rod OD	±0.0004	
Guide Tube OD	±0.0000	
Minimum G.T. Thickness	+0.0005	
Fuel Tolerances, statistically combined		± 0.0073
Rack Tolerances		
Cell ID/Pitch	±0.0016	
Wall Thickness	±0.0003	
Sheathing Thkns	±0.0001	
Poison Thickness	±0.0001	
Poison Loading	±0.0025	
Rack Tolerances, statistically combined		± 0.0029
Statistical Combination of Uncertainties and Tolerances[1]		± 0.0132
Reference k_{eff} (MCNP4a)		0.9721
Total Uncertainty (above)		0.0132
Calculational Bias (see Appendix A)		0.0009
Temperature Bias		0.0046
Maximum k_{eff}		**0.9908**
Regulatory Limiting k_{eff}		**1.0000**

[1] Square root of the sum of the squares.

Table 4.1.2
Summary of the Criticality Safety Analyses for Holtec Cask Area Rack with Soluble Boron

Design Basis Burnup at 4.1 wt% ^{235}U		28.53 GWd/mtU
Soluble Boron Concentration		500 ppm
Uncertainties		
Bias Uncertainty (95%/95%)		± 0.0011
Calculational Statistics (95%/95%, 2.0×σ)		± 0.0014
Depletion Uncertainty		± 0.0099
Fuel Eccentricity		negative
Fuel Tolerances		
Fuel Density	+0.0021	
Enrichment	+0.0068	
Rod Pitch	±0.0014	
Clad-OD	±0.0008	
Minimum Clad Thickness	+0.0006	
Fuel Rod OD	±0.0004	
Guide Tube OD	±0.0000	
Minimum G.T. Thickness	+0.0005	
Fuel Tolerances, statistically combined		± 0.0073
Rack Tolerances		
Cell ID/Pitch	±0.0016	
Wall Thickness	±0.0003	
Sheathing Thkns	±0.0001	
Poison Thickness	±0.0001	
Poison Loading	±0.0025	
Rack Tolerances, statistically combined		± 0.0029
Statistical Combination of Uncertainties[2]		± 0.0127
Reference k_{eff} (MCNP4a)		0.9162
Total Uncertainty (above)		0.0127
Calculational Bias (see Appendix A)		0.0009
Temperature Bias		0.0046
Maximum k_{eff}		**0.9344**
Regulatory Limiting k_{eff}		**0.9500**

[2] Square root of the sum of the squares.

Table 4.4.1
PWR Fuel Assembly Specifications

Parameter	Value	
Assembly type	STD (LOPAR)	OFA (Vantage 5)
Rod Array Size	17x17	17x17
Rod Pitch, Inches	0.496 [redacted]	0.496 [redacted]
Active Fuel Length, Inches	144	144
Stack Density	95% [redacted] of theoretical (10.96 g/cm^3)	95% [redacted] of theoretical (10.96 g/cm^3)
Total Number of Fuel Rods	264	264
Fuel Rod Outer Diameter, Inches	0.374 [redacted]	0.360 [redacted]
Fuel Rod Inner Diameter, Inches	0.329 [redacted]	0.315 [redacted]
Minimum Cladding Thickness, Inches	[redacted]	[redacted]
Cladding Material	Zr-4	Zr-4 or Zirlo
Pellet Diameter, Inches	0.3225 [redacted]	0.3088 [redacted]
Number of Guide/Instrument Tubes	24/1	24/1
Guide Tube Outer Diameter, Inches	0.482 [redacted]	0.474 [redacted]
Guide Tube Inner Diameter, Inches	0.450 [redacted]	0.442 [redacted]
Guide Tube Minimum Wall Thickness, Inches	[redacted]	[redacted]
Guide Tube Material	Zr-4	Zr-4 or Zirlo

Table 4.4.2
Core Operating Parameter for Depletion Analyses

Parameter	Value
Soluble Boron Concentration (cycle average), ppm	820
Average Linear Power, W/ft	5450
Average Fuel Temperature, °F	1310
Average Core Exit Temperature, °F	614.8
In-Core Assembly Pitch, Inches	8.466

Table 4.4.3
BPRA Design Specifications (based on [4.11] except for burnup)

Parameter	Value
Boron Loading	0.0062 g B-10/cm
Outer Clad OD (cm)	0.96774
Outer Clad ID (cm)	0.87376
Poison OD (cm)	0.85344
Poison ID (cm)	0.48260
Inner Clad OD (cm)	0.46101
Inner Clad ID (cm)	0.42799
Assembly Burnup when Absorber is removed, GWD/MTU	22

Table 4.4.4
Fuel Rack Specifications

Parameter	Value
Cell ID, Inches	8.75 [redacted] (8.85 on some peripheral cells, see text)
Box Wall Thickness, Inches	0.09 [redacted]
Sheathing Thickness, Inches	[redacted]
Poison Pocket Thickness, Inches	[redacted]
Poison Thickness, Inches	[redacted]
Poison Width, Inches	7.5 min. (7.0 min on rack exterior, see text)
Cell Pitch, Inches	8.946 [redacted]
Poison Loading, gm B-10/cm^2	[redacted]

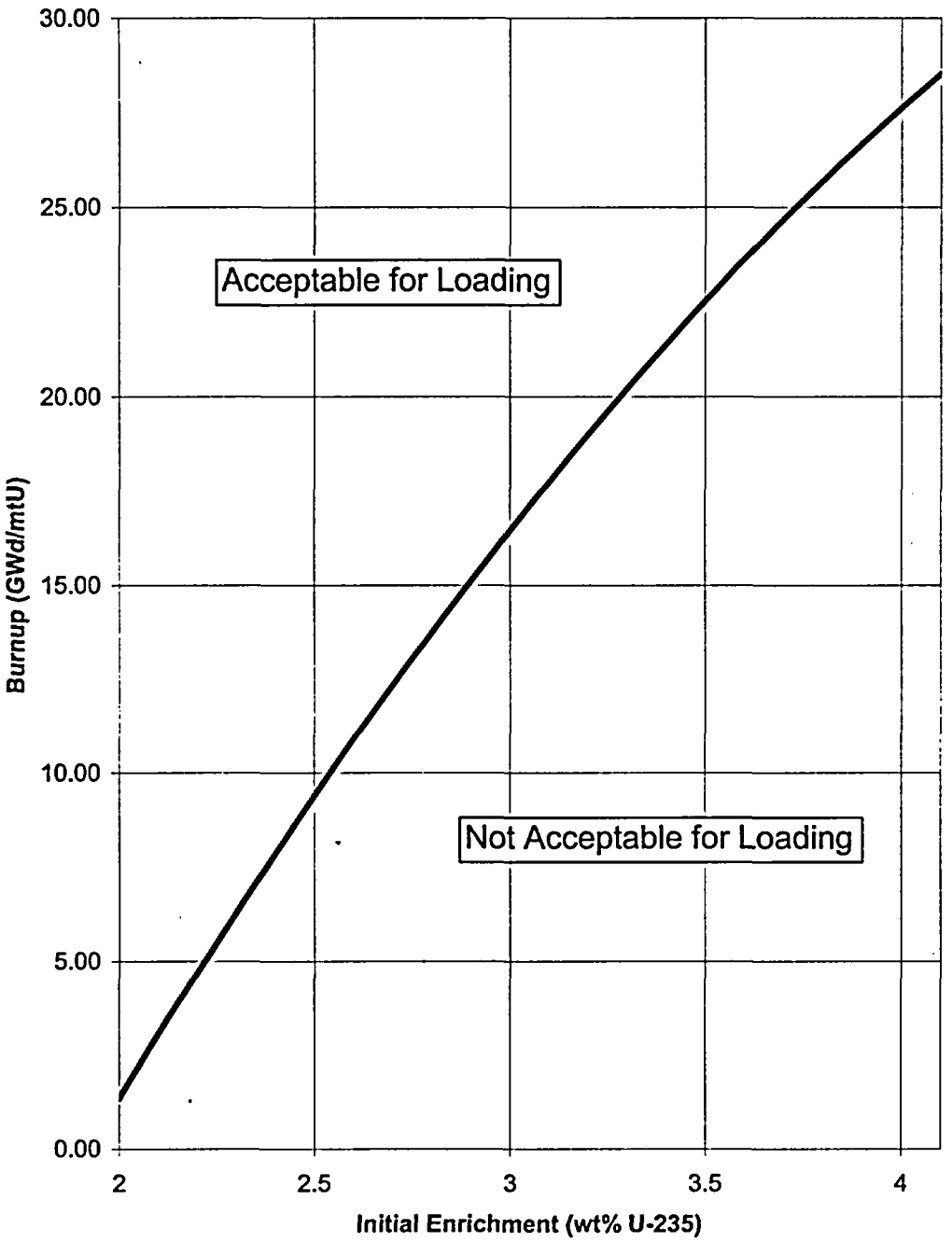

Figure 4.1.1: Cask Pit Rack Loading Curve

Appendix 4A

Benchmark Calculations

(total number of pages: 26 including this page)

APPENDIX 4A: BENCHMARK CALCULATIONS

4A.1 INTRODUCTION AND SUMMARY

Benchmark calculations have been made on selected critical experiments, chosen, in so far as possible, to bound the range of variables in the rack designs. Two independent methods of analysis were used, differing in cross section libraries and in the treatment of the cross sections. MCNP4a [4A.1] is a continuous energy Monte Carlo code and KENO5a [4A.2] uses group-dependent cross sections. For the KENO5a analyses reported here, the 238-group library was chosen, processed through the NITAWL-II [4A.2] program to create a working library and to account for resonance self-shielding in uranium-238 (Nordheim integral treatment). The 238 group library was chosen to avoid or minimize the errors† (trends) that have been reported (e.g., [4A.3 through 4A.5]) for calculations with collapsed cross section sets.

In rack designs, the three most significant parameters affecting criticality are (1) the fuel enrichment, (2) the ^{10}B loading in the neutron absorber, and (3) the lattice spacing (or water-gap thickness if a flux-trap design is used). Other parameters, within the normal range of rack and fuel designs, have a smaller effect, but are also included in the analyses.

Table 4A.1 summarizes results of the benchmark calculations for all cases selected and analyzed, as referenced in the table. The effect of the major variables are discussed in subsequent sections below. It is important to note that there is obviously considerable overlap in parameters since it is not possible to vary a single parameter and maintain criticality; some other parameter or parameters must be concurrently varied to maintain criticality.

One possible way of representing the data is through a spectrum index that incorporates all of the variations in parameters. KENO5a computes and prints the "energy of the average lethargy causing fission" (EALF). In MCNP4a, by utilizing the tally option with the identical 238-group energy structure as in KENO5a, the number of fissions in each group may be collected and the EALF determined (post-processing).

---

† Small but observable trends (errors) have been reported for calculations with the 27-group and 44-group collapsed libraries. These errors are probably due to the use of a single collapsing spectrum when the spectrum should be different for the various cases analyzed, as evidenced by the spectrum indices.

Figures 4A.1 and 4A.2 show the calculated k_{eff} for the benchmark critical experiments as a function of the EALF for MCNP4a and KENO5a, respectively (UO_2 fuel only). The scatter in the data (even for comparatively minor variation in critical parameters) represents experimental error† in performing the critical experiments within each laboratory, as well as between the various testing laboratories. The B&W critical experiments show a larger experimental error than the PNL criticals. This would be expected since the B&W criticals encompass a greater range of critical parameters than the PNL criticals.

Linear regression analysis of the data in Figures 4A.1 and 4A.2 show that there are no trends, as evidenced by very low values of the correlation coefficient (0.13 for MCNP4a and 0.21 for KENO5a). The total bias (systematic error, or mean of the deviation from a k_{eff} of exactly 1.000) for the two methods of analysis are shown in the table below.

Calculational Bias of MCNP4a and KENO5a	
MCNP4a	0.0009 ± 0.0011
KENO5a	0.0030 ± 0.0012

The bias and standard error of the bias were derived directly from the calculated k_{eff} values in Table 4A.1 using the following equations††, with the standard error multiplied by the one-sided K-factor for 95% probability at the 95% confidence level from NBS Handbook 91 [4A.18] (for the number of cases analyzed, the K-factor is ~2.05 or slightly more than 2).

$$\bar{k} = \frac{1}{n} \sum_{i}^{n} k_i \qquad (4A.1)$$

† A classical example of experimental error is the corrected enrichment in the PNL experiments, first as an addendum to the initial report and, secondly, by revised values in subsequent reports for the same fuel rods.

†† These equations may be found in any standard text on statistics, for example, reference [4A.6] (or the MCNP4a manual) and is the same methodology used in MCNP4a and in KENO5a.

$$\sigma_{\bar{k}}^2 = \frac{\sum_{i=1}^{n} k_i^2 - (\sum_{i=1}^{n} k_i)^2 / n}{n\,(n-1)} \qquad (4A.2)$$

$$Bias = (1 - \bar{k}) \pm K\,\sigma_{\bar{k}} \qquad (4A.3)$$

where k_i are the calculated reactivities of n critical experiments; $\sigma_{\bar{k}}$ is the unbiased estimator of the standard deviation of the mean (also called the standard error of the bias (mean)); K is the one-sided multiplier for 95% probability at the 95% confidence level (NBS Handbook 91 [4A.18]).

Formula 4.A.3 is based on the methodology of the National Bureau of Standards (now NIST) and is used to calculate the values presented on page 4.A-2. The first portion of the equation, (1- $\bar{k}$), is the actual bias which is added to the MCNP4a and KENO5a results. The second term, $K\sigma_{\bar{k}}$, is the uncertainty or standard error associated with the bias. The K values used were obtained from the National Bureau of Standards Handbook 91 and are for one-sided statistical tolerance limits for 95% probability at the 95% confidence level. The actual K values for the 56 critical experiments evaluated with MCNP4a and the 53 critical experiments evaluated with KENO5a are 2.04 and 2.05, respectively.

The bias values are used to evaluate the maximum k_{eff} values for the rack designs. KENO5a has a slightly larger systematic error than MCNP4a, but both result in greater precision than published data [4A.3 through 4A.5] would indicate for collapsed cross section sets in KENO5a (SCALE) calculations.

4A.2 Effect of Enrichment

The benchmark critical experiments include those with enrichments ranging from 2.46 w/o to 5.74 w/o and therefore span the enrichment range for rack designs. Figures 4A.3 and 4A.4 show the calculated k_{eff} values (Table 4A.1) as a function of the fuel enrichment reported for the critical experiments. Linear regression analyses for these data confirms that there are no trends, as indicated by low values of the correlation coefficients (0.03 for MCNP4a and 0.38 for KENO5a). Thus, there are no corrections to the bias for the various enrichments.

As further confirmation of the absence of any trends with enrichment, a typical configuration was calculated with both MCNP4a and KENO5a for various enrichments. The cross-comparison of calculations with codes of comparable sophistication is suggested in Reg. Guide 3.41. Results of this comparison, shown in Table 4A.2 and Figure 4A.5, confirm no significant difference in the calculated values of k_{eff} for the two independent codes as evidenced by the 45° slope of the curve. Since it is very unlikely that two independent methods of analysis would be subject to the same error, this comparison is considered confirmation of the absence of an enrichment effect (trend) in the bias.

4A.3 Effect of ^{10}B Loading

Several laboratories have performed critical experiments with a variety of thin absorber panels similar to the Boral panels in the rack designs. Of these critical experiments, those performed by B&W are the most representative of the rack designs. PNL has also made some measurements with absorber plates, but, with one exception (a flux-trap experiment), the reactivity worth of the absorbers in the PNL tests is very low and any significant errors that might exist in the treatment of strong thin absorbers could not be revealed.

Table 4A.3 lists the subset of experiments using thin neutron absorbers (from Table 4A.1) and shows the reactivity worth (Δk) of the absorber.†

No trends with reactivity worth of the absorber are evident, although based on the calculations shown in Table 4A.3, some of the B&W critical experiments seem to have unusually large experimental errors. B&W made an effort to report some of their experimental errors. Other laboratories did not evaluate their experimental errors.

To further confirm the absence of a significant trend with ^{10}B concentration in the absorber, a cross-comparison was made with MCNP4a and KENO5a (as suggested in Reg. Guide 3.41). Results are shown in Figure 4A.6 and Table 4A.4 for a typical geometry. These data substantiate the absence of any error (trend) in either of the two codes for the conditions analyzed (data points fall on a 45° line, within an expected 95% probability limit).

† The reactivity worth of the absorber panels was determined by repeating the calculation with the absorber analytically removed and calculating the incremental (Δk) change in reactivity due to the absorber.

4A.4 Miscellaneous and Minor Parameters

4A.4.1 Reflector Material and Spacings

PNL has performed a number of critical experiments with thick steel and lead reflectors.† Analysis of these critical experiments are listed in Table 4A.5 (subset of data in Table 4A.1). There appears to be a small tendency toward overprediction of k_{eff} at the lower spacing, although there are an insufficient number of data points in each series to allow a quantitative determination of any trends. The tendency toward overprediction at close spacing means that the rack calculations may be slightly more conservative than otherwise.

4A.4.2 Fuel Pellet Diameter and Lattice Pitch

The critical experiments selected for analysis cover a range of fuel pellet diameters from 0.311 to 0.444 inches, and lattice spacings from 0.476 to 1.00 inches. In the rack designs, the fuel pellet diameters range from 0.303 to 0.3805 inches O.D. (0.496 to 0.580 inch lattice spacing) for PWR fuel and from 0.3224 to 0.494 inches O.D. (0.488 to 0.740 inch lattice spacing) for BWR fuel. Thus, the critical experiments analyzed provide a reasonable representation of power reactor fuel. Based on the data in Table 4A.1, there does not appear to be any observable trend with either fuel pellet diameter or lattice pitch, at least over the range of the critical experiments applicable to rack designs.

4A.4.3 Soluble Boron Concentration Effects

Various soluble boron concentrations were used in the B&W series of critical experiments and in one PNL experiment, with boron concentrations ranging up to 2550 ppm. Results of MCNP4a (and one KENO5a) calculations are shown in Table 4A.6. Analyses of the very high boron concentration experiments (> 1300 ppm) show a tendency to slightly overpredict reactivity for the three experiments exceeding 1300 ppm. In turn, this would suggest that the evaluation of the racks with higher soluble boron concentrations could be slightly conservative.

---

† Parallel experiments with a depleted uranium reflector were also performed but not included in the present analysis since they are not pertinent to the Holtec rack design.

4A.5 MOX Fuel

The number of critical experiments with PuO_2 bearing fuel (MOX) is more limited than for UO_2 fuel. However, a number of MOX critical experiments have been analyzed and the results are shown in Table 4A.7. Results of these analyses are generally above a k_{eff} of 1.00, indicating that when Pu is present, both MCNP4a and KENO5a overpredict the reactivity. This may indicate that calculation for MOX fuel will be expected to be conservative, especially with MCNP4a. It may be noted that for the larger lattice spacings, the KENO5a calculated reactivities are below 1.00, suggesting that a small trend may exist with KENO5a. It is also possible that the overprediction in k_{eff} for both codes may be due to a small inadequacy in the determination of the Pu-241 decay and Am-241 growth. This possibility is supported by the consistency in calculated k_{eff} over a wide range of the spectral index (energy of the average lethargy causing fission).

4A.6 References

[4A.1] J.F. Briesmeister, Ed., "MCNP4a - A General Monte Carlo N-Particle Transport Code, Version 4A; Los Alamos National Laboratory, LA-12625-M (1993).

[4A.2] SCALE 4.3, "A Modular Code System for Performing Standardized Computer Analyses for Licensing Evaluation", NUREG-0200 (ORNL-NUREG-CSD-2/U2/R5, Revision 5, Oak Ridge National Laboratory, September 1995.

[4A.3] M.D. DeHart and S.M. Bowman, "Validation of the SCALE Broad Structure 44-G Group ENDF/B-Y Cross-Section Library for Use in Criticality Safety Analyses", NUREG/CR-6102 (ORNL/TM-12460) Oak Ridge National Laboratory, September 1994.

[4A.4] W.C. Jordan et al., "Validation of KENOV.a", CSD/TM-238, Martin Marietta Energy Systems, Inc., Oak Ridge National Laboratory, December 1986.

[4A.5] O.W. Hermann et al., "Validation of the Scale System for PWR Spent Fuel Isotopic Composition Analysis", ORNL-TM-12667, Oak Ridge National Laboratory, undated.

[4A.6] R.J. Larsen and M.L. Marx, An Introduction to Mathematical Statistics and its Applications, Prentice-Hall, 1986.

[4A.7] M.N. Baldwin et al., Critical Experiments Supporting Close Proximity Water Storage of Power Reactor Fuel, BAW-1484-7, Babcock and Wilcox Company, July 1979.

[4A.8] G.S. Hoovier et al., Critical Experiments Supporting Underwater Storage of Tightly Packed Configurations of Spent Fuel Pins, BAW-1645-4, Babcock & Wilcox Company, November 1991.

[4A.9] L.W. Newman et al., Urania Gadolinia: Nuclear Model Development and Critical Experiment Benchmark, BAW-1810, Babcock and Wilcox Company, April 1984.

[4A.10] J.C. Manaranche et al., "Dissolution and Storage Experimental Program with 4.75 w/o Enriched Uranium-Oxide Rods," Trans. Am. Nucl. Soc. 33: 362-364 (1979).

[4A.11] S.R. Bierman and E.D. Clayton, Criticality Experiments with Subcritical Clusters of 2.35 w/o and 4.31 w/o ^{235}U Enriched UO_2 Rods in Water with Steel Reflecting Walls, PNL-3602, Battelle Pacific Northwest Laboratory, April 1981.

[4A.12] S.R. Bierman et al., Criticality Experiments with Subcritical Clusters of 2.35 w/o and 4.31 w/o ^{235}U Enriched UO_2 Rods in Water with Uranium or Lead Reflecting Walls, PNL-3926, Battelle Pacific Northwest Laboratory, December, 1981.

[4A.13] S.R. Bierman et al., Critical Separation Between Subcritical Clusters of 4.31 w/o ^{235}U Enriched UO_2 Rods in Water with Fixed Neutron Poisons, PNL-2615, Battelle Pacific Northwest Laboratory, October 1977.

[4A.14] S.R. Bierman, Criticality Experiments with Neutron Flux Traps Containing Voids, PNL-7167, Battelle Pacific Northwest Laboratory, April 1990.

[4A.15] B.M. Durst et al., Critical Experiments with 4.31 wt % ^{235}U Enriched UO_2 Rods in Highly Borated Water Lattices, PNL-4267, Battelle Pacific Northwest Laboratory, August 1982.

[4A.16] S.R. Bierman, Criticality Experiments with Fast Test Reactor Fuel Pins in Organic Moderator, PNL-5803, Battelle Pacific Northwest Laboratory, December 1981.

[4A.17] E.G. Taylor et al., Saxton Plutonium Program Critical Experiments for the Saxton Partial Plutonium Core, WCAP-3385-54, Westinghouse Electric Corp., Atomic Power Division, December 1965.

[4A.18] M.G. Natrella, Experimental Statistics, National Bureau of Standards, Handbook 91, August 1963.

Table 4A.1

Summary of Criticality Benchmark Calculations

	Reference	Identification	Enrich.	Calculated k_{eff}		EALF † (eV)	
				MCNP4a	KENO5a	MCNP4a	KENO5a
1	B&W-1484 (4A.7)	Core I	2.46	0.9964 ± 0.0010	0.9898± 0.0006	0.1759	0.1753
2	B&W-1484 (4A.7)	Core II	2.46	1.0008 ± 0.0011	1.0015 ± 0.0005	0.2553	0.2446
3	B&W-1484 (4A.7)	Core III	2.46	1.0010 ± 0.0012	1.0005 ± 0.0005	0.1999	0.1939
4	B&W-1484 (4A.7)	Core IX	2.46	0.9956 ± 0.0012	0.9901 ± 0.0006	0.1422	0.1426
5	B&W-1484 (4A.7)	Core X	2.46	0.9980 ± 0.0014	0.9922 ± 0.0006	0.1513	0.1499
6	B&W-1484 (4A.7)	Core XI	2.46	0.9978 ± 0.0012	1.0005 ± 0.0005	0.2031	0.1947
7	B&W-1484 (4A.7)	Core XII	2.46	0.9988 ± 0.0011	0.9978 ± 0.0006	0.1718	0.1662
8	B&W-1484 (4A.7)	Core XIII	2.46	1.0020 ± 0.0010	0.9952 ± 0.0006	0.1988	0.1965
9	B&W-1484 (4A.7)	Core XIV	2.46	0.9953 ± 0.0011	0.9928 ± 0.0006	0.2022	0.1986
10	B&W-1484 (4A.7)	Core XV ††	2.46	0.9910 ± 0.0011	0.9909 ± 0.0006	0.2092	0.2014
11	B&W-1484 (4A.7)	Core XVI ††	2.46	0.9935 ± 0.0010	0.9889 ± 0.0006	0.1757	0.1713
12	B&W-1484 (4A.7)	Core XVII	2.46	0.9962 ± 0.0012	0.9942 ± 0.0005	0.2083	0.2021
13	B&W-1484 (4A.7)	Core XVIII	2.46	1.0036 ± 0.0012	0.9931 ± 0.0006	0.1705	0.1708

Table 4A.1

Summary of Criticality Benchmark Calculations

	Reference	Identification	Enrich.	Calculated k_{eff}		EALF † (eV)	
				MCNP4a	KENO5a	MCNP4a	KENO5a
14	B&W-1484 (4A.7)	Core XIX	2.46	0.9961 ± 0.0012	0.9971 ± 0.0005	0.2103	0.2011
15	B&W-1484 (4A.7)	Core XX	2.46	1.0008 ± 0.0011	0.9932 ± 0.0006	0.1724	0.1701
16	B&W-1484 (4A.7)	Core XXI	2.46	0.9994 ± 0.0010	0.9918 ± 0.0006	0.1544	0.1536
17	B&W-1645 (4A.8)	S-type Fuel, w/886 ppm B	2.46	0.9970 ± 0.0010	0.9924 ± 0.0006	1.4475	1.4680
18	B&W-1645 (4A.8)	S-type Fuel, w/746 ppm B	2.46	0.9990 ± 0.0010	0.9913 ± 0.0006	1.5463	1.5660
19	B&W-1645 (4A.8)	SO-type Fuel, w/1156 ppm B	2.46	0.9972 ± 0.0009	0.9949 ± 0.0005	0.4241	0.4331
20	B&W-1810 (4A.9)	Case 1 1337 ppm B	2.46	1.0023 ± 0.0010	NC	0.1531	NC
21	B&W-1810 (4A.9)	Case 12 1899 ppm B	2.46/4.02	1.0060 ± 0.0009	NC	0.4493	NC
22	French (4A.10)	Water Moderator 0 gap	4.75	0.9966 ± 0.0013	NC	0.2172	NC
23	French (4A.10)	Water Moderator 2.5 cm gap	4.75	0.9952 ± 0.0012	NC	0.1778	NC
24	French (4A.10)	Water Moderator 5 cm gap	4.75	0.9943 ± 0.0010	NC	0.1677	NC
25	French (4A.10)	Water Moderator 10 cm gap	4.75	0.9979 ± 0.0010	NC	0.1736	NC
26	PNL-3602 (4A.11)	Steel Reflector, 0 separation	2.35	NC	1.0004 ± 0.0006	NC	0.1018

Table 4A.1

Summary of Criticality Benchmark Calculations

	Reference	Identification	Enrich.	Calculated k_{eff}		EALF † (eV)	
				MCNP4a	KENO5a	MCNP4a	KENO5a
27	PNL-3602 (4A.11)	Steel Reflector, 1.321 cm sepn.	2.35	0.9980 ± 0.0009	0.9992 ± 0.0006	0.1000	0.0909
28	PNL-3602 (4A.11)	Steel Reflector, 2.616 cm sepn	2.35	0.9968 ± 0.0009	0.9964 ± 0.0006	0.0981	0.0975
29	PNL-3602 (4A.11)	Steel Reflector, 3.912 cm sepn.	2.35	0.9974 ± 0.0010	0.9980 ± 0.0006	0.0976	0.0970
30	PNL-3602 (4A.11)	Steel Reflector, infinite sepn.	2.35	0.9962 ± 0.0008	0.9939 ± 0.0006	0.0973	0.0968
31	PNL-3602 (4A.11)	Steel Reflector, 0 cm sepn.	4.306	NC	1.0003 ± 0.0007	NC	0.3282
32	PNL-3602 (4A.11)	Steel Reflector, 1.321 cm sepn.	4.306	0.9997 ± 0.0010	1.0012 ± 0.0007	0.3016	0.3039
33	PNL-3602 (4A.11)	Steel Reflector, 2.616 cm sepn.	4.306	0.9994 ± 0.0012	0.9974 ± 0.0007	0.2911	0.2927
34	PNL-3602 (4A.11)	Steel Reflector, 5.405 cm sepn.	4.306	0.9969 ± 0.0011	0.9951 ± 0.0007	0.2828	0.2860
35	PNL-3602 (4A.11)	Steel Reflector, Infinite sepn. ††	4.306	0.9910 ± 0.0020	0.9947 ± 0.0007	0.2851	0.2864
36	PNL-3602 (4A.11)	Steel Reflector, with Boral Sheets	4.306	0.9941 ± 0.0011	0.9970 ± 0.0007	0.3135	0.3150
37	PNL-3926 (4A.12)	Lead Reflector, 0 cm sepn.	4.306	NC	1.0003 ± 0.0007	NC	0.3159
38	PNL-3926 (4A.12)	Lead Reflector, 0.55 cm sepn.	4.306	1.0025 ± 0.0011	0.9997 ± 0.0007	0.3030	0.3044
39	PNL-3926 (4A.12)	Lead Reflector, 1.956 cm sepn.	4.306	1.0000 ± 0.0012	0.9985 ± 0.0007	0.2883	0.2930

Table 4A.1

Summary of Criticality Benchmark Calculations

	Reference	Identification	Enrich.	Calculated k_{eff}		EALF † (eV)	
				MCNP4a	KENO5a	MCNP4a	KENO5a
40	PNL-3926 (4A.12)	Lead Reflector, 5.405 cm sepn.	4.306	0.9971 ± 0.0012	0.9946 ± 0.0007	0.2831	0.2854
41	PNL-2615 (4A.13)	Experiment 004/032 - no absorber	4.306	0.9925 ± 0.0012	0.9950 ± 0.0007	0.1155	0.1159
42	PNL-2615 (4A.13)	Experiment 030 - Zr plates	4.306	NC	0.9971 ± 0.0007	NC	0.1154
43	PNL-2615 (4A.13)	Experiment 013 - Steel plates	4.306	NC	0.9965 ± 0.0007	NC	0.1164
44	PNL-2615 (4A.13)	Experiment 014 - Steel plates	4.306	NC	0.9972 ± 0.0007	NC	0.1164
45	PNL-2615 (4A.13)	Exp. 009 1.05% Boron-Steel plates	4.306	0.9982 ± 0.0010	0.9981 ± 0.0007	0.1172	0.1162
46	PNL-2615 (4A.13)	Exp. 012 1.62% Boron-Steel plates	4.306	0.9996 ± 0.0012	0.9982 ± 0.0007	0.1161	0.1173
47	PNL-2615 (4A.13)	Exp. 031 - Boral plates	4.306	0.9994 ± 0.0012	0.9969 ± 0.0007	0.1165	0.1171
48	PNL-7167 (4A.14)	Experiment 214R - with flux trap	4.306	0.9991 ± 0.0011	0.9956 ± 0.0007	0.3722	0.3812
49	PNL-7167 (4A.14)	Experiment 214V3 - with flux trap	4.306	0.9969 ± 0.0011	0.9963 ± 0.0007	0.3742	0.3826
50	PNL-4267 (4A.15)	Case 173 - 0 ppm B	4.306	0.9974 ± 0.0012	NC	0.2893	NC
51	PNL-4267 (4A.15)	Case 177 - 2550 ppm B	4.306	1.0057 ± 0.0010	NC	0.5509	NC
52	PNL-5803 (4A.16)	MOX Fuel - Type 3.2 Exp. 21	20% Pu	1.0041 ± 0.0011	1.0046 ± 0.0006	0.9171	0.8868

Table 4A.1

Summary of Criticality Benchmark Calculations

	Reference	Identification	Enrich.	Calculated k_{eff}		EALF† (eV)	
				MCNP4a	KENO5a	MCNP4a	KENO5a
53	PNL-5803 (4A.16)	MOX Fuel - Type 3.2 Exp. 43	20% Pu	1.0058 ± 0.0012	1.0036 ± 0.0006	0.2968	0.2944
54	PNL-5803 (4A.16)	MOX Fuel - Type 3.2 Exp. 13	20% Pu	1.0083 ± 0.0011	0.9989 ± 0.0006	0.1665	0.1706
55	PNL-5803 (4A.16)	MOX Fuel - Type 3.2 Exp. 32	20% Pu	1.0079 ± 0.0011	0.9966 ± 0.0006	0.1139	0.1165
56	WCAP-3385 (4A.17)	Saxton Case 52 PuO2 0.52" pitch	6.6% Pu	0.9996 ± 0.0011	1.0005 ± 0.0006	0.8665	0.8417
57	WCAP-3385 (4A.17)	Saxton Case 52 U 0.52" pitch	5.74	1.0000 ± 0.0010	0.9956 ± 0.0007	0.4476	0.4580
58	WCAP-3385 (4A.17)	Saxton Case 56 PuO2 0.56" pitch	6.6% Pu	1.0036 ± 0.0011	1.0047 ± 0.0006	0.5289	0.5197
59	WCAP-3385 (4A.17)	Saxton Case 56 borated PuO2	6.6% Pu	1.0008 ± 0.0010	NC	0.6389	NC
60	WCAP-3385 (4A.17)	Saxton Case 56 U 0.56" pitch	5.74	0.9994 ± 0.0011	0.9967 ± 0.0007	0.2923	0.2954
61	WCAP-3385 (4A.17)	Saxton Case 79 PuO2 0.79" pitch	6.6% Pu	1.0063 ± 0.0011	1.0133 ± 0.0006	0.1520	0.1555
62	WCAP-3385 (4A.17)	Saxton Case 79 U 0.79" pitch	5.74	1.0039 ± 0.0011	1.0008 ± 0.0006	0.1036	0.1047

Notes: NC stands for not calculated.

† EALF is the energy of the average lethargy causing fission.

†† These experimental results appear to be statistical outliers ($>3\sigma$) suggesting the possibility of unusually large experimental error. Although they could justifiably be excluded, for conservatism, they were retained in determining the calculational basis.

Table 4A.2

COMPARISON OF MCNP4a AND KENO5a CALCULATED REACTIVITIES[†] FOR VARIOUS ENRICHMENTS

Enrichment	Calculated $k_{eff} \pm 1\sigma$	
	MCNP4a	KENO5a
3.0	0.8465 ± 0.0011	0.8478 ± 0.0004
3.5	0.8820 ± 0.0011	0.8841 ± 0.0004
3.75	0.9019 ± 0.0011	0.8987 ± 0.0004
4.0	0.9132 ± 0.0010	0.9140 ± 0.0004
4.2	0.9276 ± 0.0011	0.9237 ± 0.0004
4.5	0.9400 ± 0.0011	0.9388 ± 0.0004

† Based on the GE 8x8R fuel assembly.

Table 4A.3

MCNP4a CALCULATED REACTIVITIES FOR
CRITICAL EXPERIMENTS WITH NEUTRON ABSORBERS

Ref.	Experiment		Δk Worth of Absorber	MCNP4a Calculated k_{eff}	EALF † (eV)
4A.13	PNL-2615	Boral Sheet	0.0139	0.9994±0.0012	0.1165
4A.7	B&W-1484	Core XX	0.0165	1.0008±0.0011	0.1724
4A.13	PNL-2615	1.62% Boron-steel	0.0165	0.9996±0.0012	0.1161
4A.7	B&W-1484	Core XIX	0.0202	0.9961±0.0012	0.2103
4A.7	B&W-1484	Core XXI	0.0243	0.9994±0.0010	0.1544
4A.7	B&W-1484	Core XVII	0.0519	0.9962±0.0012	0.2083
4A.11	PNL-3602	Boral Sheet	0.0708	0.9941±0.0011	0.3135
4A.7	B&W-1484	Core XV	0.0786	0.9910±0.0011	0.2092
4A.7	B&W-1484	Core XVI	0.0845	0.9935±0.0010	0.1757
4A.7	B&W-1484	Core XIV	0.1575	0.9953±0.0011	0.2022
4A.7	B&W-1484	Core XIII	0.1738	1.0020±0.0011	0.1988
4A.14	PNL-7167	Expt 214R flux trap	0.1931	0.9991±0.0011	0.3722

†EALF is the energy of the average lethargy causing fission.

Table 4A.4

COMPARISON OF MCNP4a AND KENO5a
CALCULATED REACTIVITIES† FOR VARIOUS ^{10}B LOADINGS

^{10}B, g/cm^2	Calculated $k_{eff} \pm 1\sigma$	
	MCNP4a	KENO5a
0.005	1.0381 ± 0.0012	1.0340 ± 0.0004
0.010	0.9960 ± 0.0010	0.9941 ± 0.0004
0.015	0.9727 ± 0.0009	0.9713 ± 0.0004
0.020	0.9541 ± 0.0012	0.9560 ± 0.0004
0.025	0.9433 ± 0.0011	0.9428 ± 0.0004
0.03	0.9325 ± 0.0011	0.9338 ± 0.0004
0.035	0.9234 ± 0.0011	0.9251 ± 0.0004
0.04	0.9173 ± 0.0011	0.9179 ± 0.0004

† Based on a 4.5% enriched GE 8x8R fuel assembly.

Table 4A.5

CALCULATIONS FOR CRITICAL EXPERIMENTS WITH THICK LEAD AND STEEL REFLECTORS†

Ref.	Case	E, wt%	Separation, cm	MCNP4a k_{eff}	KENO5a k_{eff}
4A.11	Steel Reflector	2.35	1.321	0.9980±0.0009	0.9992±0.0006
		2.35	2.616	0.9968±0.0009	0.9964±0.0006
		2.35	3.912	0.9974±0.0010	0.9980±0.0006
		2.35	∞	0.9962±0.0008	0.9939±0.0006
4A.11	Steel Reflector	4.306	1.321	0.9997±0.0010	1.0012±0.0007
		4.306	2.616	0.9994±0.0012	0.9974±0.0007
		4.306	3.405	0.9969±0.0011	0.9951±0.0007
		4.306	∞	0.9910±0.0020	0.9947±0.0007
4A.12	Lead Reflector	4.306	0.55	1.0025±0.0011	0.9997±0.0007
		4.306	1.956	1.0000±0.0012	0.9985±0.0007
		4.306	5.405	0.9971±0.0012	0.9946±0.0007

† Arranged in order of increasing reflector-fuel spacing.

Table 4A.6

CALCULATIONS FOR CRITICAL EXPERIMENTS WITH VARIOUS SOLUBLE BORON CONCENTRATIONS

Reference	Experiment	Boron Concentration, ppm	Calculated k_{eff}	
			MCNP4a	KENO5a
4A.15	PNL-4267	0	0.9974 ± 0.0012	-
4A.8	B&W-1645	886	0.9970 ± 0.0010	0.9924 ± 0.0006
4A.9	B&W-1810	1337	1.0023 ± 0.0010	-
4A.9	B&W-1810	1899	1.0060 ± 0.0009	-
4A.15	PNL-4267	2550	1.0057 ± 0.0010	-

Table 4A.7

CALCULATIONS FOR CRITICAL EXPERIMENTS WITH MOX FUEL

Reference	Case†	MCNP4a		KENO5a	
		k_{eff}	EALF††	k_{eff}	EALF††
PNL-5803 [4A.16]	MOX Fuel - Exp. No. 21	1.0041±0.0011	0.9171	1.0046±0.0006	0.8868
	MOX Fuel - Exp. No. 43	1.0058±0.0012	0.2968	1.0036±0.0006	0.2944
	MOX Fuel - Exp. No. 13	1.0083±0.0011	0.1665	0.9989±0.0006	0.1706
	MOX Fuel - Exp. No. 32	1.0079±0.0011	0.1139	0.9966±0.0006	0.1165
WCAP-3385-54 [4A.17]	Saxton @ 0.52" pitch	0.9996±0.0011	0.8665	1.0005±0.0006	0.8417
	Saxton @ 0.56" pitch	1.0036±0.0011	0.5289	1.0047±0.0006	0.5197
	Saxton @ 0.56" pitch borated	1.0008±0.0010	0.6389	NC	NC
	Saxton @ 0.79" pitch	1.0063±0.0011	0.1520	1.0133±0.0006	0.1555

Note: NC stands for not calculated

† Arranged in order of increasing lattice spacing.

†† EALF is the energy of the average lethargy causing fission.

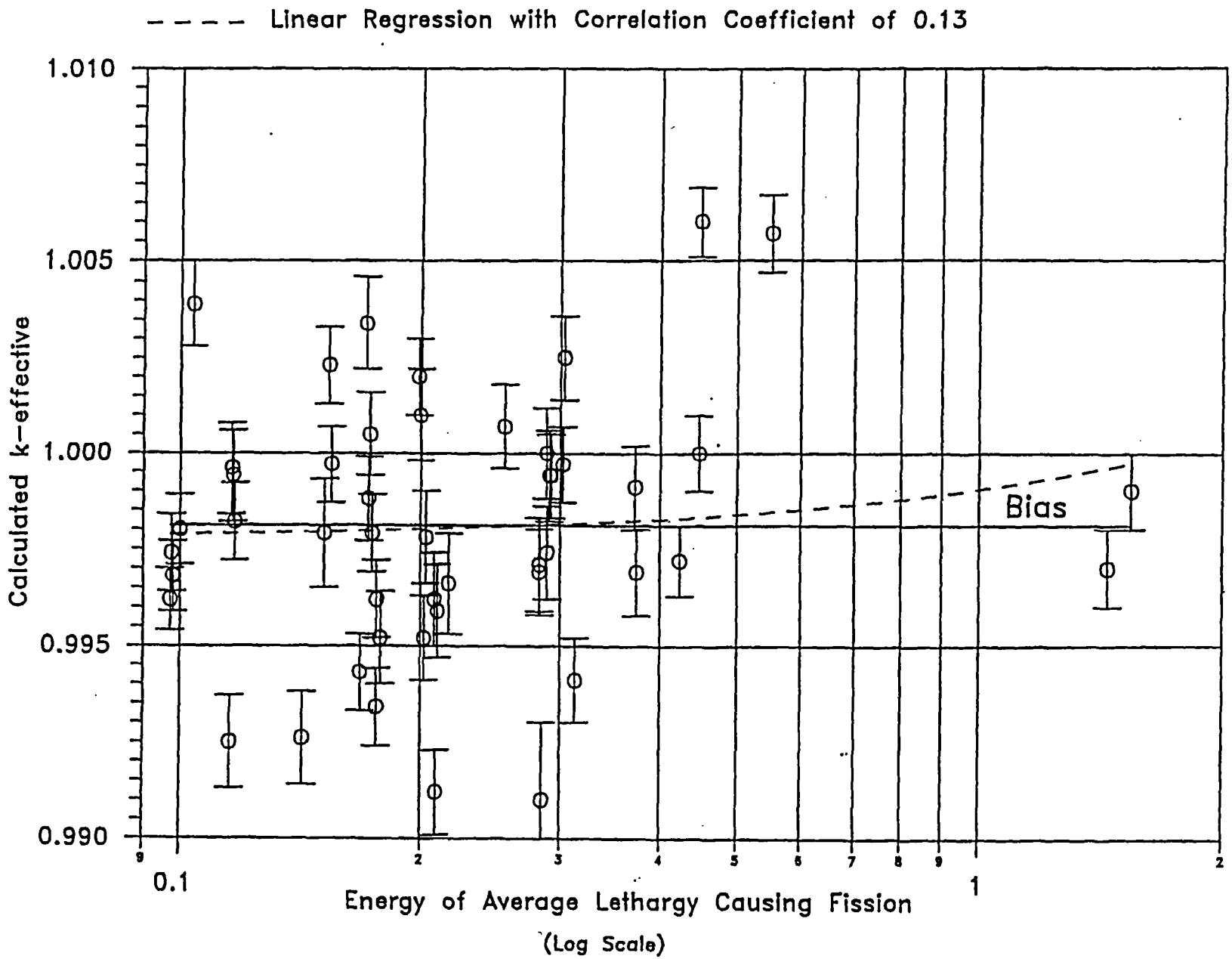

FIGURE 4A.1 MCNP CALCULATED k-eff VALUES for VARIOUS VALUES OF THE SPECTRAL INDEX

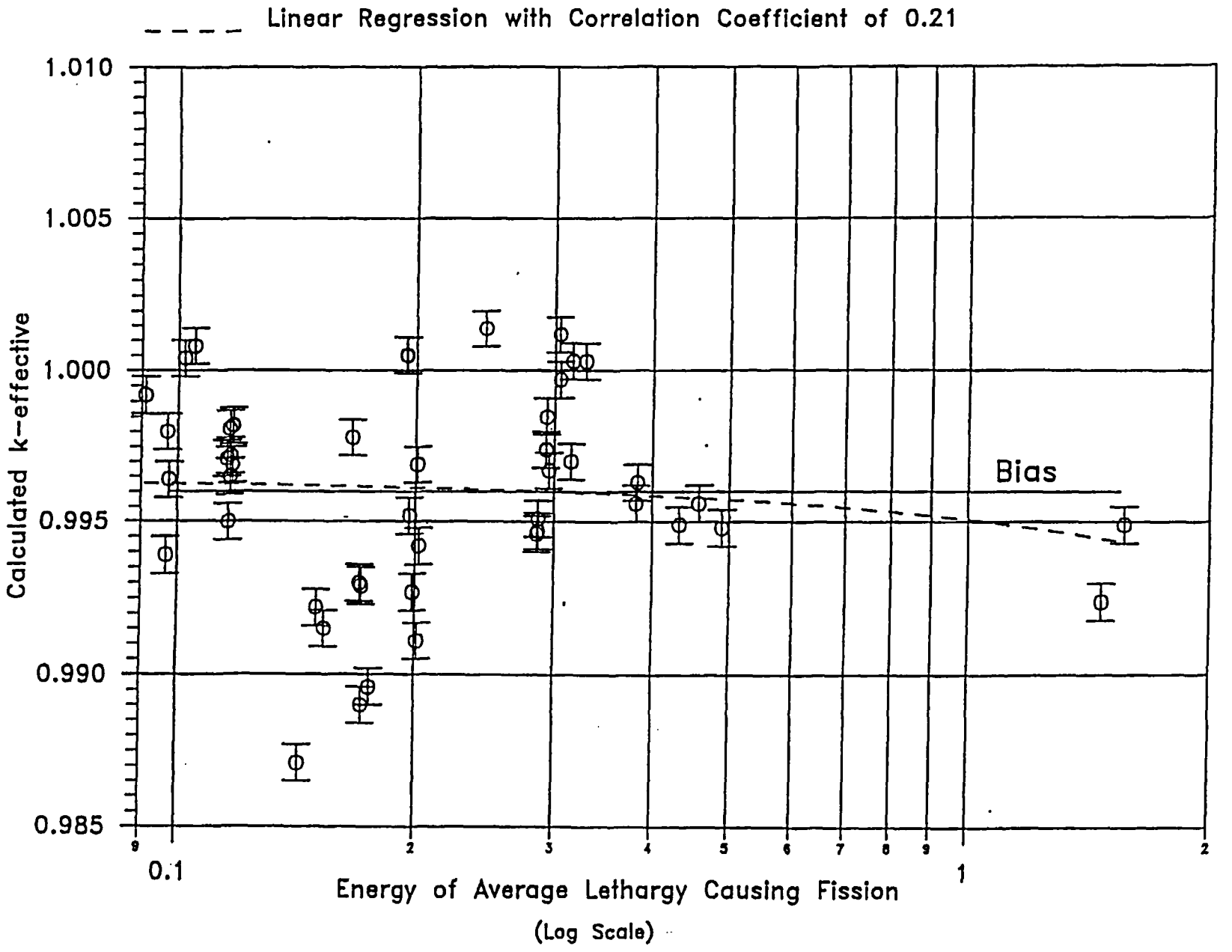

FIGURE 4A.2 KENO5a CALCULATED k-eff VALUES FOR VARIOUS VALUES OF THE SPECTRAL INDEX

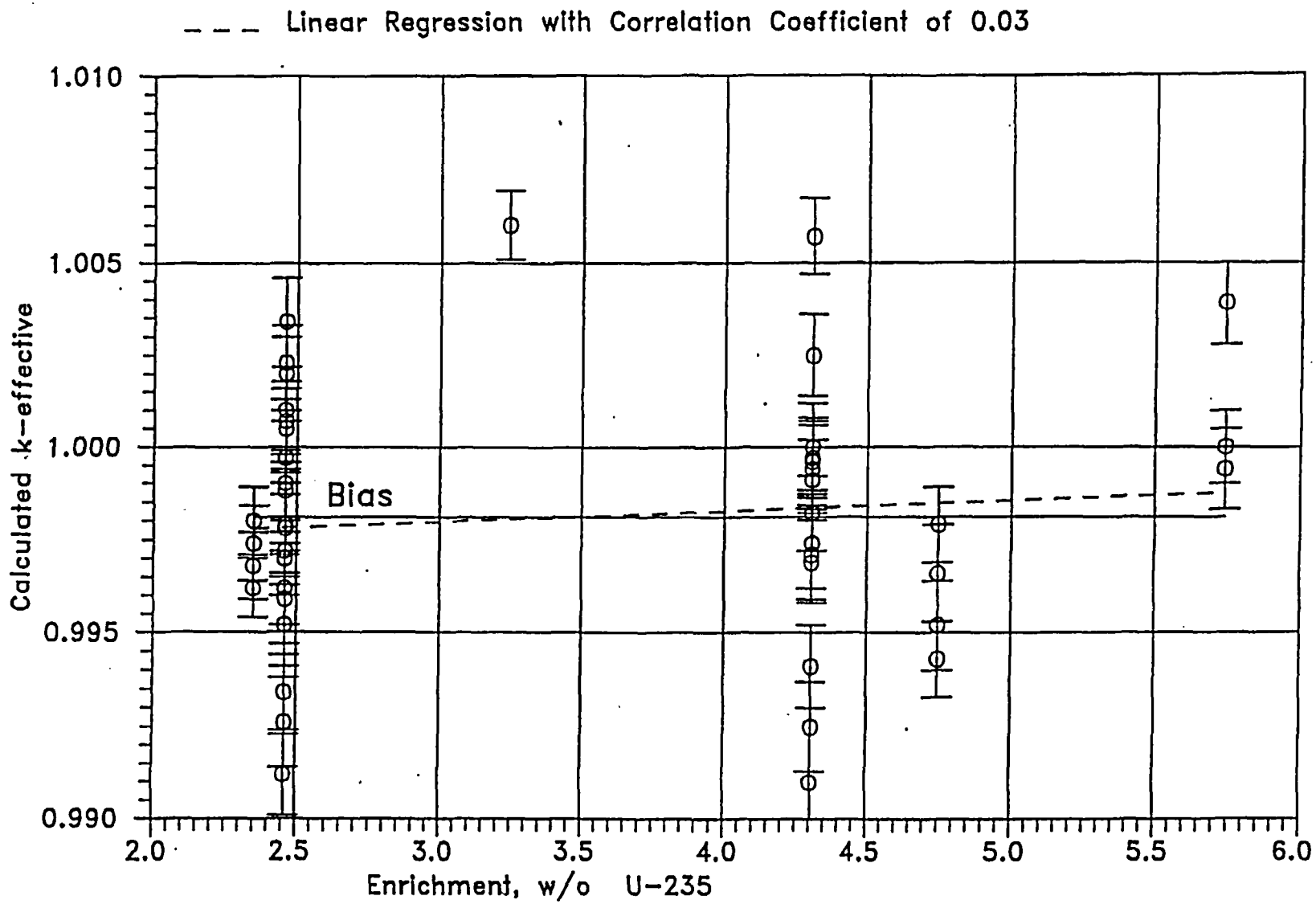

FIGURE 4A.3 MCNP CALCULATED k-eff VALUES AT VARIOUS U-235 ENRICHMENTS

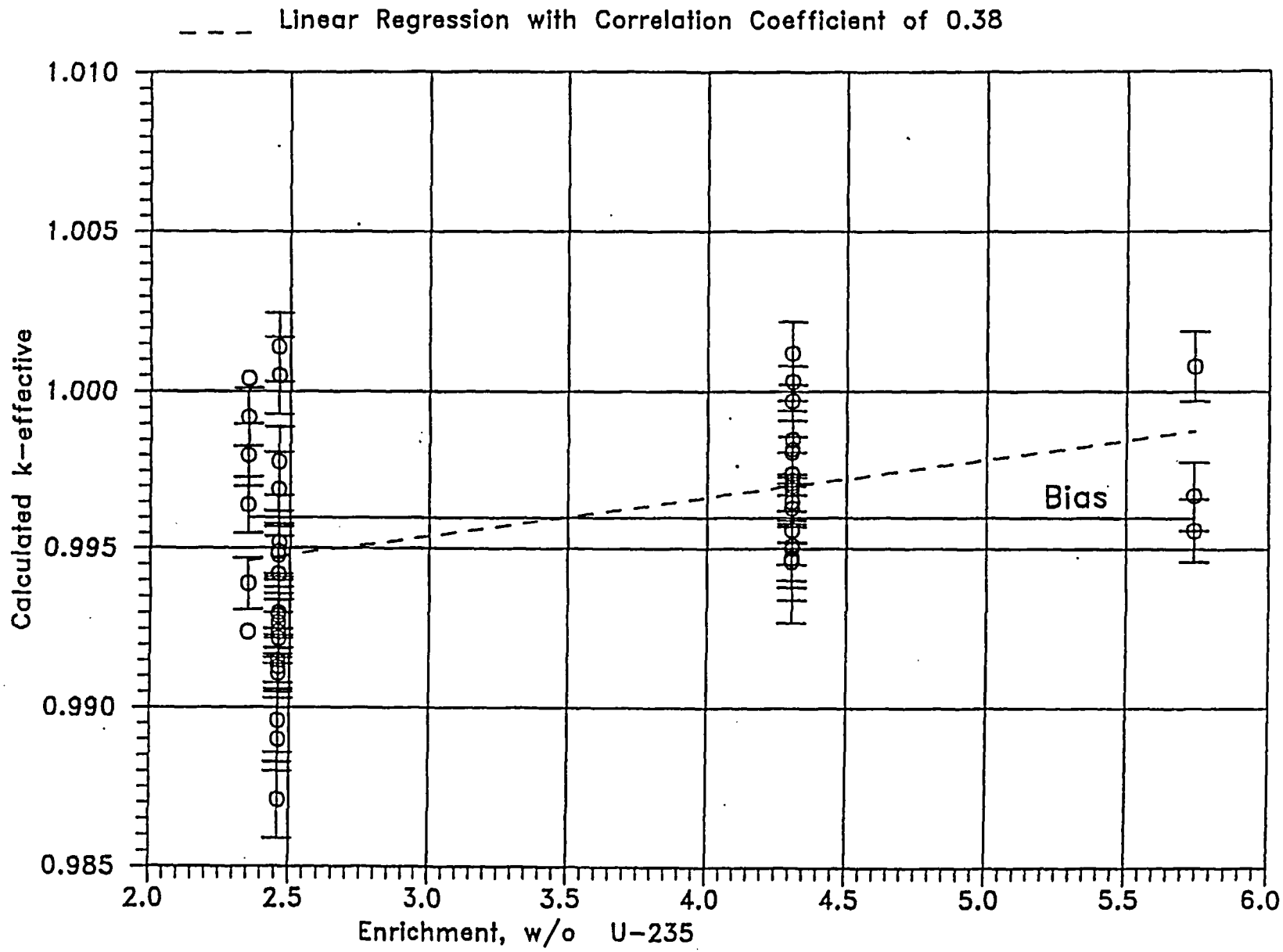

FIGURE 4A.4. KENO CALCULATED k-eff VALUES AT VARIOUS U-235 ENRICHMENTS

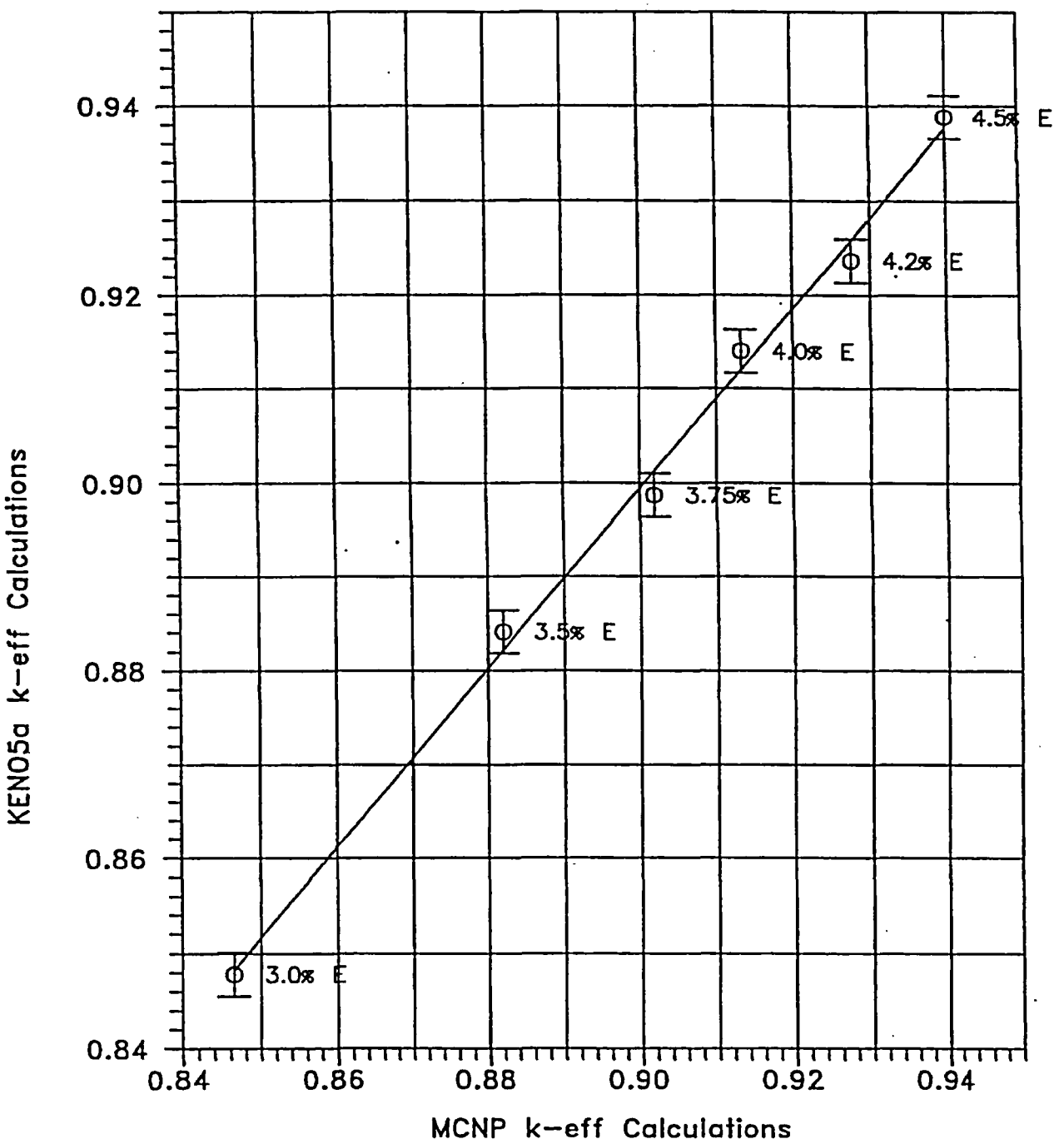

FIGURE 4A.5 COMPARISON OF MCNP AND KENO5A CALCULATIONS FOR VARIOUS FUEL ENRICHMENTS

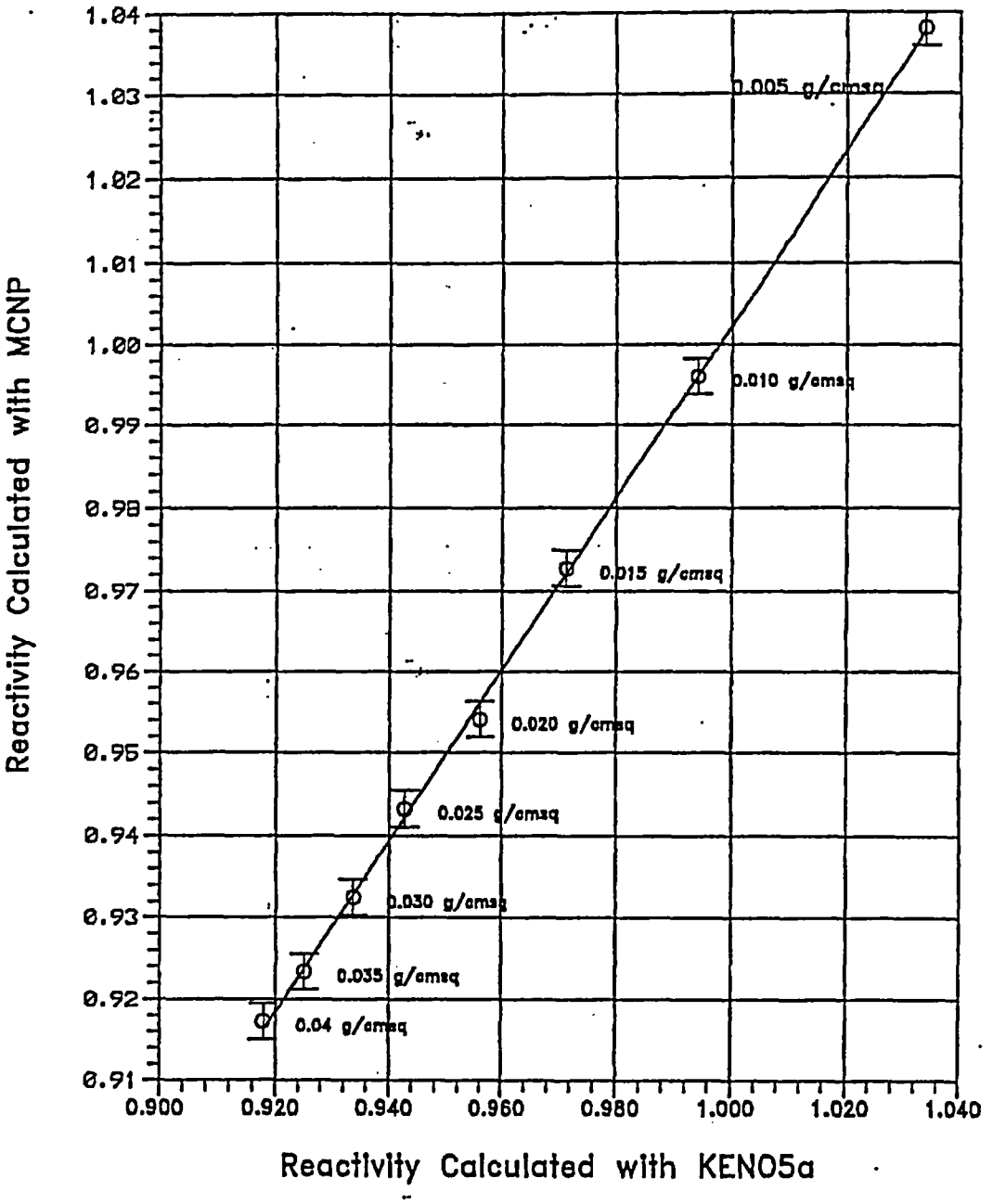

FIGURE 4A.6 : COMPARISON OF MCNP AND KENO5a CALCULATIONS FOR VARIOUS BORON-10 AREAL DENSITIES

5.0 THERMAL-HYDRAULIC CONSIDERATIONS

5.1 Introduction

This section provides a summary of the analyses performed to demonstrate the compliance of the Diablo Canyon Units 1 and 2 spent fuel pools (SFPs) and their attendant cooling systems with the appropriate provisions of USNRC Standard Review Plan (SRP) 9.1.3 (Spent Fuel Pool Cooling and Cleanup System, Rev. 1, July 1981), Section III of the USNRC "OT Position Paper for Review and Acceptance of Spent Fuel Storage and Handling Applications," (April 14, 1978), and the existing Diablo Canyon Power Plant (DCPP) licensing bases. Similar methods of thermal-hydraulic analysis have been used in the licensing evaluations for other SFP capacity expansion projects.

The thermal-hydraulic qualification analyses for the expanded rack array may be broken down into the following categories:

i. Evaluation of the maximum SFP bulk temperatures for the design-basis offload scenarios, to establish that maximum bulk temperature limits are not exceeded.

ii. Evaluation of loss-of-forced cooling scenarios, to establish minimum times to boil, maximum boil-off rates and the minimum time for the SFP level to reach 10 feet above the stored fuel. This establishes the minimum times to perform corrective actions, and the associated makeup water requirements.

iii. Determination of the maximum local water temperature, at the instant when the bulk temperature reaches its maximum value, to establish that localized boiling in the fuel storage racks is not possible while forced cooling is operating.

iv. Evaluation of the maximum fuel rod cladding temperature, at the instant when the bulk temperature reaches its maximum value, to establish that nucleate boiling is not possible while forced cooling is operating.

The following sections present plant system descriptions, analysis methodologies and assumptions, a synopsis of the input data employed and summaries of the calculated results.

5.2 Cooling Systems Description

The existing spent fuel pool cooling system (SFPCS) licensing basis for both units requires that the system must maintain the SFP bulk temperature below the following limits:

- Following a partial core offload of 76 fuel assemblies the SFP bulk temperature must not exceed 140.0°F and following a partial core offload of 96 fuel assemblies the SFP bulk temperature must not exceed 147.3°F.
- Following a full core offload (either planned or unplanned), the SFP bulk temperature must not exceed 174.3°F.

The SFPCS at each unit consists of two parallel cooling pumps discharging to a single shell and tube heat exchanger. SFP water is circulated through the heat exchanger tubes and heat is transferred to component cooling water circulating through the shell side. Only one pump is operated at a time, providing for a single active failure without any reduction in system capacity.

5.3 Offload Scenarios

Three offload scenarios are postulated in this evaluation. These scenarios are as follows:

Scenario 1

A partial core offload is comprised of 96 assemblies offloaded into the SFP, filling all but 142 storage locations when the cask pit rack is in place. All 96 offloaded assemblies are assumed to have 52000 MWD/MTU of burnup. The minimum decay time of the previously offloaded fuel assemblies for this offload scenario is 18 months.

Scenario 2

A full core offload is comprised of 193 assemblies offloaded into the SFP, filling all but 45 storage locations when the cask pit rack is in place. The 193 offloaded assemblies are separated into two distinct groups: 101 assemblies with 52000 MWD/MTU of burnup and 92 assemblies with 25000 MWD/MTU of burnup. The minimum decay time of the previously offloaded fuel assemblies for this scenario is 18 months.

Scenario 3

A planned refueling is completed in 30 days, leaving 104 recently discharged assemblies in the SFP at restart. After 36 days of operation at 100% power an emergency full core offload is performed, resulting in a total SFP inventory of 1537 assemblies, which conservatively exceeds the SFP capacity. The 193 offloaded assemblies are separated into two distinct groups: 113 assemblies with 40000 MWD/MTU of burnup and 80 assemblies with 3000 MWD/MTU of burnup.

Each of these offload/cooling scenarios is evaluated to determine the peak SFP bulk temperature.

5.4 Maximum Pool Bulk Temperatures

In this section, we present the methodology for calculating the maximum SFP bulk temperatures for the scenarios presented in the preceding section.

The transient thermal response of the SFP and the attendant cooling systems is governed by a first-order, ordinary differential equation. The governing differential equation can be written by utilizing conservation of energy as:

$$C\frac{dT}{d\tau} = Q(\tau) - Q_{HX}(T) - Q_{ENV}(T) \qquad (5\text{-}1)$$

where:

C = SFP thermal capacity, Btu/°F
T = SFP bulk temperature, °F
τ = Time after reactor shutdown, hr

$Q(\tau)$ = Time varying decay heat generation rate, Btu/hr
$Q_{HX}(T)$ = Temperature dependent SFPCS heat rejection rate, Btu/hr
$Q_{ENV}(T)$ = Temperature dependent passive heat loss to the environment, Btu/hr

$Q_{HX}(T)$ in Equation 5-1 is a function of the SFP bulk temperature and the coolant water flow rate and temperature, and can be written in terms of the temperature effectiveness (p) as follows:

$$Q_{HX}(T) = W_t \, C_t \, p \, (T - t_i) \tag{5-2}$$

where:

W_t = Coolant water flow rate, lb/hr
C_t = Coolant water specific heat capacity, Btu/(lb-°F)
p = SFPCS heat exchanger(s) temperature effectiveness
T = SFP bulk water temperature, °F
t_i = Coolant water inlet temperature, °F

The temperature effectiveness, a measure of the heat transfer efficiency of the heat exchanger(s), is defined as:

$$p = \frac{t_o - t_i}{T - t_i} \tag{5-3}$$

where t_o is the coolant outlet temperature (°F) and all other terms are as defined above. The SFPCS heat exchanger(s) coolant outlet temperature (t_o) for various SFP bulk temperatures (T) are determined using the Holtec QA validated computer program STER [5.4.7].

The following conservatisms are applied in the maximum SFP bulk temperature calculations:

- The reactor thermal power level is increased by 5% to account for burnup uncertainty.
- Appropriate parameters (i.e., burnup, batch size, assembly uranium weight and initial enrichment) are used for all projected offloads.
- The thermal performance of the SFPCS heat exchanger(s) is determined with all heat transfer surfaces fouled to their design-basis maximum levels.
- The thermal performance of the SFPCS heat exchanger(s) is determined assuming 5% tube plugging.
- The thermal inertia (thermal capacity) of the SFP is based on the net water volume only. This conservatively neglects the considerable thermal inertia of the fuel assemblies and the SFP structure.
- Every fuel assembly in the SFP is assumed to be the heavier LOPAR design with a control rod inserted. This yields a conservative value for the calculated net water volume within the SFP.

The differential equation that defines the transient thermal response of the SFP (Equation 5-1) is solved numerically. The decay heat load from previously offloaded fuel assemblies is assumed to be constant and is calculated using Holtec's QA validated LONGOR computer program [5.4.3]. This program incorporates the ORIGEN2 computer code [5.4.4] to perform the decay heat calculations. The transient decay heat loads and SFP bulk temperatures are calculated using Holtec's QA validated BULKTEM computer program [5.4.5], which also incorporates the ORIGEN2 computer code. The maximum SFP bulk temperatures are extracted from the results

of the transient evaluations. Table 5.4.1 presents the historic and projected offload schedule used for these analyses. The other major input values for these analyses are summarized in Table 5.4.2.

5.5 Minimum Time-to-Boil and Maximum Boiloff Rate

In this section, we present the methodology for calculating the minimum time-to-boil and corresponding maximum boiloff rate for the scenarios presented in Section 5.3.

The governing enthalpy balance equation for this condition, subject to these conservative assumptions, can be written as:

$$C(\tau)\frac{dT}{d\tau} = Q(\tau + \tau_0) - Q_{ENV}(T) \qquad (5\text{-}5)$$

where:

$C(\tau)$ = Time-varying SFP thermal capacity
τ = Time after cooling is lost (hr)
τ_0 = Loss of cooling time after shutdown (hr)

All other terms in this equation are the same as defined for Equation 5-1 in Section 5.4.

The following conservatisms and assumptions are applied in the time-to-boil and boiloff rate calculations:

- During the loss of forced cooling evaluations, no credit is taken for any makeup water.
- The loss of forced cooling is assumed to occur coincident with the peak SFP bulk temperature. Maximizing the initial temperature will conservatively minimize the calculated time-to-boil.
- The decay heat load in the SFP is assumed constant that the value that corresponds to the peak SFP bulk temperature, neglecting the reduction in decay heat with time.

- The passive heat losses from the SFP surface to the building air are evaluated assuming the relative humidity of the building air is 100%. This minimizes the evaporation driving force and reduces the resulting heat losses.

- The thermal inertia (thermal capacity) of the SFP is based on the net water volume only. This conservatively neglects the considerable thermal inertia of the fuel assemblies and the SFP structure.

Equation 5-5 is solved using a numerical solution technique to obtain the bulk pool temperature as a function of time. The time-to-boil, boil-off rate and water depth versus time are calculated using Holtec's QA validated TBOIL program [5.4.6]. Calculations also determined the time required for the water level to reduce to within 10' of the top of the spent fuel storage racks. The major input values for these analyses are summarized in Table 5.5.1.

5.6 Maximum SFP Local Water Temperature

In this section, a summary of the methodology for evaluating the maximum local water temperatures within the fuel racks in the SFP is presented. The results of these evaluations are maximum local water temperatures.

To demonstrate adequate cooling of hot fuel in the SFP, it is necessary to rigorously quantify the coupled velocity and temperature fields created by the interaction of buoyancy driven and forced water flows. A Computational Fluid Dynamics (CFD) analysis for this demonstration is required. The objective of this study is to demonstrate that the thermal-hydraulic criterion of ensuring local subcooled conditions in the SFP is met for all postulated fuel offload/cooling alignment scenarios. The local thermal-hydraulic analysis is performed such that partial cell blockage and slight fuel assembly variations are bounded. An outline of the CFD approach is described in the following.

There are several significant geometric and thermal-hydraulic features of the Diablo Canyon SFPs that need to be considered for a rigorous CFD analysis. From a fluid flow modeling standpoint, there are two regions to be considered. One region is the SFP bulk region where the

classical Navier-Stokes equations [5.6.1] are solved, with turbulence effects included. The other region is the fuel storage racks containing heat generating fuel assemblies, located near the bottom of the SFP. In this region, water flow is directed vertically upwards due to buoyancy forces through relatively small flow channels formed by rods of the fuel assemblies in each rack cell. This situation is modeled as a porous solid region with pressure drop in the flowing fluid governed by Darcy's Law as:

$$\frac{\partial P}{\partial X_i} = -\frac{\mu}{K(i)} V_i - C \rho |V| \frac{V_i}{2} \qquad (5\text{-}6)$$

where $\partial P/\partial X_i$ is the pressure gradient, K(i), V_i and C are the corresponding permeability, velocity and inertial resistance parameters and μ is the fluid viscosity. These terms are added to the classic Navier-Stokes equations. The permeability and inertial resistance parameters for the rack cells loaded with fuel assemblies are determined based on friction factor correlations for the laminar flow conditions that would exist due to the low buoyancy induced velocities and the small size of the flow channels.

The Diablo Canyon SFP geometries require an adequate portrayal of both large scale and small scale features, spatially distributed heat sources in the racks and water inlet/outlet piping. Relatively cooler bulk water normally flows down between the fuel racks outline and wall liner, a clearance known as the downcomer. Near the bottom of the racks the flow turns from a vertical to horizontal direction into the bottom plenum, supplying cooling water to the rack cells. Heated water issuing out of the top of the racks mixes with the bulk water. An adequate modeling of these features on the CFD program involves meshing the large scale bulk SFP region and small scale downcomer and bottom plenum regions with a sufficient number of computational cells to capture both the global and local features of the flow field.

The distributed heat sources in the racks are modeled by identifying distinct heat generation zones considering recently offloaded fuel, bounding peaking effects, and the presence of background decay heat from previous offloads. Three heat generating zones are identified. The first consists of background fuel from previous offloads. The second and third zones consist of

fuel from recently offloaded fuel assemblies. The two recent offload zones are differentiated by one zone with higher than average decay heat generation (hottest assemblies in full core) and the other with less than average decay heat generation (remainder of full core). This is a conservative model, since all of the fuel with higher than average decay heat is placed in a contiguous area. A uniformly distributed heat generation rate was applied throughout each distinct zone (i.e., there were no variations in heat generation rate within a single zone).

In order to determine an upper bound on the maximum local water temperature, a series of conservative assumptions are made. The most important of these assumptions are:

- The walls and floor of the SFP are all modeled as adiabatic surfaces, thereby neglecting conduction heat loss through these items.
- Heat losses by thermal radiation and natural convection from the hot SFP surface to the environment are neglected.
- No downcomer flow is assumed to exist between the rack modules.
- The hydraulic resistance of every fuel storage rack cell is determined based on the most hydraulically limiting (i.e., highest hydraulic resistance) fuel assembly type.
- The hydraulic resistance parameters for the rack cells, permeability and inertial resistance, are conservatively adjusted by 5%.
- The bottom plenum heights used in the model are less than the actual heights to conservatively reduce the area for cooling water flow to the inlets of the rack cells.
- The hydraulic resistance of every fuel storage rack cell is determined based on the most restrictive water inlet geometry of the cells over rack support pedestals (i.e., all baseplate holes are completely blocked). These cells have a reduced water entrance area, caused by the pedestal blocking the baseplate hole, and a correspondingly increased hydraulic resistance.
- The hydraulic resistance of every fuel storage rack cell includes the effects of blockage due to an assumed dropped fuel assembly lying horizontally on top of the racks.

- The fuel assemblies with the highest decay heat generation rates are grouped together in the center of the model. This conservatively maximizes the distance between these highest heat fuel assemblies and the rack-to-wall downcomers, so the cooled water from the SFPCS must travel farther along the SFP floor to cool them. Discharge of these assemblies into any rack locations that are closer to a downcomer is bounded by the analyzed configuration.

The CFD analysis was performed on the commercially available FLUENT [5.6.2] computational fluid dynamics program, which has been benchmarked under Holtec's QA program. The FLUENT code enables buoyancy flow and turbulence effects to be included in the CFD analysis. Buoyancy forces are included by specifying a temperature-dependent density for water and applying an appropriate gravity vector. Turbulence effects are modeled by relating time-varying Reynolds' Stresses to the mean bulk flow quantities with the standard k-ε turbulence model.

Some of the major input values for this analysis are summarized in Table 5.6.1. An isometric view of the assembled CFD model for the DCPP units is presented in Figure 5.6.1.

5.7 Fuel Rod Cladding Temperature

In this section, the method to calculate the temperature of the fuel rod cladding is presented. The maximum local water temperature and peak heat flux are considered to occur coincidentally. The superposition of these two maximum values ensures that the calculated peak fuel cladding temperature bounds the fuel cladding temperature anywhere along the length of the fuel assembly. As previously stated in Section 5.1, the maximum fuel rod cladding temperature is determined to establish that nucleate boiling is not possible while forced cooling is operating. This requires demonstrating that the highest fuel rod cladding temperatures are less than the local saturation temperature of the adjacent SFP water. The saturation temperature of water increases with increasing pressure and, subsequently, increasing depth. The critical location for localized boiling in the fuel racks is at the top of the active fuel length. The minimum depth of water at the top of the active fuel length is greater than 24 feet. At a water depth of 24 feet, the saturation temperature of water is approximately 240°F.

A fuel rod can produce F_z times the average heat emission rate over a small length, where F_z is the axial peaking factor. The axial heat distribution in a rod is generally a maximum in the central region, and tapers off at its two extremities. Thus, peak cladding heat flux over an infinitesimal rod section is given by the equation:

$$q_c = \frac{Q \times F_z}{A_c} \tag{5-7}$$

where Q is the rod average heat emission and A_c is the total cladding external heat transfer area in the active fuel length region. The axial peaking factor is obtained by dividing the total assembly peaking factor by the radial assembly peaking factor, both given in Table 5.6.1.

As described previously, the maximum local water temperature was computed. Within each fuel assembly sub-channel, water is continuously heated by the cladding as it moves axially upwards under laminar flow conditions. Rohsenow and Hartnett [5.7.1] report a Nusselt-number for laminar flow heat transfer in a heated channel. The film temperature driving force (ΔT_f) at the peak cladding flux location is calculated as follows:

$$\Delta T_f = \frac{q_c}{h_f}$$
$$h_f = Nu \frac{Kw}{D_h} \tag{5-8}$$

where h_f is the waterside film heat transfer coefficient, D_h is the sub-channel hydraulic diameter, Kw is the water thermal conductivity and Nu is the Nusselt number for laminar flow heat transfer.

In order to introduce some additional conservatism in the analysis, we assume that the fuel cladding has a crud deposit resistance R_c (equal to 0.0005 ft^2-hr-°F/Btu) which covers the entire surface. Thus, including the temperature drop across the crud resistance, the cladding to water local temperature difference (ΔT_c) is given by the equation $\Delta T_c = \Delta T_f + R_c \times q_c$.

5.8 Results

This section contains results from the analyses performed for the postulated offload scenarios.

5.8.1 Maximum Pool Bulk Temperatures

For the offload/cooling scenarios described in Section 5.3, the maximum calculated bulk temperatures are summarized in Table 5.8.1. Given the conservatisms incorporated into the calculations, actual bulk temperatures will be lower than these calculated values. Figures 5.8.1 through 5.8.3 each present profiles of net decay heat load, passive heat losses and bulk temperature versus time for the evaluated transient scenarios.

The results presented in Table 5.8.1 demonstrate that calculated bulk temperatures for all scenarios remain below the allowable bulk temperature limit. The maximum bulk temperature, the time after reactor shutdown that the maximum temperature is reached and the coincident net heat load are given for three core offload scenarios.

5.8.2 Minimum Time-to-Boil and Maximum Boiloff Rate

For the offload/cooling described in Section 5.3, the calculated times-to-boil and maximum boil-off rates are summarized in Table 5.8.2. Given the conservatisms incorporated into the calculations, actual times-to-boil will be higher than these calculated values and actual boil-off rates will be lower than calculated. The results show that the minimum time-to-boil is greater than the current licensing basis value of 2.5 hours and the maximum boil-off rate is less than the current licensing basis value of 44,905 lb/hr (93.6 gpm).

5.8.3 Local Water and Fuel Cladding Temperatures

Consistent with the approach to make conservative assessments of temperature, the local water temperature calculations are performed for a bounding condition with the maximum SFP bulk temperature (from Scenario 3), the maximum coincident total SFP decay heat load (also from Scenario 3) and the maximum coincident individual fuel assembly decay heat load (from Scenario 1). The peak fuel clad superheat (i.e., the maximum clad-to-local water temperature difference) is determined for a bounding scenario. The resultant bounding superheat value was then used to calculate a bounding maximum fuel clad temperature.

The numeric results of the maximum local water temperature and the bounding fuel cladding temperature evaluations are presented in Table 5.8.3. Figure 5.8.4 presents converged temperature contours in a vertical slice through the hot fuel region of the SFP.

The maximum local water temperature and the bounding maximum fuel clad temperature are both lower than the 240°F local boiling temperature at the top of the racks and are also both below the current licensing basis values of 219.5°F and 254.3°F, respectively. These results demonstrate that boiling, including nucleate boiling on clad surfaces cannot occur.

5.9 References

[5.4.1] "Heat Loss to the Ambient from Spent Fuel Pools: Correlation of Theory with Experiment", Holtec Report HI-90477, Revision 0, April 3, 1990.

[5.4.2] "An Improved Correlation for Evaporation from Spent Fuel Pools", Holtec Report HI-971664, Revision 0.

[5.4.3] "QA Documentation for LONGOR," Holtec Report HI-951390, Revision 0.

[5.4.4] A.G. Croff, "ORIGEN2 - A Revised and Updated Version of the Oak Ridge Isotope Generation and Depletion Code," ORNL-5621, Oak Ridge National Laboratory, 1980.

[5.4.5] "QA Documentation for BULKTEM," Holtec Report HI-951391, Revision 1.

[5.4.6] "QA Documentation for TBOIL," Holtec Report HI-92832, Revision 5.

[5.4.7] "QA Documentation for STER", Holtec Report HI-92776, Revision 11.

[5.6.1] Batchelor, G.K., "An Introduction to Fluid Dynamics", Cambridge University Press, 1967.

[5.6.2] "Validation of FLUENT Version 6.1.18", Holtec Report HI-2032998, Revision 0.

[5.7.1] Rohsenow, N.M., and Hartnett, J.P., "Handbook of Heat Transfer", McGraw Hill Book Company, New York, 1973.

Table 5.4.1 Historic and Projected Fuel Offload Schedule				
Initial ^{235}U Enrichment (wt.%)	Average Burnup (MWD/MTU)	Number of Assemblies	Assembly ^{n}U Weight (kgU)	Offload Date (dd/mm/yyyy)
Previously Discharged Fuel Assemblies				
2.123	16165	37	460.1	3/4/1987
2.795	29192	74	459.8	17/9/1988
3.199	33512	84	462.5	4/3/1990
3.419	37609	113	463.3	31/8/1991
3.552	37328	88	436.4	6/3/1993
4.162	44578	88	424.8	24/9/1994
4.289	45117	80	424.5	6/4/1996
4.320	48085	69	425.3	14/2/1998
4.685	50328	101	425.1	26/9/1999
4.444	49065	93	418.7	28/4/2001
4.512	49048	101	417.7	3/2/2003
4.396	52000	104	423.0	3/8/2004
4.396	52000	104	423.0	3/2/2006
4.396	52000	104	423.0	3/8/2007
Partial Core Offload Scenario 1				
4.7	52000	96	472.6	3/2/2009
Full Core Offload Scenario 2				
4.7	52000	101	472.6	3/2/2009
4.7	25000	92	472.6	3/2/2009
Emergency Core Offload Scenario 3				
4.7	52000	104	472.6	3/2/2009
4.7	40000	113	472.6	10/4/2009
4.7	3000	80	472.6	10/4/2009

Table 5.4.2 Key Input Data for Bulk Temperature Evaluation	
Parameter	**Value**
Number of Storage Cells in SFP	1478
Reactor Thermal Power	3411 MWt
Reactor Core Size	193 assemblies
Burnup Uncertainty	5%
SFPCS HX Coolant (CCW) Inlet Temperature	75°F
SFPCS HX Coolant (CCW) Flow Rate	3400 gpm
SFPCS HX SFP Water Flow Rate	1,140,000 lb/hr
In-Core Hold Time Before Transfer	100 hrs
Fuel Assembly Transfer Rate	4 per hr

Table 5.5.1 Key Input Data for Time-To-Boil Evaluation	
Parameter	**Value**
SFP Surface Area	1394 ft^2
Minimum Pool Water Depth	38.3 ft
Fuel Racks Displaced Volume	771 ft^3
Fuel Assemblies Displaced Volume	5,840 ft^3
SFP Net Water Volume	47,215 ft^3

Table 5.6.1 Key Design Data for Local Temperature Evaluation	
Parameter	**Value**
Radial Assembly Peaking (Nuclear Enthalpy Rise Hot Channel) Factor	1.7
Total Assembly Peaking (Heat Flux Hot Channel) Factor	2.7
Cooled SFP Water Flow Rate through SFPCS Heat Exchange	1,140,000 lb/hr
Hydraulically Limiting Fuel Assembly	Westinghouse 17×17 Standard (LOPAR)
Fuel Rod Outer Diameter	0.374 in
Active Fuel Length	144 in
Number of Fuel Rods per Assembly	264
Rack Cell Inner Dimension (Min.)	8.75 in
Rack Cell Length	169 in
Modeled Bottom Plenum Height	2 in

Table 5.8.1 Result of Transient Bulk Temperature Evaluations			
Scenario	**Maximum Bulk Temperature (°F)**	**Time After Reactor Shutdown (hrs)**	**Coincident Net Heat Load (Btu/hr)**
1 - Partial Core	127.21	139	22.92×10^6
2 - Full Core	156.99	159	36.67×10^6
3 – Emergency Core	161.50	159 (1)	38.71×10^6

(1) For the Emergency Core Offload (Scenario 3) only, the time after reactor shutdown is measured from the second reactor shutdown.

Table 5.8.2 Results of Loss-of-Forced Cooling Evaluations			
Scenario	**Minimum Time-to-Boil (hrs)**	**Maximum Boiloff Rate (gpm)**	**Minimum Time to Reach 10' Above Racks (hrs)**
1 - Partial Core	11.27	50.34	58
2 - Full Core	4.35	82.45	33
3 – Emergency Core	3.76	87.37	30

Table 5.8.3 Results of Maximum Local Water and Fuel Cladding Temperature Evaluations	
Maximum Local Water Temperature	188°F
Bounding Fuel Clad Superheat	25°F
Bounding Fuel Clad Temperature	213°F

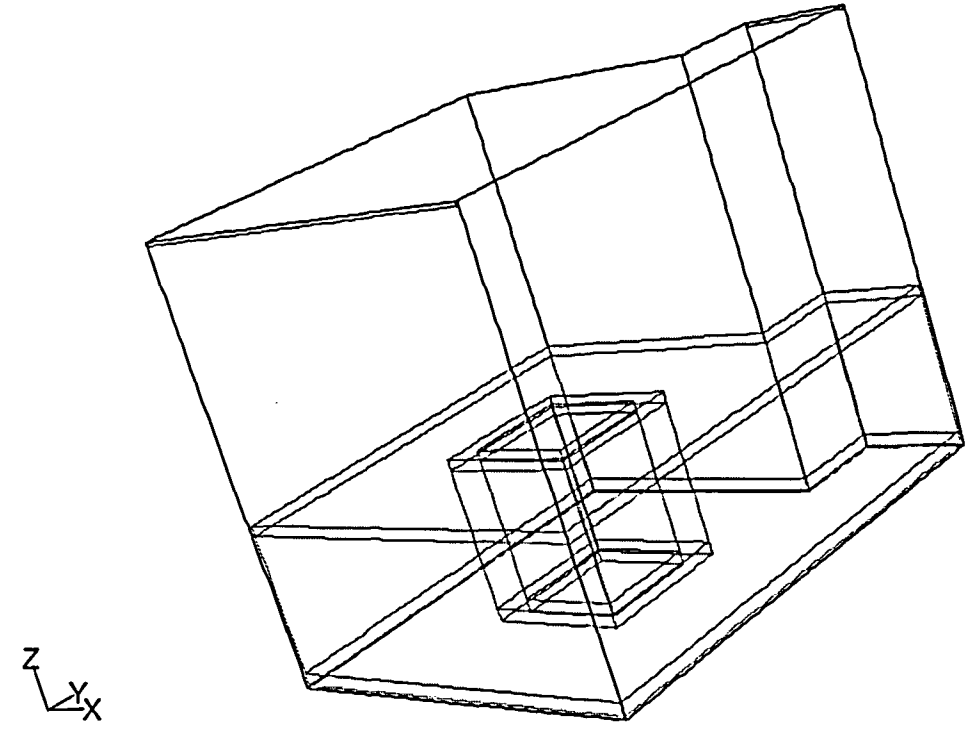

Figure 5.6.1 – CFD Model Isometric View

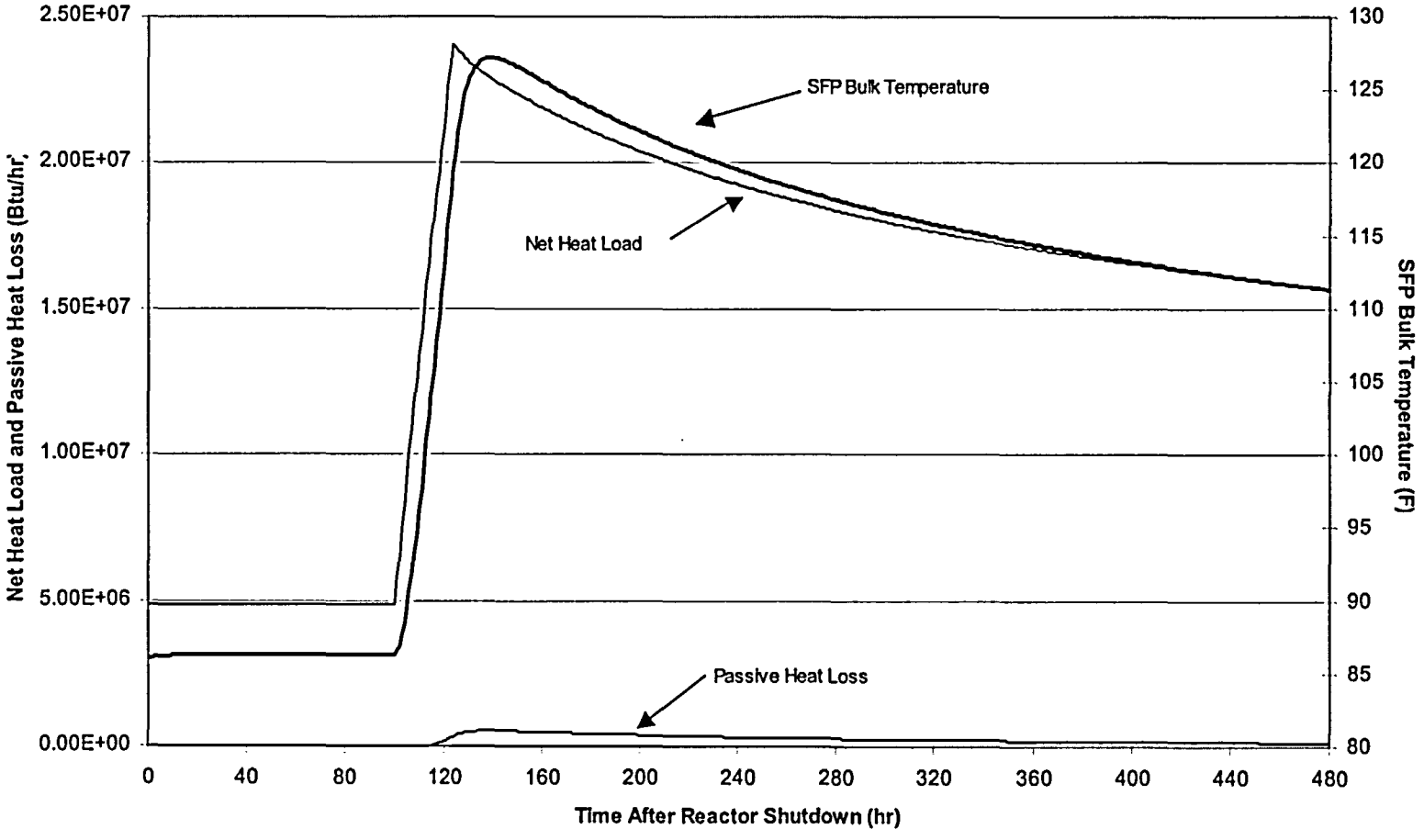

Figure 5.8.1 –Scenario 1 – Partial Core Discharge

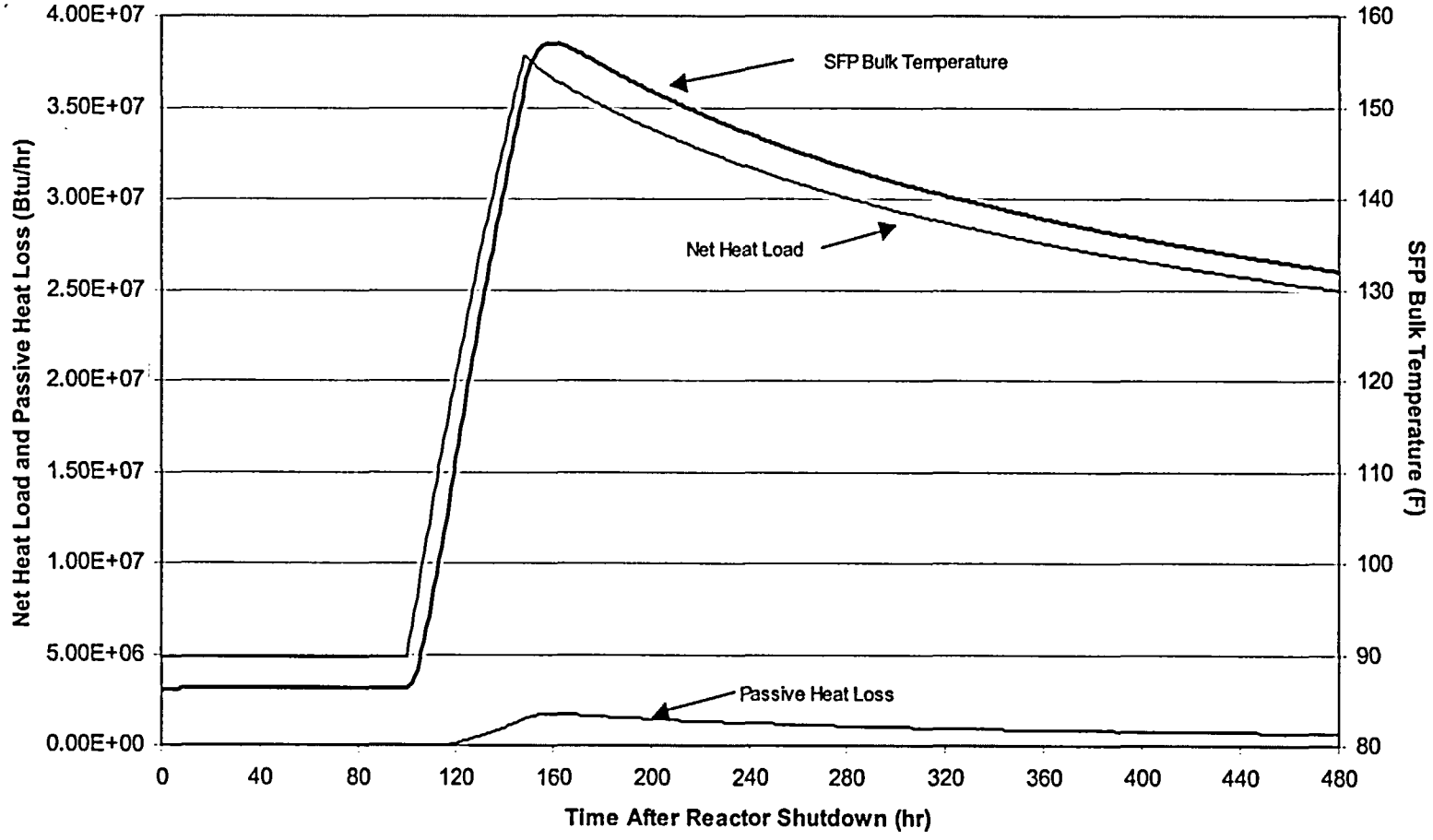

Figure 5.8.2 –Scenario 2 – Full Core Discharge

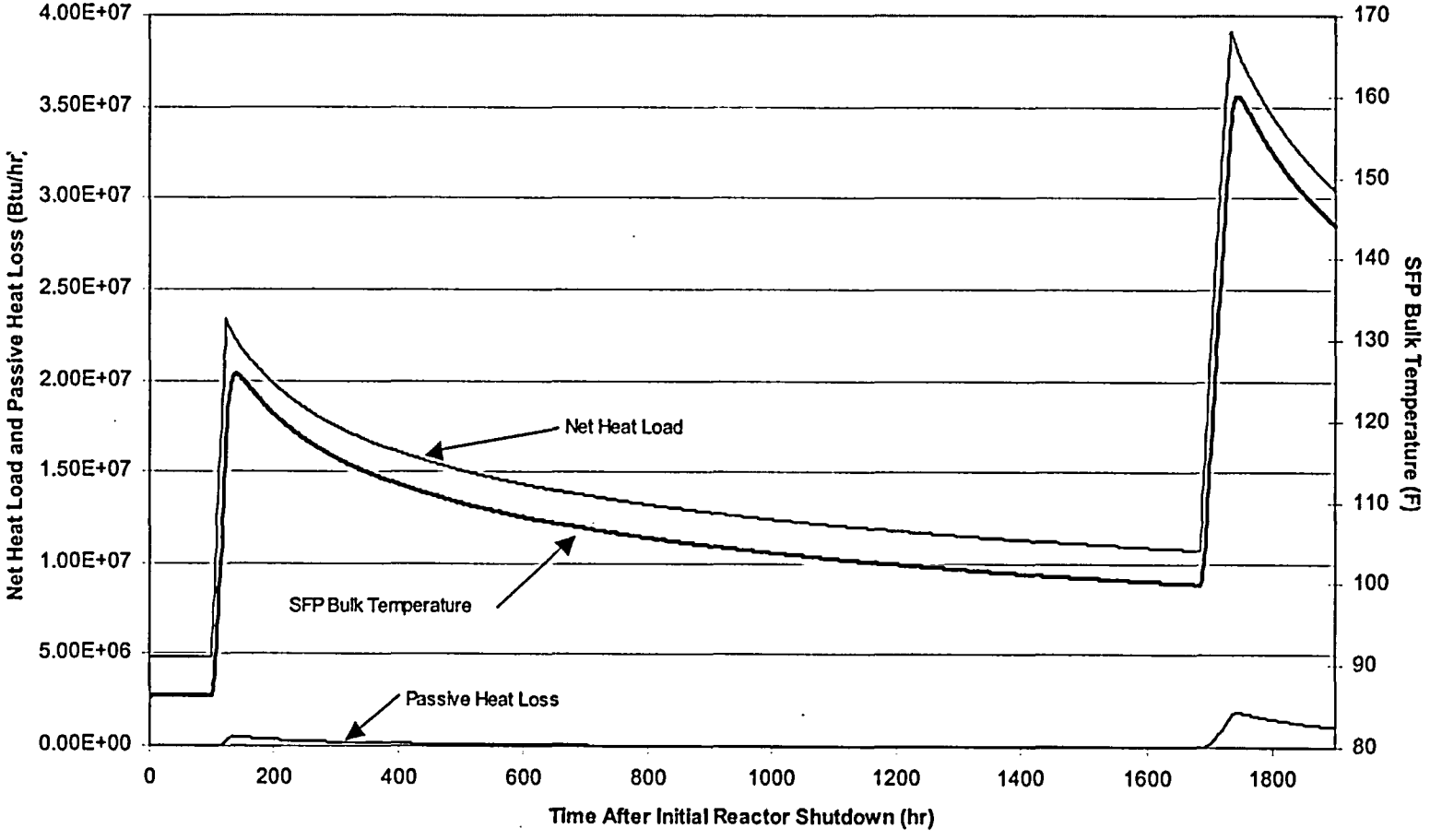

Figure 5.8.3 – Scenario 3 – Emergency Full Core Discharge

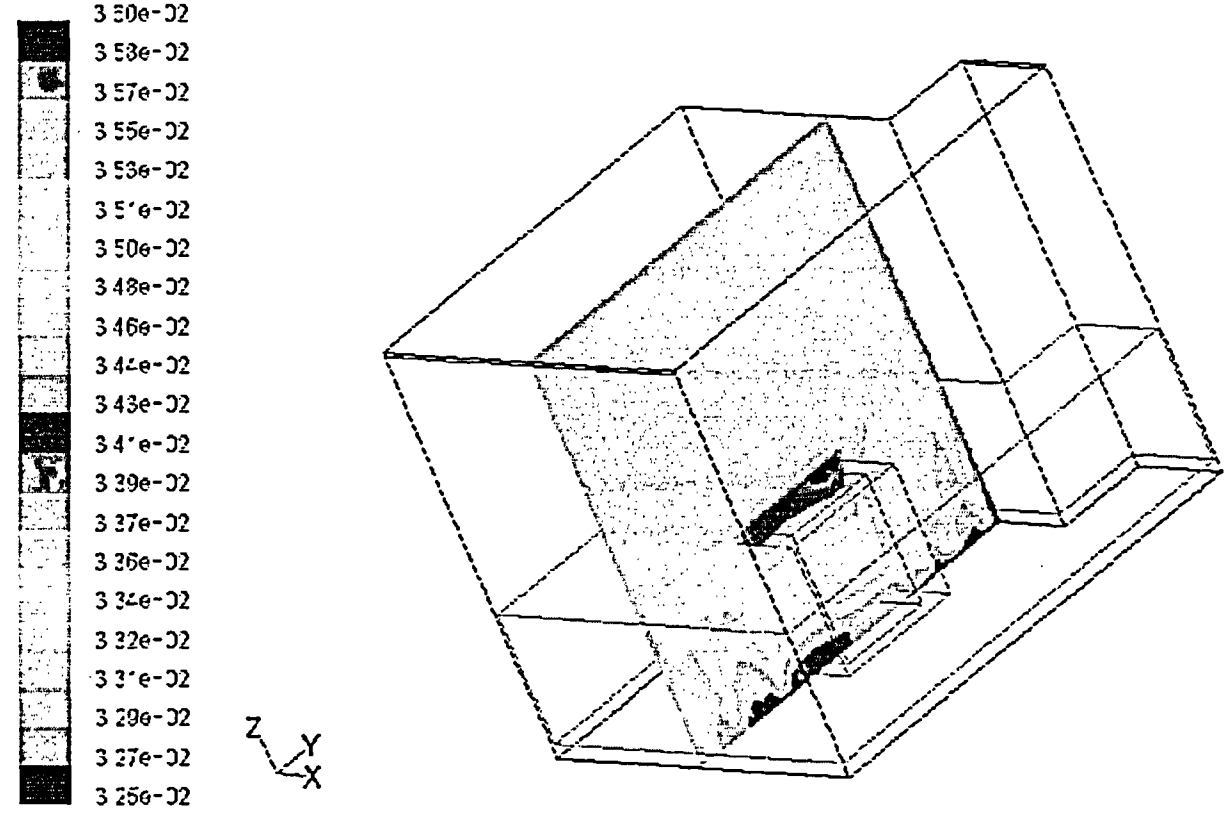

Figure 5.8.4 –CFD Model with Converged Temperature Contours

6.0 RACK STRUCTURAL INTEGRITY CONSIDERATIONS

6.1 Introduction

The structural integrity evaluations performed on the new cask pit rack in each of the two DCPP pools is presented in this section. The analyzed storage rack configuration is depicted in Figure 1.1.1. Inasmuch as the two DCPP pools are mirror images of each other, Figure 1.1.1 represents both pools with appropriately assigned local coordinates.

The analyses undertaken to confirm the structural integrity of the new racks are performed in compliance with the USNRC Standard Review Plan [6.1.1] and the OT Position Paper [6.1.2]. A summary of the key input data, an abstract of the methodology, modeling assumptions, key results, and quantification of the minimum kinematic and stress margins for each of the applicable load combinations is provided in this section.

6.2 Structural Characteristics of the New Cask Pit Rack

The Cask Pit region of the DCPP fuel pools is integral to the fuel pool cavity space wherein 16 freestanding modules containing a total of 1,324 storage locations are presently employed. The cask pit region, situated in a corner of the rectangular pool planform space, is surrounded by reinforced concrete walls on two sides and by a welded steel framework (intended to serve as a barrier against excessive sliding of the fuel pool racks adjacent to the pit) on the two other sides. The cask pit floor liner is approximately 51 inches lower in elevation than the floor liner in the main pool. Below the elevation of the main pool floor, the cask pit is surrounded on all four sides by reinforced concrete lined with ¼" thick stainless steel liner plate.

To ensure that the top of the new rack will be coplanar with the existing racks (to facilitate fuel handling), a stainless steel platform is provided that is engineered to be emplaced in the pit with a snug fit with the four stainless liner-equipped reinforced concrete walls in the cask pit cavity. This so-called "cask pit platform", which is discussed in Section 2.1 and illustrated in Figure 2.1.2, is thus a laterally immovable and extremely stiff weldment that is engineered to serve as a staging surface for the cask pit rack.

The four corners of the platform are equipped with precisely machined recesses (see Figure 2.1.3) that are coaxial with and approximately 3/4" larger in diameter than the 5" diameter rack support pedestals, shown in Figure 2.6.4. Thus, when staged on the platform, the sliding of the rack (under inertia loads) is severely restricted while the clearance between the recess and the rack pedestal precludes any differential thermal expansion-related concerns. Finally, to prevent a vertical lift-off of the rack from the platform, two specially machined "connector links" made of stainless steel at each corner of the rack are installed through storage cells adjacent to the pedestal location. The design of the "connector link" is intended to prevent a separation between the rack and the platform and thus prevent excessive sidesway and uplift of the rack during a seismic event. Thus, the combined effect of the lateral confinement of the support pedestals and vertical fixity (Figure 2.1.4) is to limit the kinematic movement of the cask pit rack under seismic events. Because the fluid coupling forces increase with a rack's motion, a chief structural consequence of the above rack staging configuration is to virtually eliminate any significant hydrodynamic coupling between the cask pit racks and the existing array of racks in the main pool. The virtual elimination of a cross coupling between the new rack and the neighboring existing racks in the main pool is further helped by the large gap between them (minimum gap in excess of 20 inches).

The high bending rigidity of the honeycomb cellular design of the racks (described in Section 2) prevents any significant flexural bending of module during the seismic event, thus ensuring that the cask pit rack will not impact any adjacent structures (reinforced concrete wall or the seismic restraint structure). Thus, while the existing racks in the pool are permitted to impact each other, the new rack is engineered to preclude impact with any external surface. This helps mitigate stress levels and maximize the computed safety margins. Nevertheless, in recognition of the rather severe earthquakes postulated for DCPP, the metal thicknesses of the storage cell walls in the cask pit modules is at least 20% greater than a similar rack of recent vintage at any other nuclear plant. The benefits of the design approach summarized in the foregoing become apparent in the stress levels computed for the cask pit rack under the applicable seismic events, as presented in a later subsection herein.

6.3 Applicable Load Combinations

The applicable loads and their combinations that must be considered in structural qualification of the cask pit rack module are excerpted from References [6.1.1] and [6.1.2] in the following:

Load Combination	Service Level Per the ASME Code [6.3.1]
$D+L$ $D+L+T_o$ $D+L+T_o+E$	Level A (Normal Operating Condition)
$D+L+T_a+E$ $D+L+T_o+P_f$	Level B (Upset Condition)
$D+L+T_a+E'$ $D+L+T_o+F_d$	Level D (Faulted Condition)

where:

D = Dead weight-induced loads (including stored spent nuclear fuel and control elements)

L = Live Load

P_f = Force on the racks caused by the removal of a postulated stuck fuel assembly.

F_d = Impact force from accidental drop of the heaviest load from the maximum possible height.

E = Operating Basis Earthquake (OBE)

E' = Safe Shutdown Earthquake (SSE)

T_o = Differential thermal expansion induced loads

T_a = Differential thermal expansion induced loads under postulated abnormal conditions

As for the rack itself, T_o and T_a produce thermal stresses that are of the self-limiting (secondary) genre since the rack is free to expand or contract due to the existence of gaps between the rack support pedestals and the recessed holes in the platform. Therefore, T_o and T_a are not germane to the stress analysis of the cask pit rack. As for the cask pit platform, the thermal loads (T_o and T_a) produce primary stresses in the platform since the platform is restrained from thermal growth by

the lateral support shims. Therefore, thermal loads are a contributing factor in the platform stress analysis.

The inertia loading corresponding to the Operating Basis Earthquake (OBE) and Safe Shutdown Earthquake (SSE) in [6.1.1] are termed Design Earthquake (DE) and Double Design Earthquake (DDE), respectively, in the DCPP FSAR.

In addition to DE and DDE, the plant's owner (PG&E) has also defined two other earthquakes, named Hosgri earthquake (HE) and LTSP (acronym for the Long Term Seismic Program), for which the cask pit rack assembly is analyzed and the resulting stresses are compared with Level D condition limits.

In accordance with the recommendation of Section IV.2 of the OT Position Paper [6.1.2] the cask pit rack will be designed in accordance with ASME Code Section III, Subsection NF limits. Because of the honeycomb construction of the rack, the effect of mechanical loads such as P_f and F_d result in local stresses and possibly plastic strains that are not within the purview of the stress limits for Class 3 "NF" linear structures. Therefore, mechanical loads are treated separately, mainly with the goal to quantify the extent of local damage sustained by the rack under localized loads, as discussed in Section 7 of this report.

6.4 Synthetic Time-Histories

Because the fuel rack is a highly non-linear structure, the applicable earthquakes must be cast in terms of acceleration time-histories for analysis purposes.

The synthetic time-histories in three orthogonal directions (N-S, E-W, and vertical) were accordingly generated in accordance with the provisions of SRP 3.7.1 [6.1.1] for each of the four earthquakes (DE, DDE, HE, and LTSP). The structural damping value used in the generation of the synthetic time-histories utilizes the values prescribed in the DCPP FSAR. No credit for material damping (hysterisis) or fluid damping is incorporated in the time-history generation algorithm for conservatism.

As suggested in SRP 3.7.1 [6.1.1], both the response spectrum and the power spectral density corresponding to the generated acceleration time-history should envelope their target (design basis) counterparts with only finite enveloping infractions. The time-histories for the pool slab for all four earthquakes have been generated to satisfy the above enveloping criteria. Finally, the three orthogonal time-histories for each earthquake are required to meet the criterion of statistical independence (i.e., cross correlation factor between any two components, c). The conventional limit for c is 0.15.

Figures 6.4.1 through 6.4.12 provide plots of the time-history accelerograms corresponding to the four discrete earthquakes (DE, DDE, HE and LTSP). These artificial time-histories are used in the non-linear dynamic simulations of the racks to quantify the structural margins of safety.

For reference purposes, the peak accelerations for the twelve time-histories are summarized in Table 6.4.1 below.

Table 6.4.1

ZPA VALUES (in g's) FOR THE APPLICABLE EARTHQUAKES

Earthquake	Horizontal (N-S)	Horizontal (E-W)	Vertical
DE	0.334	0.260	0.130
DDE	0.520	0.520	0.270
HE	0.710	0.750	0.565
LTSP	0.846	0.987	0.670

6.5 Analysis Methodology

6.5.1 Overview

The response of a free-standing rack module (free to move to the extent of available gaps between the rack support pedestal and the recessed holes in the platform) to seismic inputs is highly nonlinear and involves a complex combination of motions (sliding, rocking, twisting, and turning), resulting from an interplay of inertia, friction, impact, and damping effects. Some of the unique attributes of the rack dynamic behavior include a large fraction of the total structural

mass in a confined rattling motion, frictional effect at the bottom surface of the pedestal, and fluid coupling effects due to deep submergence. Evidently, linear methods, such as modal analysis and response spectrum techniques, cannot accurately simulate the structural response of such a highly nonlinear structure to seismic excitation. An accurate simulation is obtained only by direct integration of the nonlinear equations of motion with the three acceleration time-histories applied as the forcing functions acting simultaneously.

The DYNARACK solver [6.5.1], the vehicle previously utilized in virtually all rerack O.L. amendment requests over the past two decades (see Table 6.5.1 below) to simulate the dynamic behavior of the complex storage rack structures, is also used to analyze the DCPP cask pit rack and platform. The analytical premise of DYNARACK is provided in a published technical paper [6.5.2].

Table 6.5.1

PARTIAL LISTING OF FUEL RACK APPLICATIONS USING DYNARACK

PLANT	DOCKET NUMBER(s)	YEAR
Enrico Fermi Unit 2	USNRC 50-341	1980
Quad Cities 1 & 2	USNRC 50-254, 50-265	1981
Rancho Seco	USNRC 50-312	1982
Grand Gulf Unit 1	USNRC 50-416	1984
Oyster Creek	USNRC 50-219	1984
Pilgrim	USNRC 50-293	1985
V.C. Summer	USNRC 50-395	1984
Diablo Canyon Units 1 & 2	USNRC 50-275, 50-323	1986
Byron Units 1 & 2	USNRC 50-454, 50-455	1987
Braidwood Units 1 & 2	USNRC 50-456, 50-457	1987
Vogtle Unit 2	USNRC 50-425	1988
St. Lucie Unit 1	USNRC 50-335	1987

Table 6.5.1 PARTIAL LISTING OF FUEL RACK APPLICATIONS USING DYNARACK		
PLANT	**DOCKET NUMBER(s)**	**YEAR**
Millstone Point Unit 1	USNRC 50-245	1989
Chinshan	Taiwan Power Company	1988
D.C. Cook Units 1 & 2	USNRC 50-315, 50-316	1992
Indian Point Unit 2	USNRC 50-247	1990
Three Mile Island Unit 1	USNRC 50-289	1991
James A. FitzPatrick	USNRC 50-333	1990
Shearon Harris Unit 2	USNRC 50-401	1991
Hope Creek	USNRC 50-354	1990
Kuosheng Units 1 & 2	Taiwan Power Company	1990
Ulchin Unit 2	Korea Electric Power Co.	1990
Laguna Verde Units 1 & 2	Comision Federal de Electricidad	1991
Zion Station Units 1 & 2	USNRC 50-295, 50-304	1992
Sequoyah	USNRC 50-327, 50-328	1992
LaSalle Unit 1	USNRC 50-373	1992
Duane Arnold Energy Center	USNRC 50-331	1992
Fort Calhoun	USNRC 50-285	1992
Nine Mile Point Unit 1	USNRC 50-220	1993
Beaver Valley Unit 1	USNRC 50-334	1992
Salem Units 1 & 2	USNRC 50-272, 50-311	1993
Limerick	USNRC 50-352, 50-353	1994
Ulchin Unit 1	KINS	1995
Yonggwang Units 1 & 2	KINS	1996

Table 6.5.1

PARTIAL LISTING OF FUEL RACK APPLICATIONS USING DYNARACK

PLANT	DOCKET NUMBER(s)	YEAR
Kori-4	KINS	1996
Connecticut Yankee	USNRC 50-213	1996
Angra Unit 1	Brazil	1996
Sizewell B	United Kingdom	1996
Waterford 3	USNRC 50-382	1996
Vogtle	USNRC 50-424	1997
J. A. Fitzpatrick	USNRC 50-333	1997
Vermont Yankee	USNRC 50-271	1998
Callaway	USNRC 50-483	1998
Nine Mile	USNRC 50-220	1998
Chin Shan	Taiwan Power Company	1998
Millstone 3	USNRC 50-423	1998
Byron/Braidwood	USNRC 50-454, 50-455, 50-567, 50-457	1999
Wolf Creek	USNRC 50-482	1999
Plant Hatch Units 1 & 2	USNRC 50-321, 50-366	1999
Harris Pools C and D	USNRC 50-401	1999
Davis-Besse	USNRC 50-346	1999
Enrico Fermi Unit 2	USNRC 50-341	2000
Kewaunee	USNRC 50-305	2001
V.C. Summer	USNRC 50-395	2001
St. Lucie	USNRC 50-335, 50-389	2002
Turkey Point	USNRC 50-250, 251	2002

Recognizing that the analysis work effort must deal with both stress and displacement criteria, the sequence of model development and analysis steps that are undertaken are summarized in the following:

a. Prepare 3-D dynamic rack/platform coupled models suitable for a time-history analysis. Include all fluid coupling interactions and mechanical coupling appropriate to performing an accurate non-linear simulation.

b. Perform 3-D dynamic analyses on various physical conditions (such as coefficient of friction and extent of cells containing fuel assemblies). Archive appropriate displacement and load outputs from the dynamic model for post-processing.

c. Perform stress analysis of high stress areas for the limiting case of all the rack dynamic analyses. Demonstrate compliance with ASME Code Section III, Subsection NF limits.

6.5.2 Rack/Platform Coupled Dynamic Model

The dynamic modeling of the rack structure is prepared with special consideration of all nonlinearities and fluid effects inherent to the physical problem. Particulars of modeling details and assumptions for the analysis of racks are summarized below.

a. The cask pit rack structure motion is captured by modeling the rack as a 12 degree-of-freedom structure. Movement of the rack cross-section at any height is described by six degrees-of-freedom of the rack base and six degrees-of-freedom at the rack top with appropriate bending and shear springs [6.5.3] providing the structural connectivity between the lumped masses. The cask pit platform is modeled, beneath the rack, as a six degree-of-freedom rigid body with appropriate overall dimensions and mass properties.

b. Fuel assemblies that are free to rattle within the rack are modeled by five lumped masses located at H, 0.75H, 0.5H, 0.25H, and at the rack base (H is the rack height measured above the baseplate). Each lumped fuel mass has two horizontal displacement degrees-of-freedom. Vertical motion of the fuel assembly mass is assumed equal to rack vertical motion at the baseplate level. The centroid of each fuel assembly mass can be located off-center, relative to the rack structure centroid at that level, to simulate a partially loaded rack (see Figure 6.5.1).

c. Seismic motion of a fuel rack is characterized by random rattling of fuel assemblies in their individual storage locations. All fuel assemblies are assumed to move in-phase within a rack. This exaggerates computed dynamic loading on the rack structure and, therefore, yields conservative results.

d. Fluid coupling between rack and fuel assemblies, and between rack and wall, is simulated by appropriate inertial coupling in the system kinetic energy. Inclusion of these effects uses the methods of references [6.5.4-6.5.8].

e. Fluid damping and form drag are conservatively neglected.

f. Because the top of the rack is over 25' below the pool's free water surface, the sloshing effect is negligible in the water mass surrounding the rack and, therefore, neglected in the rack dynamic model.

g. Potential impacts between the cell walls of the new rack and the contained fuel assemblies are accounted for by appropriate compression-only gap elements between masses involved (see Figure 6.5.2).

h. The cask pit rack is connected to the cask pit platform structure at each corner by a pair of tension-only springs that represent the axial stiffnesses of the connector links.

i. Each rack support pedestal is linked to its support structure by two piece-wise linear orthogonally-disposed friction springs. In addition, the lateral motion of each of the four rack support pedestals in the horizontal direction is constrained by the clearance gap with the recessed holes in the platform.

j. Rattling of fuel assemblies inside the storage locations causes the gap between fuel assemblies and cell wall to change from a maximum of twice the nominal gap to a theoretical zero gap. Fluid coupling coefficients are based on the nominal gap in order to provide a conservative measure of fluid resistance to gap closure.

Table 6.5.2 provides a complete listing of each of the 28 degrees-of-freedom for the rack/platform model. Six translational and six rotational degrees-of-freedom (three of each type on each end) describe the motion of the rack structure. Rattling fuel mass motions (shown at nodes 1^*, 2^*, 3^*, 4^*, and 5^* in Figure 6.5.1) are described by ten horizontal translational degrees-of-freedom (two at each of the five fuel masses). The vertical fuel mass motion is assumed (and modeled) to be the same as that of the rack baseplate. The five masses are connected to each other by an axially rigid member, which enables the fuel masses to vibrate in unison with the rack in the vertical direction. Therefore, the masses represented by the fuel assemblies vibrate independently in the horizontal direction and are driven by the inertia loads and local impact loads. The five fuel masses are connected to the rack model via impact gap elements. Impact loads between the fuel masses and the rack cell wall are obtained upon closure of this gap element. The gap dimensions are determined at each time step by establishing the independent displacements of the fuel masses and the rack geometric centerline displacement corresponding

to the same elevation. Therefore, the outer boxes surrounding the fuel masses shown in Figure 6.5.2 depict the inside of the fuel cell. The final six degrees-of-freedom are assigned to the platform. The interface between the cask pit rack and the platform is modeled by a series of gap elements and friction springs at the correct locations, which simulate the rack support pedestals, connector links, and recessed holes in the platform.

Table 6.5.2

Degrees-of-Freedom

LOCATION (Node)	DISPLACEMENT			ROTATION		
	U_x	U_y	U_z	θ_x	θ_y	θ_z
1	p_1	p_2	p_3	q_4	q_5	q_6
2	p_7	p_8	p_9	q_{10}	q_{11}	q_{12}
3	p_{23}	p_{24}	p_{25}	q_{26}	q_{27}	q_{28}
Node 1 is assumed to be attached to the rack at the bottom most point. Node 2 is assumed to be attached to the rack at the top most point. Node 3 is assumed to be attached to the platform at its centroid. Refer to Figures 6.5.1 and 6.5.3 for node identification.						
2*	p_{13}	p_{14}				
3*	p_{15}	p_{16}				
4*	p_{17}	p_{18}				
5*	p_{19}	p_{20}				
1*	p_{21}	p_{22}				

where the relative displacement variables q_i are defined as:

$p_i = q_i(t) + U_x(t)$ $\quad i = 1, 7, 13, 15, 17, 19, 21, 23$

$= q_i(t) + U_y(t)$ $\quad i = 2, 8, 14, 16, 18, 20, 22, 24$

$= q_i(t) + U_z(t)$ $\quad i = 3, 9, 25$

$= q_i(t)$ $\quad i = 4, 5, 6, 10, 11, 12, 26, 27, 28$

p_i denotes absolute displacement (or rotation) with respect to inertial space

q_i denotes relative displacement (or rotation) with respect to the floor slab

* denotes fuel mass nodes

U(t) are the three known earthquake displacements

Finally, to eliminate the uncertainty in rack/platform dynamic analyses because of the uncertainty in the extent of friction at the pedestal/platform and platform/liner interfaces, multiple simulations are performed by adjusting the friction coefficient. These friction coefficients are chosen consistent with the two bounding extremes from Rabinowicz's data [6.5.9]†.

6.5.3 Governing Equations of Motion

Using the structural model discussed in the foregoing, equations of motion corresponding to each degree-of-freedom are obtained using Lagrange's Formulation [6.5.2, 6.5.3]. The system kinetic energy includes contributions from solid structures and from trapped and surrounding fluid. The final system of equations obtained have the matrix form:

$$[M]\left[\frac{d^2q}{dt^2}\right]=[Q]+[G]$$

where:

- [M] - total mass matrix (including structural and fluid mass contributions). The size of this matrix will be 28 x 28.
- q - the nodal displacement vector relative to the pool slab displacement (the term with q indicates the second derivative with respect to time, i.e., acceleration)
- [G] - a vector dependent on the given ground acceleration
- [Q] - a vector dependent on the spring forces (linear and nonlinear) and the coupling between degrees-of-freedom

† The coefficient of friction (μ) between the pedestal supports and the bearing pad is indeterminate. According to Rabinowicz [6.5.9], results of 199 tests performed on austenitic stainless steel plates submerged in water show a mean value of μ to be 0.503 with standard deviation of 0.125. Upper and lower bounds (based on twice standard deviation) are 0.753 and 0.253, respectively. Analyses are therefore performed for coefficient of friction values of 0.2 (lower limit) and for 0.8 (upper limit). The bounding values of μ = 0.2 and 0.8 have been found to envelope the upper limit of module response in previous rerack projects.

The above column vectors have a length of 28. The equations can be rewritten as follows:

$$\left[\frac{d^2q}{dt^2}\right] = [M]^{-1}[Q] + [M]^{-1}[G]$$

This equation set is mass uncoupled, displacement coupled at each instant in time. The numerical solution uses a central difference scheme built into the proprietary computer program DYNARACK [6.5.1].

6.6 Acceptance Criteria

6.6.1 Kinematic and Stress Acceptance Criteria

There are two sets of criteria to be satisfied by the rack modules:

a. Kinematic Criteria

Although the OT Position Paper [6.1.2] does not prohibit impact between the rack and neighboring structures, such impact is not permitted under any of the four earthquake scenarios under the kinematic acceptance criteria conservatively set down for the new rack.

b. Stress Criteria

The stress limits applicable to the rack structure are derived from the ASME Code, Section III, Subsection NF [6.3.1]. The terminology used hereunder is in accordance with the ASME Code.

(i) Normal and Upset Conditions (Level A or Level B)

a. Allowable stress in tension on a net section is:

$F_t = 0.6\ S_y$

Where, S_y = yield stress at temperature, and F_t is equivalent to primary membrane stress.

b. Allowable stress in shear on a net section is:

$F_v = .4\ S_y$

c. Allowable stress in compression on a net section is given by:

$$F_a = S_y\left(.47 - \frac{k\ell}{444\,r}\right)$$

where kl/r for the main rack body is based on the full height and cross section of the honeycomb region and does not exceed 120 for all sections.

l = unsupported length of component

k = length coefficient which gives influence of boundary conditions. The following values are appropriate for the described end conditions:

= 1 (simple support both ends)

= 2 (cantilever beam)

= 0.5 (clamped at both ends)

r = radius of gyration of component

d. Maximum allowable bending stress at the outermost fiber of a net section, due to flexure about one plane of symmetry is:

$F_b = 0.60\ S_y$ (equivalent to primary bending)

e. Combined bending and compression on a net section satisfies:

$$\frac{f_a}{F_a} + \frac{C_{mx}\,f_{bx}}{D_x\,F_{bx}} + \frac{C_{my}\,f_{by}}{D_y\,F_{by}} < 1$$

where:

f_a = Direct compressive stress in the section

f_{bx} = Maximum bending stress along x-axis

f_{by} = Maximum bending stress along y-axis

C_{mx} = 0.85

C_{my} = 0.85

D_x = $1 - (f_a/F'_{cx})$

D_y = $1 - (f_a/F'_{cy})$

$F'_{cx,cy}$ = $(\pi^2 E)/(2.15\ (kl/r)^2_{x,y})$

E = Young's Modulus

and subscripts x,y reflect the particular bending plane.

f. Combined flexure and compression (or tension) on a net section:

$$\frac{f_a}{0.6S_y}+\frac{f_{bx}}{F_{bx}}+\frac{f_{by}}{F_{by}}<1.0$$

The above requirements are to be met for both direct tension or compression.

g. Welds

Allowable maximum shear stress on the net section of a weld is given by:

$$F_w = 0.3\ S_u$$

where S_u is the weld material ultimate strength at temperature. For fillet weld legs in contact with base metal, the shear stress on the gross section is limited to $0.4S_y$, where S_y is the base material yield strength at the service temperature.

(ii) Level D Service Limits

Based on Section F-1334 (ASME Section III, Appendix F) [6.6.1], the limits for the Level D condition are the smaller of 1.2 (S_y/F_t) or ($0.7S_u/F_t$) times the corresponding limits for the Level A condition. S_u is ultimate tensile stress at the specified rack design temperature.

Exceptions to the above general multiplier are the following:

a) Stresses in shear shall not exceed the lesser of $0.72S_y$ or $0.42S_u$. In the case of the material used here, $0.72S_y$ governs.

b) Axial Compression Loads shall be limited to 2/3 of the calculated buckling load.

c) Combined Axial Compression and Bending - The equations for Level A conditions shall apply except that:

F_a = 0.667 x Buckling Load/ Gross Section Area,

and the terms F'_{cx} and F'_{cy} may be increased by the factor 1.65.

d) For welds, the Level D allowable maximum weld stress is not specified in Appendix F of the ASME Code. An appropriate limit for weld throat stress is conservatively set here as:

$F_w = 0.3\ S_u\ f$

where:

f = (Level D shear stress limit)/(Level A shear stress limit)

6.6.2 Dimensionless Stress Factors

As is customary in fuel rack stress analysis, the stress results are presented in dimensionless form. Dimensionless stress factors are defined as the ratio of the actual developed stress to the specified limiting value. The limiting value of each stress factor is 1.0.

The applicable stress factors are:

R_1 = Ratio of direct tensile or compressive stress on a net section to its allowable value (note pedestals only resist compression)

R_2 = Ratio of gross shear on a net section in the x-direction to its allowable value

R_3 = Ratio of maximum x-axis bending stress to its allowable value for the section

R_4 = Ratio of maximum y-axis bending stress to its allowable value for the section

R_5 = Combined flexure and compressive factor (as defined in the foregoing)

R_6 = Combined flexure and tension (or compression) factor (as defined in the foregoing)

R_7 = Ratio of gross shear on a net section in the y-direction to its allowable value

6.6.3 Allowable g-Load on the Stored Fuel

The permissible lateral load on an irradiated fuel assembly has been studied by the Lawrence Livermore National Laboratory. The LLNL report [6.6.2] states that "...for the most vulnerable fuel assembly, the axial buckling load varies from 82g's at initial storage to 95g's after 20 years storage. In a side drop, no yielding is expected below 63g's at initial storage to 74g's after 20 years {dry} storage." The most significant load on the fuel assembly arises from rattling during the seismic event.

6.7 Key Input Data and Dynamic Simulations

6.7.1 Key Input Data

The principal input data used in the seismic analysis of the cask pit rack and platform are summarized in Table 6.7.1 below.

Table 6.7.1

PRINCIPAL INPUT DATA

Item	Value
Weight of empty rack, (lb)	27,200
Height of rack above baseplate, H (inch)	169
Number of storage cells in the N-S direction †	12
Number of storage cells in the E-W direction †	13
Nominal height of support pedestal	Per Table 2.5.1
Storage rack prismatic envelope ††, (inch)	107.9 x 116.8
Storage cell prismatic (square) opening, (inch)	8.75
Weight of fuel assembly, (lb)	1,616
Material properties of structural components	Per Table 6.7.2
Structural damping (percent of critical) DE	2%
Structural damping (percent of critical) DDE and HOSGRI	4%
Structural damping (percent of critical) LTSP	5%
Weight of platform, (lb)	28,775
Height of platform, (inch)	54.1
Planar dimensions of platform, (inch)	117 x 117

† Two corner cells are eliminated from each rack, as shown in Figures 1.0.1 and 1.0.2, to avoid interference with the cask restraint system.

†† The prismatic envelope is defined as the rectangular envelope, including verticality tolerances, but not including poison, sheathing or baseplate extensions.

The input quantities presented in Table 6.7.1, wherever applicable, are bounding values rather than nominal data to maximize response. Thus, for example, assuming an upper bound weight of the rack, platform, and fuel are cited because increased inertia translates into increased inertial response to seismic excitations.

The racks will be constructed of stainless steel material. The cell wall, baseplate, sheathing and female pedestal materials will all be made form SA 240, Type 304L. The male pedestals are subjected to higher stresses than the remainder of the rack components, since these members support the weight of the loaded rack and are often subjected to simultaneous axial and bending moments. The male support pedestals and the connector links will be fabricated from SA 564-630, which provides greater strength. The mechanical properties of the rack material are defined in Table 6.7.2 below.

Table 6.7.2

RACK MATERIAL PROPERTY DATA*
(ASME - Section II, Part D)

Material	Young's Modulus E (psi)	Yield Strength S_y (psi)	Ultimate Strength Su (psi)
SA240, Type 304L S.S.	27.6×10^6	21,300	66,200
SUPPORT MATERIAL DATA (200°F)			
SA240, Type 304L (upper part of support feet)	27.6×10^6	21,300	66,200
SA-564-630 (lower part of support feet; age hardened at 1100°F)	28.5×10^6	106,300	140,000
CONNECTOR LINK MATERIAL DATA (200°F)			
SA-564-630 (connector link; age hardened at 1100°F)	28.5×10^6	106,300	140,000
SA240, Type 304L (connector link nut)	27.6×10^6	21,300	66,200

* Properties correspond to the reference metal temperature = 200°F.

6.7.2 Dynamic Simulations

The plurality of earthquakes, the wide range of coefficients of friction, and the potential of a variable extent of storage cells loaded suggest the need for multiple dynamic simulations. Table 6.7.3 lists the individual scenarios that are analyzed to establish the margins of safety.

Table 6.7.3

DYNAMIC SIMULATION SCENARIOS

Scenario Number	Earthquake I.D.	Fuel Storage Configuration	Coefficient of Friction	ASME Code Service Condition
1.	DE	Full	0.2	Level B †
2.	DE	Full	0.8	Level B
3.	DE	Half Loaded (Diagonally)	0.2	Level B
4	DE	Half Loaded (Diagonally)	0.8	Level B
5.	DE	Half Loaded (E-W)	0.2	Level B
6.	DE	Half Loaded (E-W)	0.8	Level B
7.	DE	Half Loaded (N-S)	0.2	Level B
8.	DE	Half Loaded (N-S)	0.8	Level B
9.	DE	Nearly Empty	0.2	Level B
10.	DE	Nearly Empty	0.8	Level B
11.	DDE	Full	0.2	Level D
12.	DDE	Full	0.8	Level D
13.	DDE	Half Loaded (Diagonally)	0.2	Level D
14.	DDE	Half Loaded (Diagonally)	0.8	Level D
15.	DDE	Half Loaded (E-W)	0.2	Level D
16.	DDE	Half Loaded (E-W)	0.8	Level D
17.	DDE	Half Loaded (N-S)	0.2	Level D
18.	DDE	Half Loaded (N-S)	0.8	Level D
19.	DDE	Nearly Empty	0.2	Level D
20.	DDE	Nearly Empty	0.8	Level D
21.	HOSGRI	Full	0.2	Level D
22.	HOSGRI	Full	0.8	Level D
23.	HOSGRI	Half Loaded (Diagonally)	0.2	Level D
24.	HOSGRI	Half Loaded (Diagonally)	0.8	Level D
25.	HOSGRI	Half Loaded (E-W)	0.2	Level D
26.	HOSGRI	Half Loaded (E-W)	0.8	Level D
27.	HOSGRI	Half Loaded (N-S)	0.2	Level D

† The evaluation conservatively used normal (Level A) condition allowable stresses for all DE seismic cases.

Table 6.7.3

DYNAMIC SIMULATION SCENARIOS

Scenario Number	Earthquake I.D.	Fuel Storage Configuration	Coefficient of Friction	ASME Code Service Condition
28.	HOSGRI	Half Loaded (N-S)	0.8	Level D
29.	HOSGRI	Nearly Empty	0.2	Level D
30.	HOSGRI	Nearly Empty	0.8	Level D
31.	LTSP	Full	0.2	Level D
32.	LTSP	Full	0.8	Level D
33.	LTSP	Half Loaded (Diagonally)	0.2	Level D
34.	LTSP	Half Loaded (Diagonally)	0.8	Level D
35.	LTSP	Half Loaded (E-W)	0.2	Level D
36.	LTSP	Half Loaded (E-W)	0.8	Level D
37.	LTSP	Half Loaded (N-S)	0.2	Level D
38.	LTSP	Half Loaded (N-S)	0.8	Level D
39.	LTSP	Nearly Empty	0.2	Level D
40.	LTSP	Nearly Empty	0.8	Level D
41.	HOSGRI	Full	0.2	Level D
42.	HOSGRI	Full	0.8	Level D

Scenario Nos. 41 and 42 are identical to Scenario Nos. 21 and 22 except that the compression-only gap elements that represent the sixteen (16) platform lateral shims (refer to Figure 6.5.3) are preloaded to simulate the restraint of thermal expansion due to a bounding pool water temperature rise of 181°F.

6.8 Margins Against Kinematic and Stress Limits

6.8.1 Satisfaction of Kinematic Acceptance Criteria

All of the dynamic simulations listed in Table 6.7.3 show that the cask pit rack does not impact the neighboring cask pit walls or the restraint structure at *any* point in time. The ratio of the available gap to the maximum kinematic excursion towards the proximate structure is in excess of 3 in every simulation. Therefore, the prescribed criterion of no impact with adjacent structure is satisfied with large margins.

Finally, the cask pit platform structure, which serves to stage the rack, is not found to lift off the liner surface due to existence and arrangement of the 16 support shims located between the platform and cask pit wall liner.

6.8.2 Satisfaction of Stress Acceptance Criteria

As is typical of all "honeycomb connected construction" modules [6.5.2] the locations of maximum stress in the cask pit rack are (i) the base of the cell wall, just above the baseplate, (ii) the support pedestal-to-baseplate junction (welds) and (iii) the threaded joint in the adjustable pedestals. In addition, in the case of the cask pit rack, the axial stress in the connector links is a candidate for potential stress exceedance. Finally, for the stored fuel, the maximum deceleration "g" load sustained by the fuel due to its rattling in the storage cell during the seismic event is a matter of safety concern.

As described in Subsection 6.6, the margin of safety in fuel rack dynamic simulations is expressed in terms of dimensionless ratios of actual stress to allowable stress, referred to as stress factors. Table 6.8.1 provides the maximum value of stress factors for each of the Table 6.7.3 simulation scenarios at each of the above-mentioned vulnerable locations in the fuel rack.

Table 6.8.1

MAXIMUM STRESS FACTORS AT CRITICAL LOCATIONS IN THE CASK PIT RACK

Scenario	Seismic Event	Maximum Computed Stress Factor (Maximum Allowable Value = 1.0)				Maximum g-load experienced by the fuel (Allowable is 63g's, per Subsection 6.6.4)
		Base of Rack Cell Walls	Female Support Pedestal	Female Pedestal Threads	Rack-to-Platform Connector Links	
1.	DE	0.425	0.069	0.679	0.145	1.042
2.	DE	0.434	0.067	0.704	0.173	0.978
3.	DE	0.220	0.040	0.369	0.120	0.874
4.	DE	0.244	0.043	0.402	0.150	0.869
5.	DE	0.218	0.040	0.365	0.113	0.965
6.	DE	0.242	0.043	0.405	0.157	0.983
7.	DE	0.216	0.040	0.366	0.116	0.871
8.	DE	0.239	0.042	0.401	0.154	0.965
9.	DE	0.049	0.008	0.080	0.031	0.938
10.	DE	0.050	0.010	0.085	0.040	0.896
11.	DDE	0.259	0.042	0.436	0.183	1.785
12.	DDE	0.275	0.043	0.455	0.215	1.817
13.	DDE	0.125	0.022	0.242	0.107	1.614
14.	DDE	0.157	0.031	0.273	0.149	1.624
15.	DDE	0.131	0.023	0.237	0.105	1.542
16.	DDE	0.166	0.034	0.282	0.157	1.713
17.	DDE	0.130	0.022	0.223	0.102	1.540
18.	DDE	0.157	0.030	0.273	0.145	1.582
19.	DDE	0.029	0.005	0.047	0.025	1.572
20.	DDE	0.039	0.008	0.081	0.063	1.597
21.	HOSGRI	0.362	0.054	0.555	0.282	2.587

Table 6.8.1

MAXIMUM STRESS FACTORS AT CRITICAL LOCATIONS IN THE CASK PIT RACK

Scenario	Seismic Event	Maximum Computed Stress Factor (Maximum Allowable Value = 1.0)				Maximum g-load experienced by the fuel (Allowable is 63g's, per Subsection 6.6.4)
		Base of Rack Cell Walls	Female Support Pedestal	Female Pedestal Threads	Rack-to-Platform Connector Links	
22.	HOSGRI	0.386	0.077	0.612	0.413	2.926
23.	HOSGRI	0.198	0.028	0.287	0.152	2.500
24.	HOSGRI	0.243	0.058	0.391	0.293	2.606
25.	HOSGRI	0.168	0.025	0.273	0.128	2.490
26.	HOSGRI	0.236	0.058	0.375	0.285	2.834
27.	HOSGRI	0.196	0.027	0.273	0.125	2.465
28.	HOSGRI	0.241	0.059	0.389	0.299	2.639
29.	HOSGRI	0.031	0.005	0.048	0.028	2.649
30.	HOSGRI	0.048	0.011	0.085	0.065	2.649
31.	LTSP	0.341	0.063	0.636	0.308	2.010
32.	LTSP	0.410	0.085	0.761	0.469	1.993
33.	LTSP	0.176	0.034	0.349	0.165	2.079
34.	LTSP	0.247	0.048	0.470	0.277	2.163
35.	LTSP	0.177	0.034	0.349	0.165	2.092
36.	LTSP	0.247	0.046	0.470	0.277	2.327
37.	LTSP	0.177	0.034	0.346	0.165	2.092
38.	LTSP	0.247	0.047	0.470	0.277	2.193
39.	LTSP	0.035	0.006	0.063	0.043	1.980
40.	LTSP	0.064	0.015	0.130	0.109	2.017
41.	HOSGRI	0.332	0.058	0.586	0.323	2.490
42.	HOSGRI	0.387	0.089	0.640	0.481	2.941

It is evident from the summary results compiled in Table 6.8.1 that there is considerable margin in the stress factors against the allowable limit, and that the maximum "g" load experienced by the spent fuel is a fraction of the allowable.

The interface loads between the racks and the platform, obtained from the dynamic analyses, were applied to the platform to evaluate its stress compliance. Results of the stress analysis using the maximum interface loads from the totality of the dynamic simulations are presented, again, in terms of dimensionless stress factors in Table 6.8.2, which indicate large margins of safety.

Table 6.8.2

MAXIMUM STRESS FACTORS IN THE PLATFORM UNDER LIMITING INTERFACE LOADS FROM THE TABLE 6.7.3 DYNAMIC SIMULATIONS

Region	Maximum Stress Factor
Corner Support Plates	0.556
Corner Lock Plates	0.833
Welds	0.833
Mainframe	0.769

6.9 Assessment of Margin Against Fatigue Failure

The dynamic simulations described in the foregoing showed that the cask pit rack behaves primarily as a nonlinear cantilevered structure when subjected to 3-D seismic excitations. In addition to the pulsations in the vertical load at each pedestal, lateral friction forces at the pedestal/platform interface, which help prevent or mitigate lateral sliding of the rack, also exert a time-varying moment in the baseplate region of the rack. The friction-induced lateral forces act simultaneously in x and y directions with the requirement that their vectorial sum does not exceed μV, where μ is the limiting interface coefficient of friction and V is the concomitant vertical thrust on the support surface (at the *given* time instant). As the vertical thrust at a pedestal location changes, so does the maximum friction force, F, that the interface can exert. In other words, the lateral force at the pedestal/platform interface, F, is given by

$$F \leq \mu N(\tau)$$

where N (vertical thrust) is the time-varying function of τ. F does not always equal μN; rather, μN is the maximum value it can attain at any time; the actual value, of course, is determined by the dynamic equilibrium of the rack structure. If the above inequality is not satisfied then the pedestal slides, resulting in a confinement reaction from the platform recess surface. In summary, the reaction force at the pedestal/support interface is a function of time; its magnitude and direction of action varies during the earthquake event.

The time-varying lateral (horizontal) and vertical forces on the extremities of the support pedestals produce stresses at the root of the pedestals in the manner of an end-loaded cantilever. The stress field in the cellular region of the rack is quite complex, with its maximum values located in the region closest to the pedestal. The maximum magnitude of the stresses depends on the severity of the pedestal end loads and on the geometry of the pedestal/rack baseplate region.

Alternating stresses in metals produce metal fatigue if the amplitude of the stress cycles is sufficiently large. In high-density racks designed for sites with moderate to high postulated seismic action, the stress intensity amplitudes frequently reach values above the material endurance limit, leading to expenditure of the fatigue "usage" reserve in the material.

Because the locations of maximum stress (viz., the rack support pedestals and connector links) and the close placement of racks, a post-earthquake inspection of the high stressed regions in the racks is not feasible. Therefore, the racks must be engineered to withstand multiple earthquakes without reliance of nondestructive inspections for post-earthquake integrity assessment. The fatigue life evaluation of racks is an integral aspect of rack safety evaluation.

The time-history method of analysis, deployed in the evaluation of the rack structure, provides the means to obtain a complete cycle history of the stress intensities in the highly stressed regions of the rack. Having determined the amplitude of the stress intensity cycles and their number, the cumulative damage factor, U, can be determined using the classical Miner's rule:

$$U = \Sigma \frac{n_i}{N_i}$$

where n_i is the number of stress intensity cycles of amplitude σ_i, and N_i is the permissible number of cycles corresponding to σ_i from the ASME fatigue curve for the material of construction. U must be less than or equal to 1.0.

Using the archived results of the spent fuel rack dynamic analyses enables a time-history of stress intensity to be established at the most limiting location. This permits establishing a set of alternating stress intensity ranges versus cycles. Following ASME Code guidelines for computing U, it is found that U = 0.513 due to the combined effect of one SSE (see note below) and twenty OBE events. This is well below the ASME Code limit of 1.0.

Note: LTSP results, where governing, have conservatively been used in lieu of Hosgri and DDE results in determining the value for U.

6.10 References

[6.1.1] USNRC NUREG-0800, Standard Review Plan, June 1987.

[6.1.2] (USNRC Office of Technology) "OT Position for Review and Acceptance of Spent Fuel Storage and Handling Applications", dated April 14, 1978, and January 18, 1979 amendment thereto.

[6.3.1] ASME Boiler & Pressure Vessel Code, Section III, Subsection NF, 1989 Edition.

[6.5.1] A.I. Soler, "DYNARACK Validation Manual", Holtec Report No. HI-91700 (1991).

[6.5.2] Soler, A.I. and Singh, K.P., "Seismic Responses of Free Standing Fuel Rack Constructions to 3-D Motions", Nuclear Engineering and Design, Vol. 80, pp. 315-329 (1984).

[6.5.3] Levy, S. and Wilkinson, J.P.D., "The Component Element Method in Dynamics with Application to Earthquake and Vehicle Engineering," McGraw Hill, 1976.

[6.5.4] Singh, K.P. and Soler, A.I., "Dynamic Coupling in a Closely Spaced Two-Body System Vibrating in Liquid Medium: The Case of Fuel Racks," 3rd International Conference on Nuclear Power Safety, Keswick, England, May 1982.

[6.5.5] Soler, A.I. and Singh, K.P., "Some Results from Simultaneous Seismic Simulations of All Racks in a Fuel Pool", INNM Spent Fuel Management Seminar X, January 1993.

[6.5.6] Paul, B., "Fluid Coupling in Fuel Racks: Correlation of Theory and Experiment", (Proprietary), Holtec Report HI-88243.

[6.5.7] Fritz, R.J., "The Effects of Liquids on the Dynamic Motions of Immersed Solids," Journal of Engineering for Industry, Trans. of the ASME, February 1972, pp 167-172.

[6.5.8] Singh, K.P. and Soler, A.I., "Seismic Qualification of Free Standing Nuclear Fuel Storage Racks - the Chin Shan Experience, Nuclear Engineering International, UK (March 1991).

[6.5.9] Rabinowicz, E., "Friction Coefficients of Water Lubricated Stainless Steels for a Spent Fuel Rack Facility," MIT, a report for Boston Edison Company, 1976.

[6.6.1] ASME Boiler & Pressure Vessel Code, Section III, Appendices, 1989 Edition.

[6.6.1] UCID-21246, "Dynamic Impact Effects on Spent Fuel Assemblies, Lawrence Livermore National Laboratory, dated October 20, 1987.

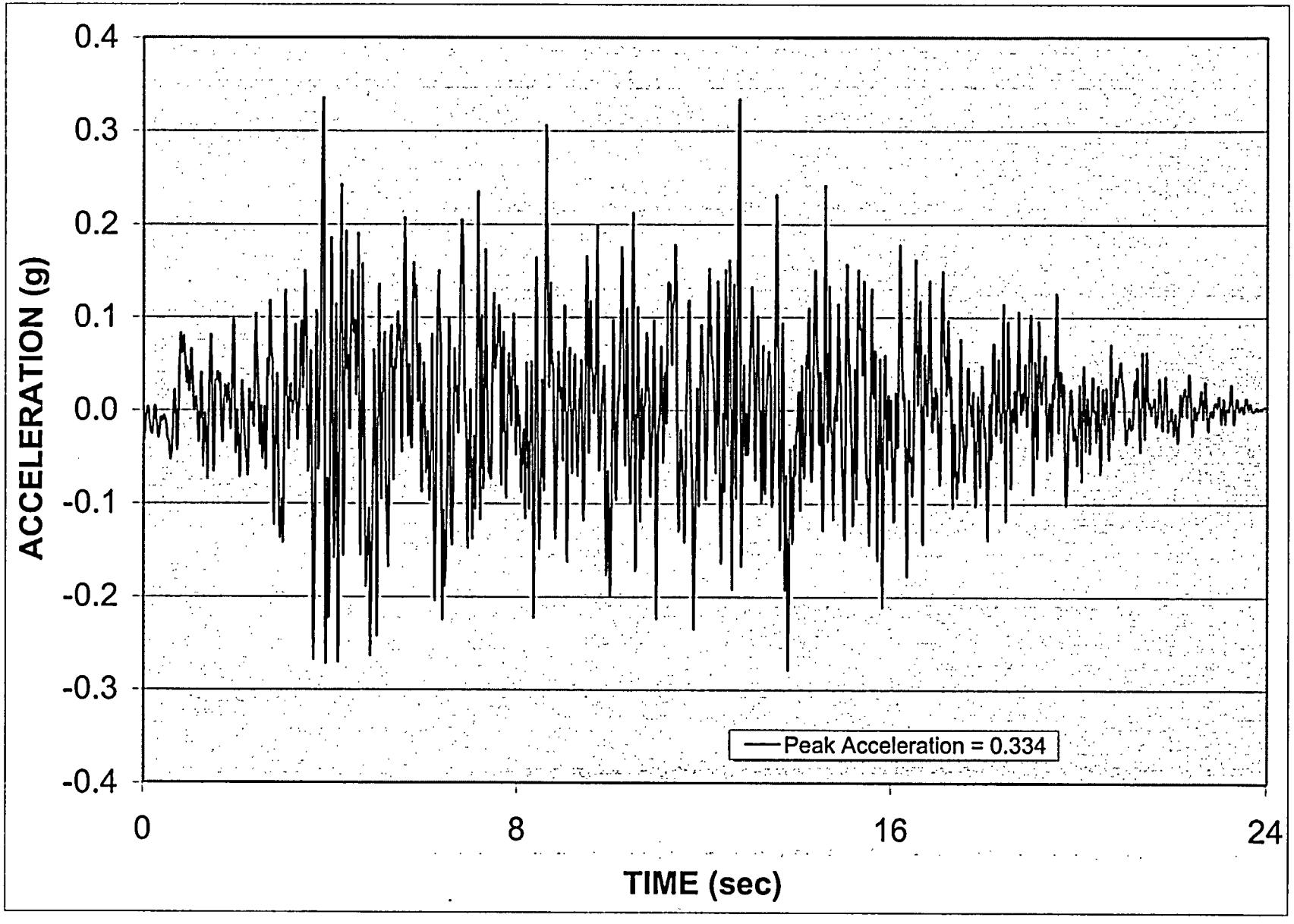

FIGURE 6.4.1
ACCELERATION TIME HISTORY DE-X

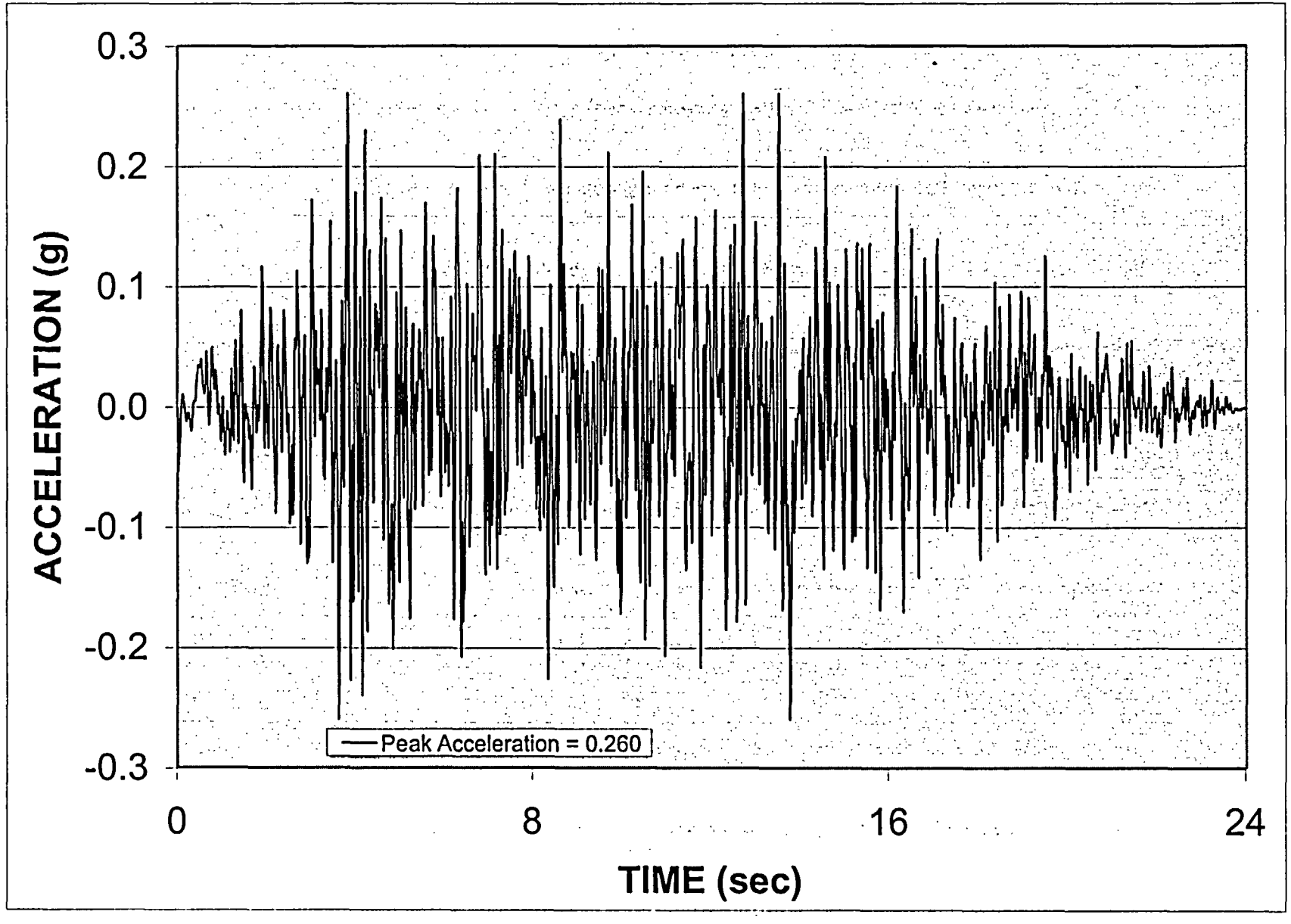

FIGURE 6.4.2
ACCELERATION TIME HISTORY DE-Y

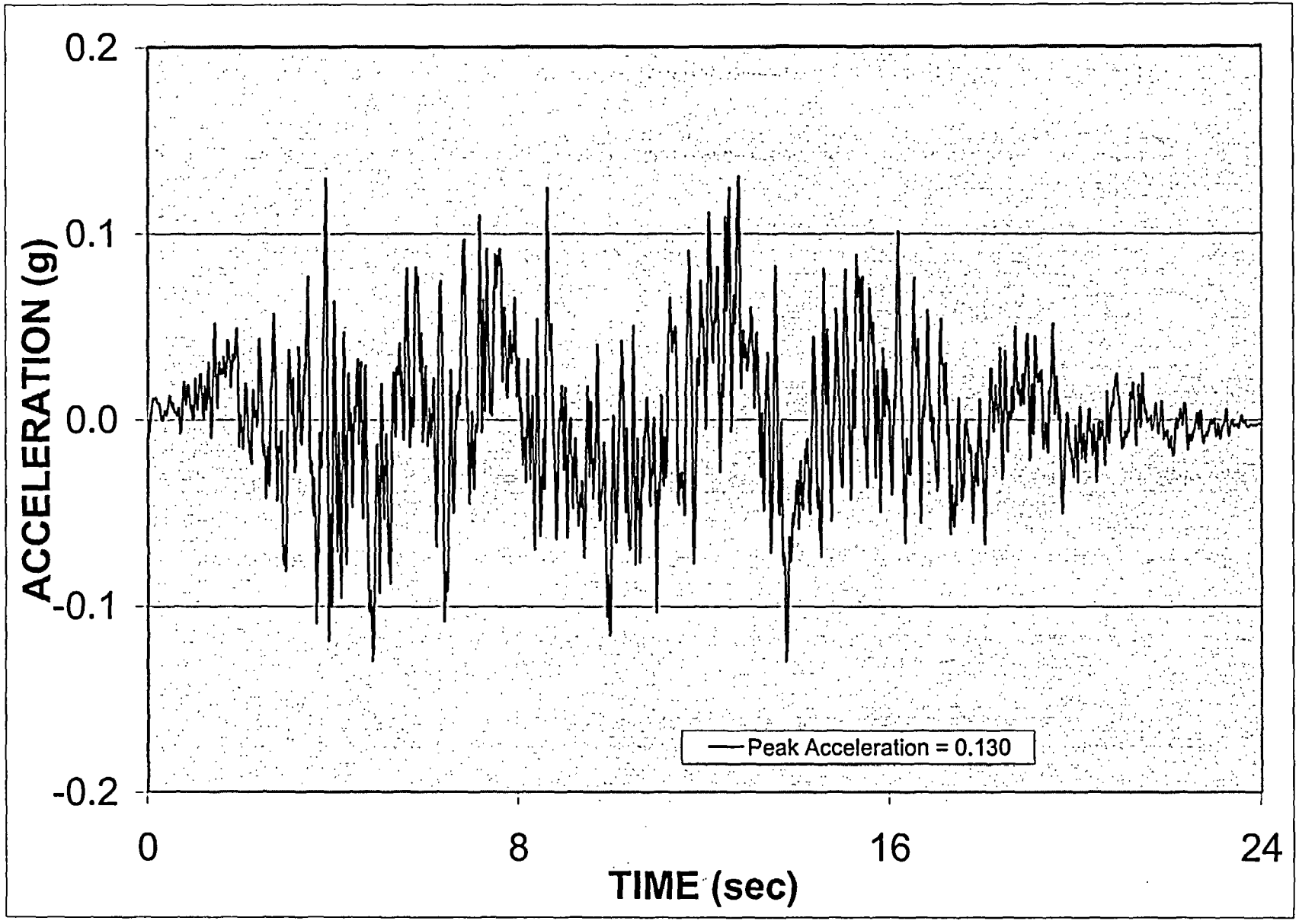

FIGURE 6.4.3
ACCELERATION TIME HISTORY DE-VT

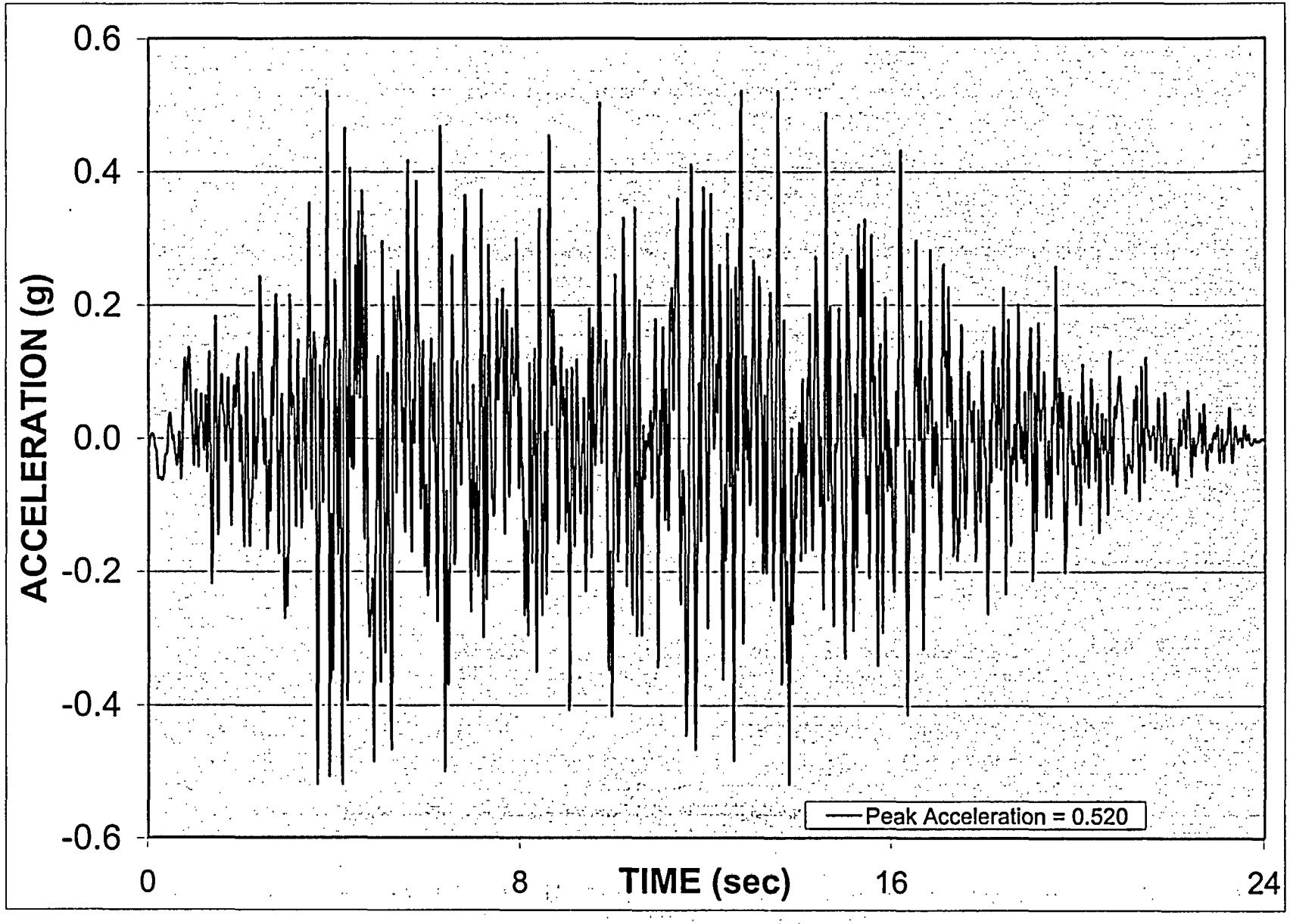

FIGURE 6.4.4
ACCELERATION TIME HISTORY DDE-E/W

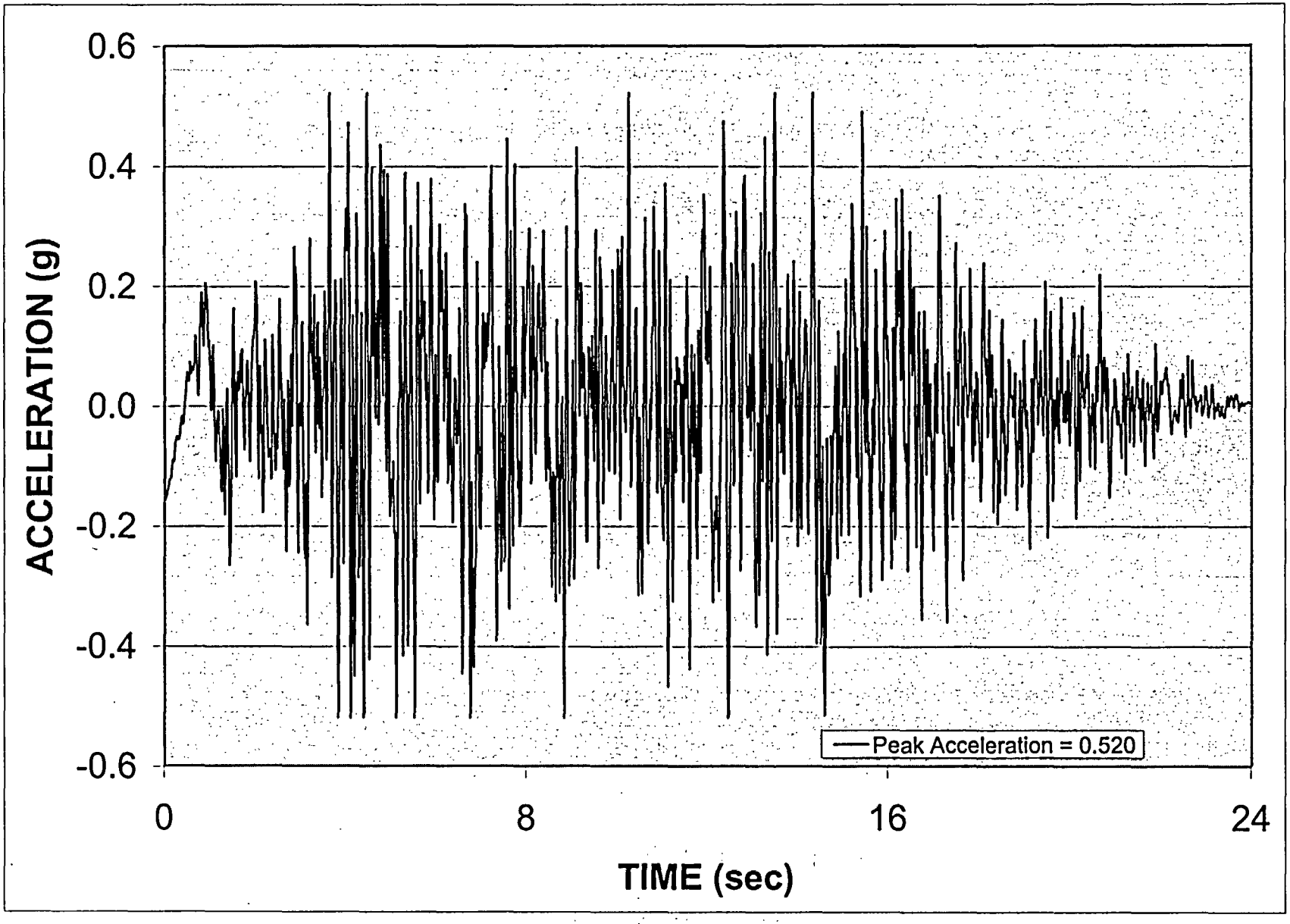

FIGURE 6.4.5
ACCELERATION TIME HISTORY DDE-N/S

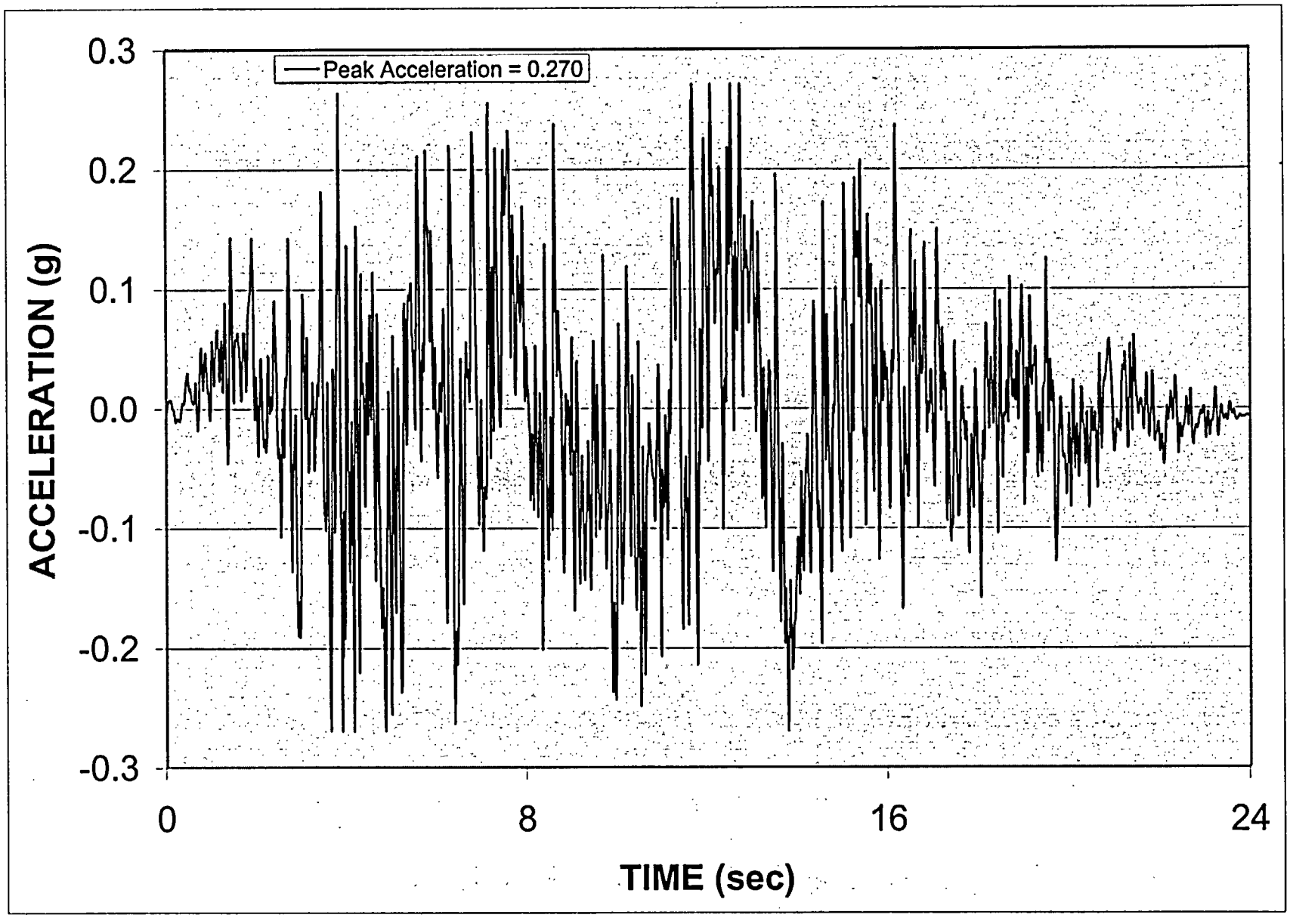

FIGURE 6.4.6
ACCELERATION TIME HISTORY DDE-VT

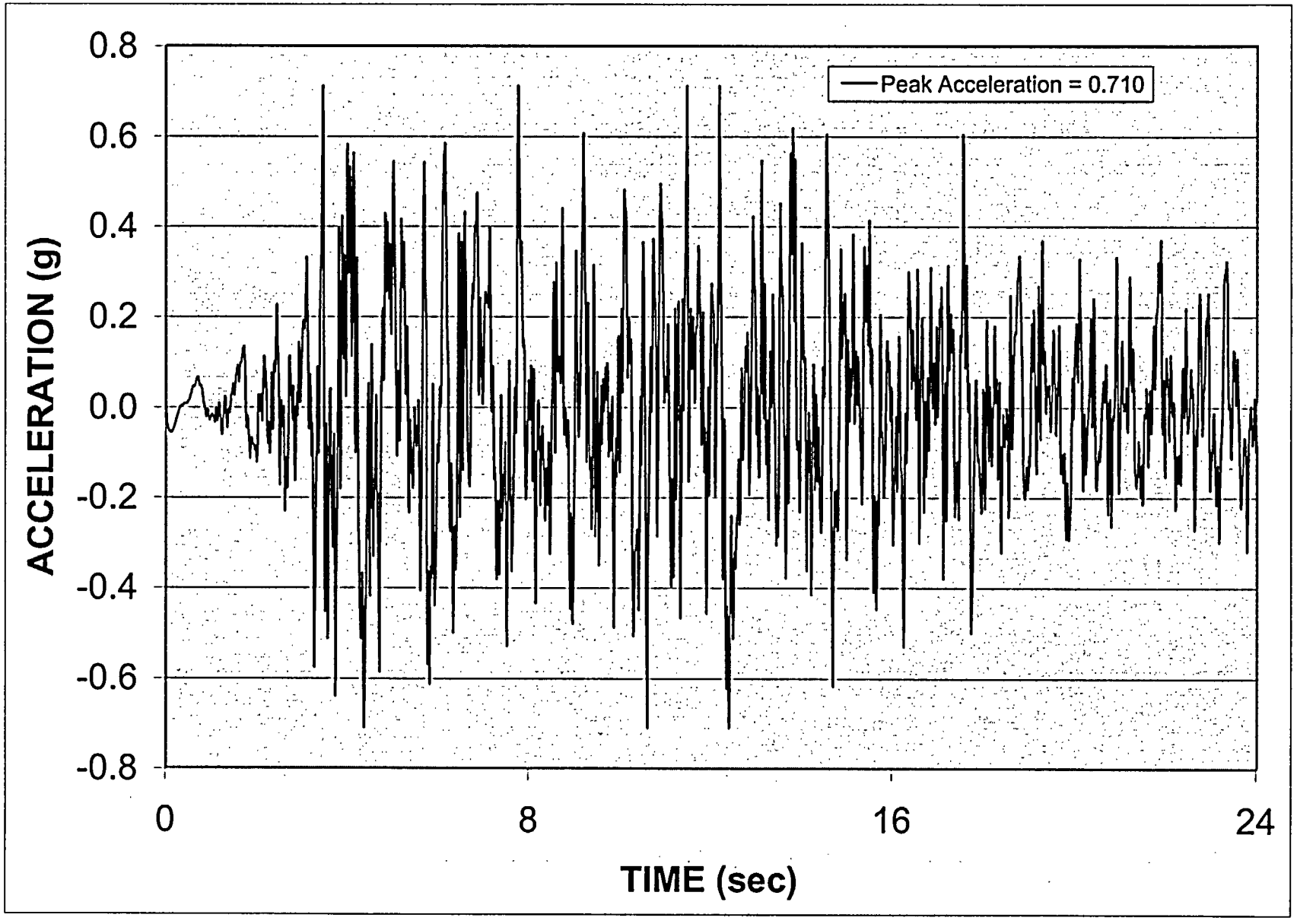

FIGURE 6.4.7
ACCELERATION TIME HISTORY HOSGRI-X

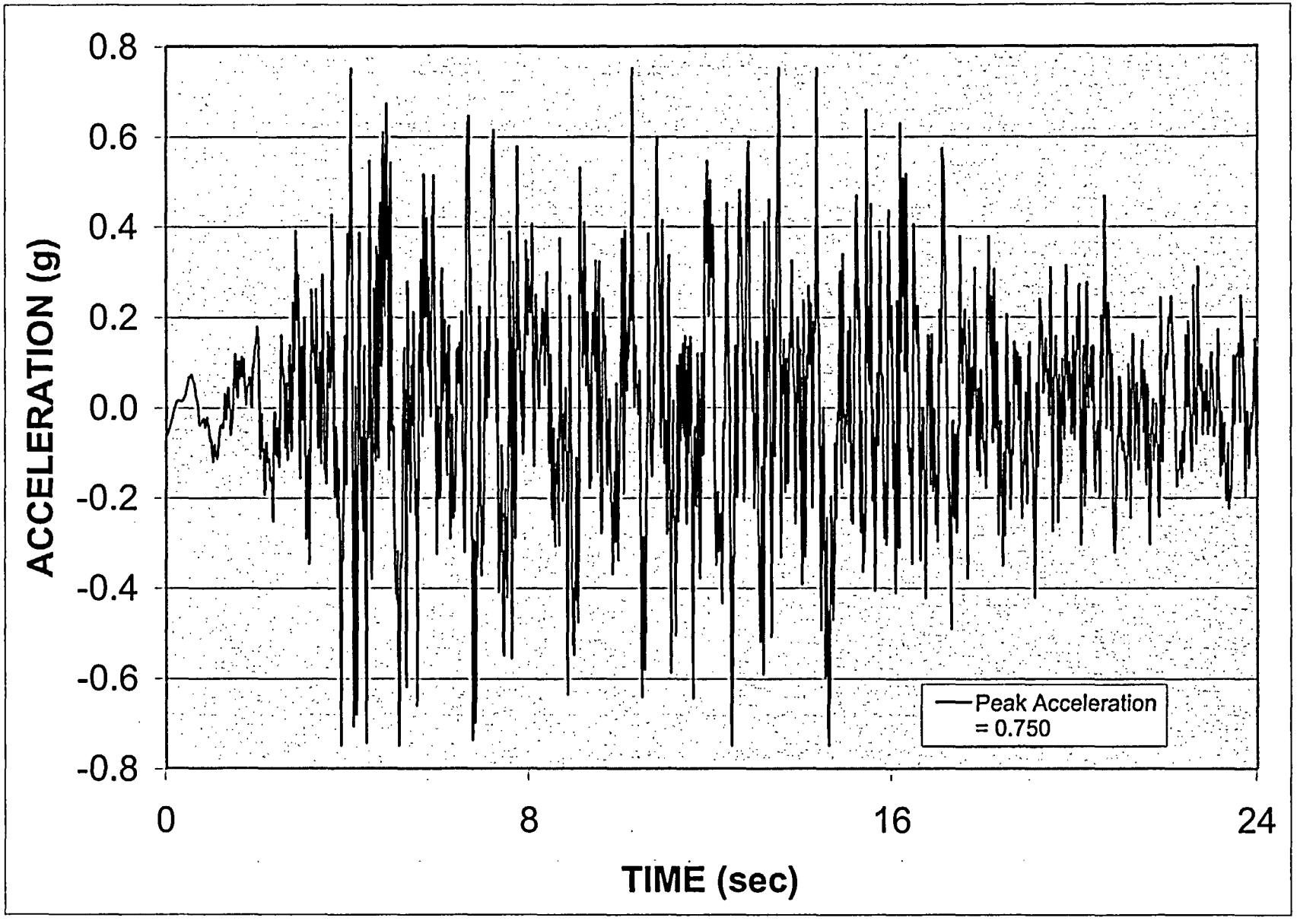

FIGURE 6.4.8
ACCELERATION TIME HISTORY HOSGRI-Y

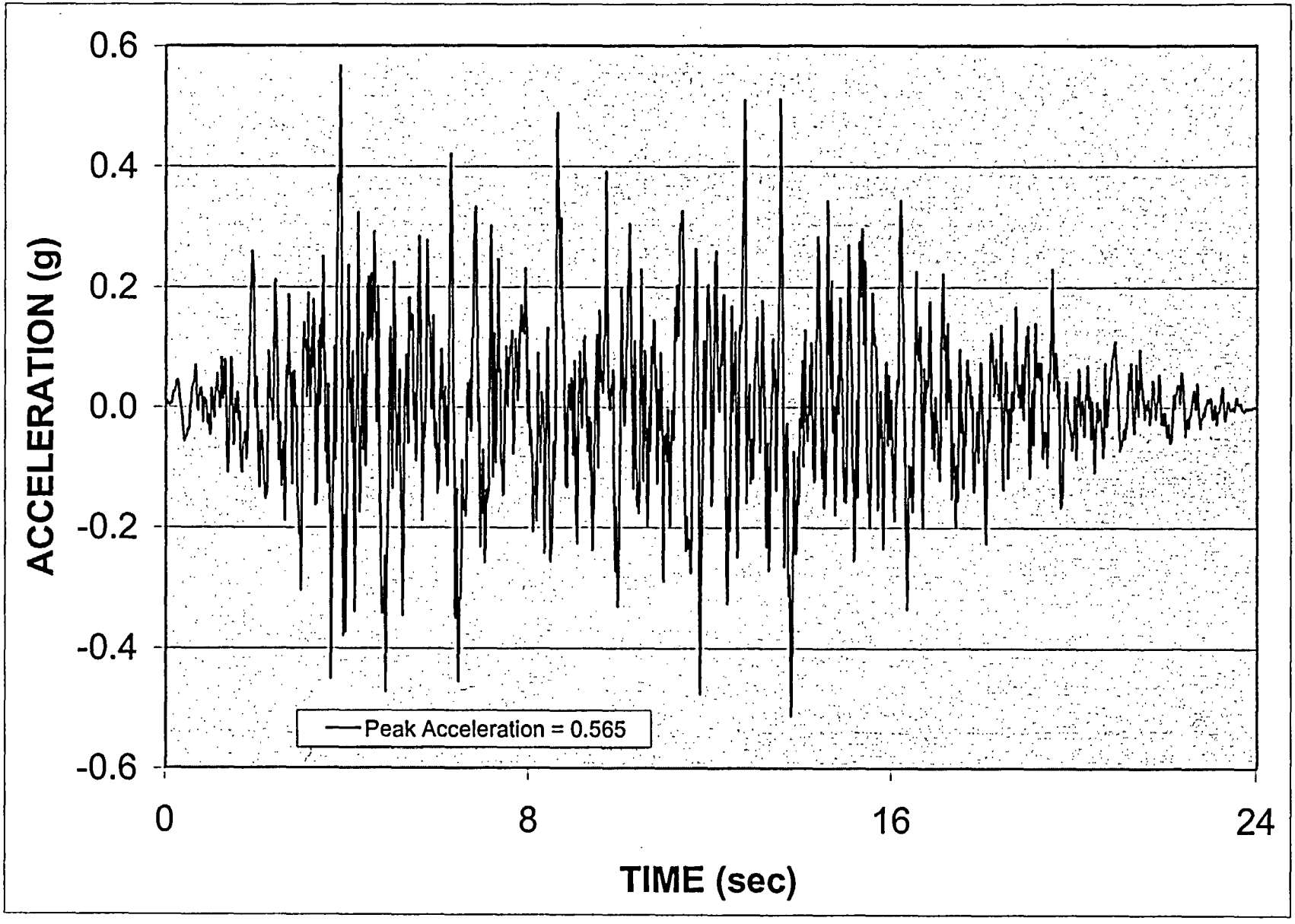

FIGURE 6.4.9
ACCELERATION TIME HISTORY HOSGRI-VT

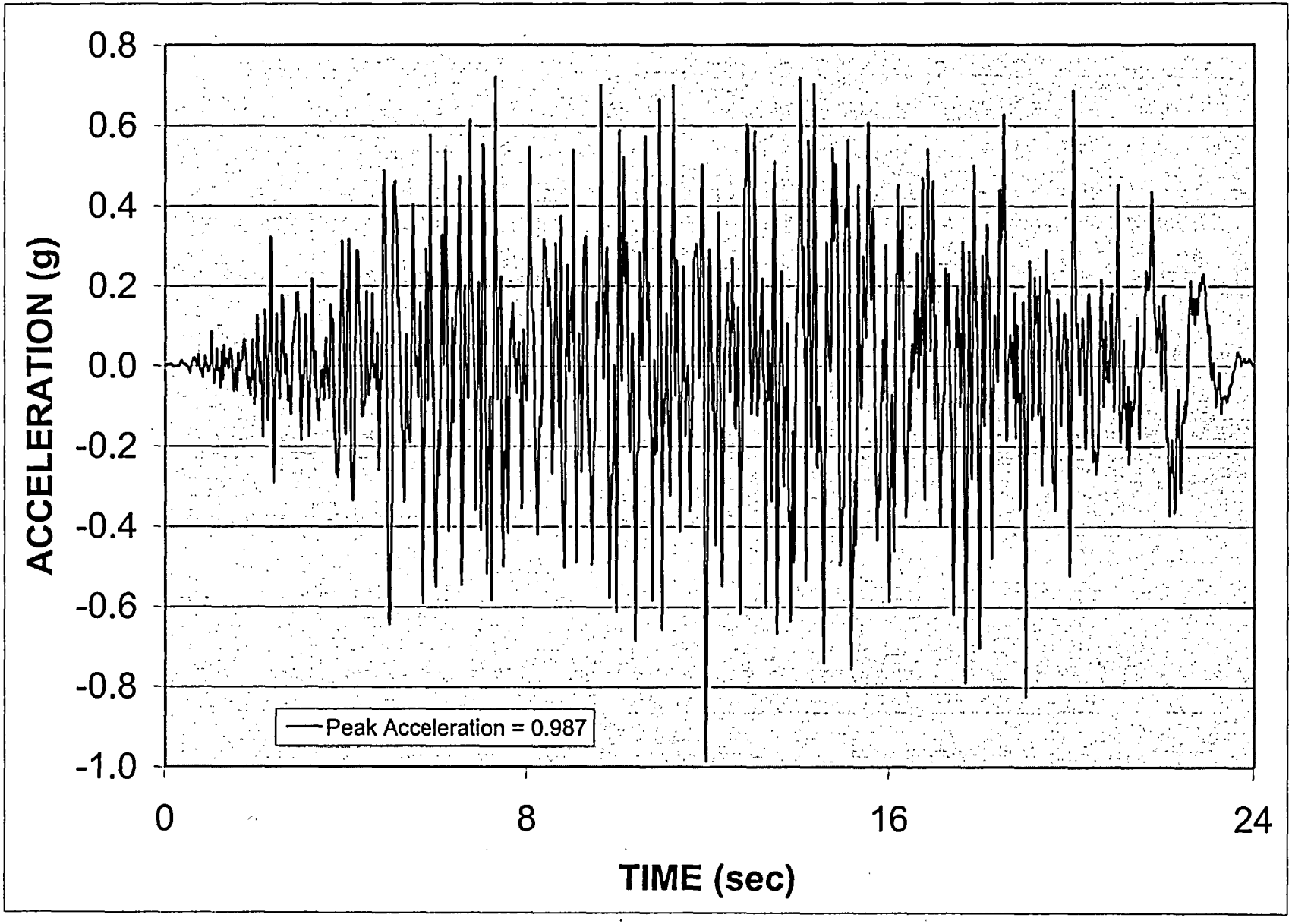

FIGURE 6.4.10
ACCELERATION TIME HISTORY LTSP-EW

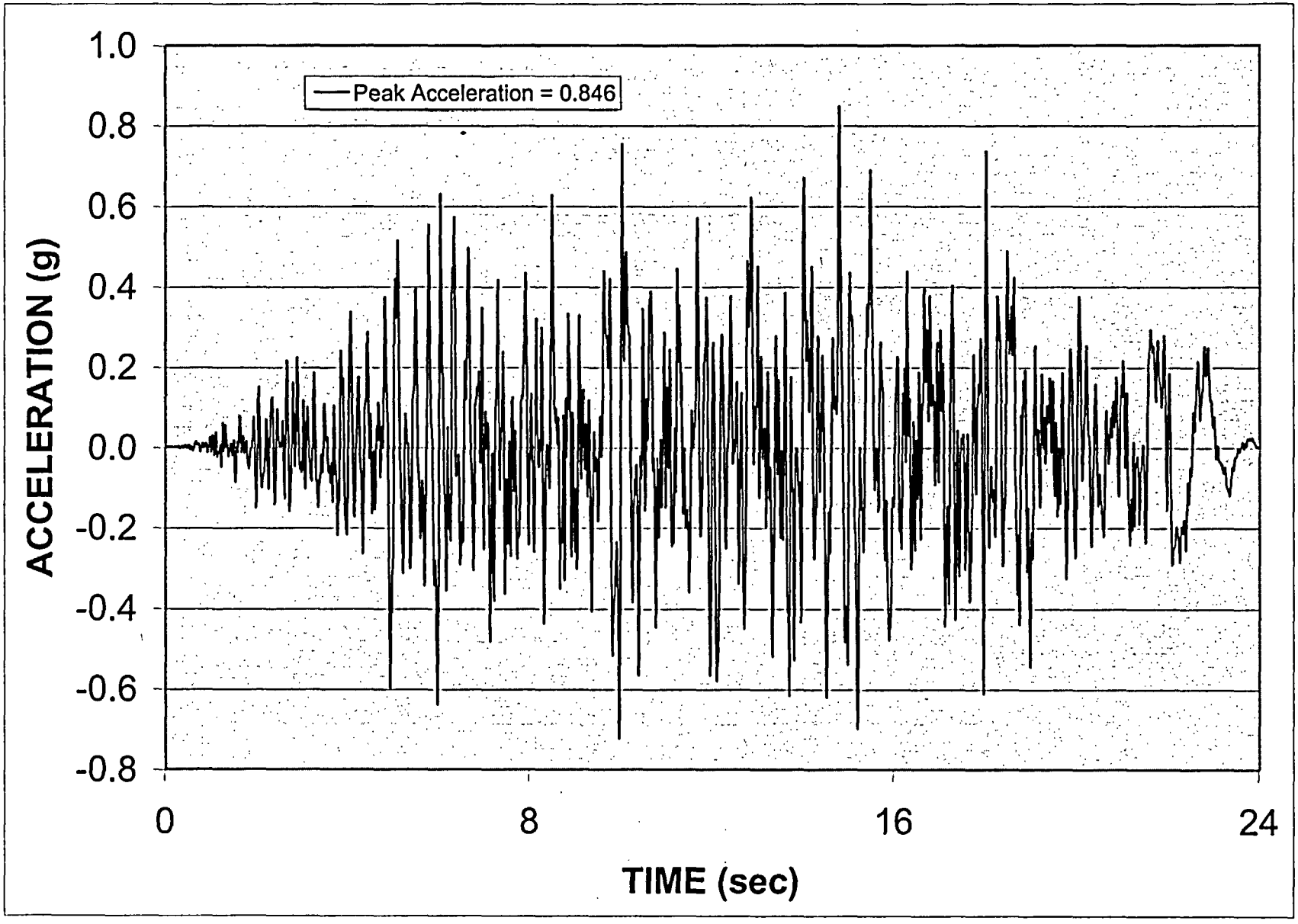

FIGURE 6.4.11
ACCELERATION TIME HISTORY LTSP-NS

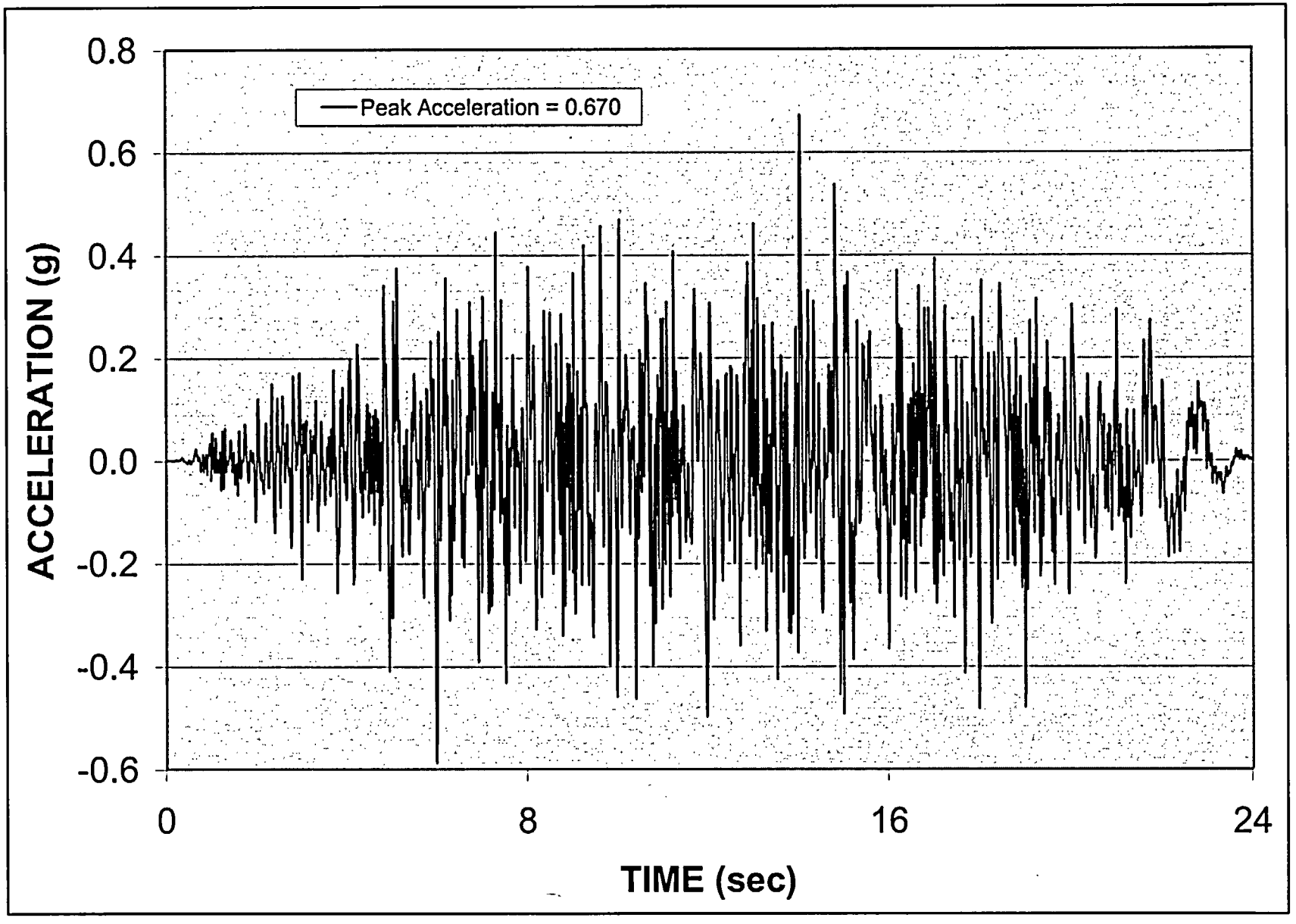

FIGURE 6.4.12
ACCELERATION TIME HISTORY LTSP-VT

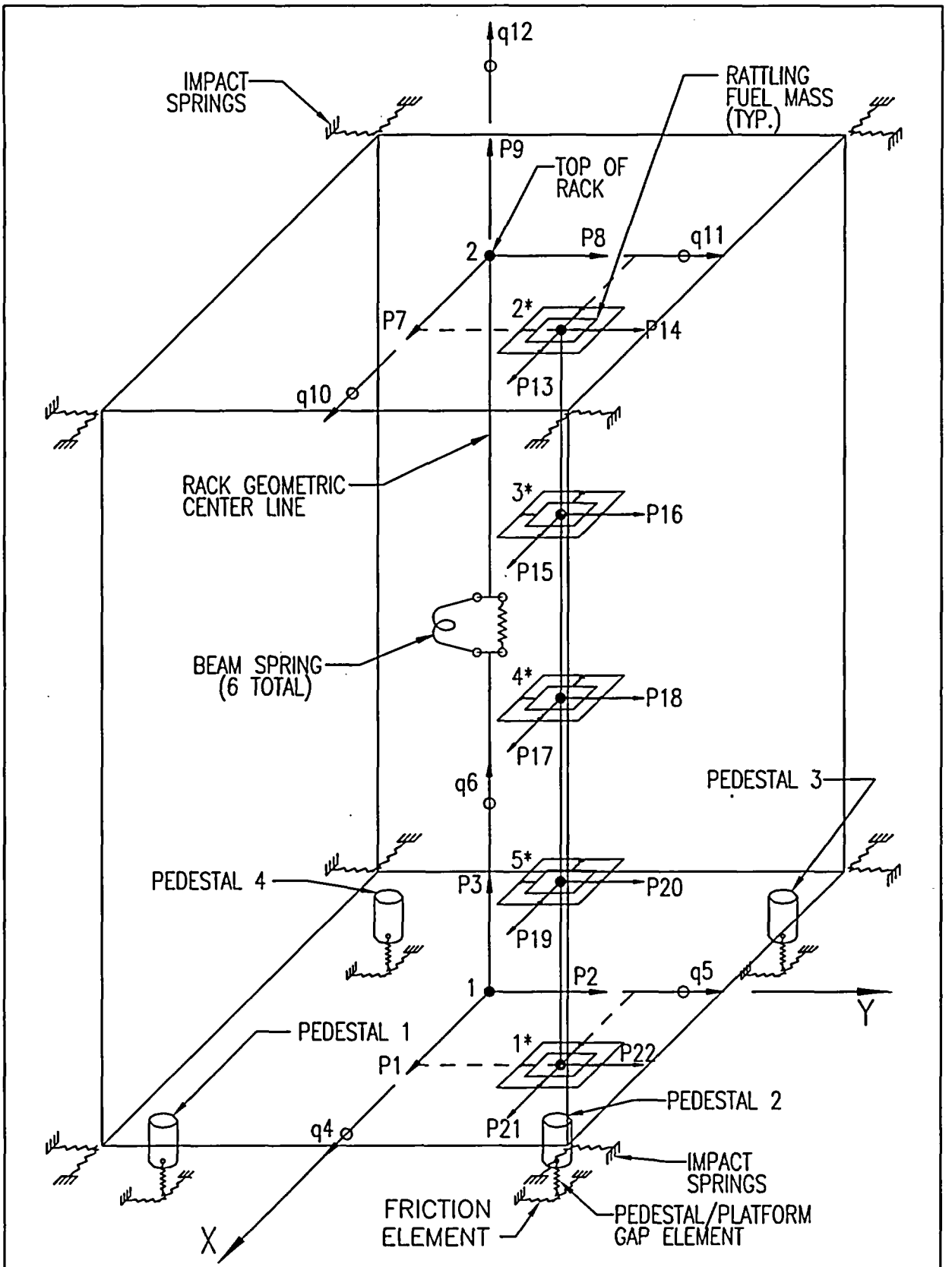

FIGURE 6.5.1; SCHEMATIC OF THE DYNAMIC MODEL OF A SINGLE RACK MODULE USED IN DYNARACK

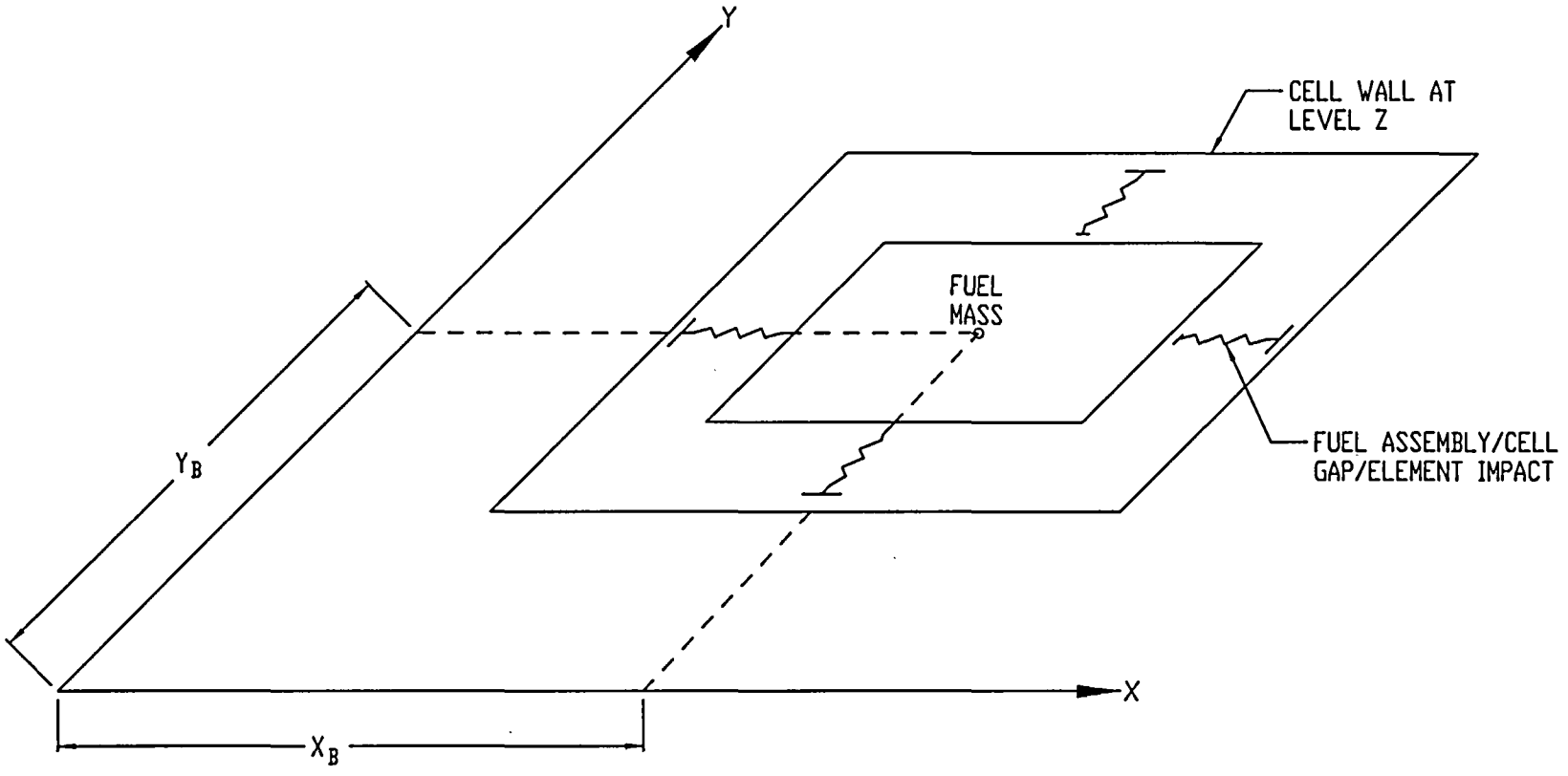

FIGURE 6.5.2; FUEL-TO-RACK GAP/IMPACT ELEMENTS AT LEVEL OF RATTLING MASS

G:\DRAWINGS\0-FIGURES\1368\REPORT-HI-2043162\CHP_6\FIGURE6.5.2

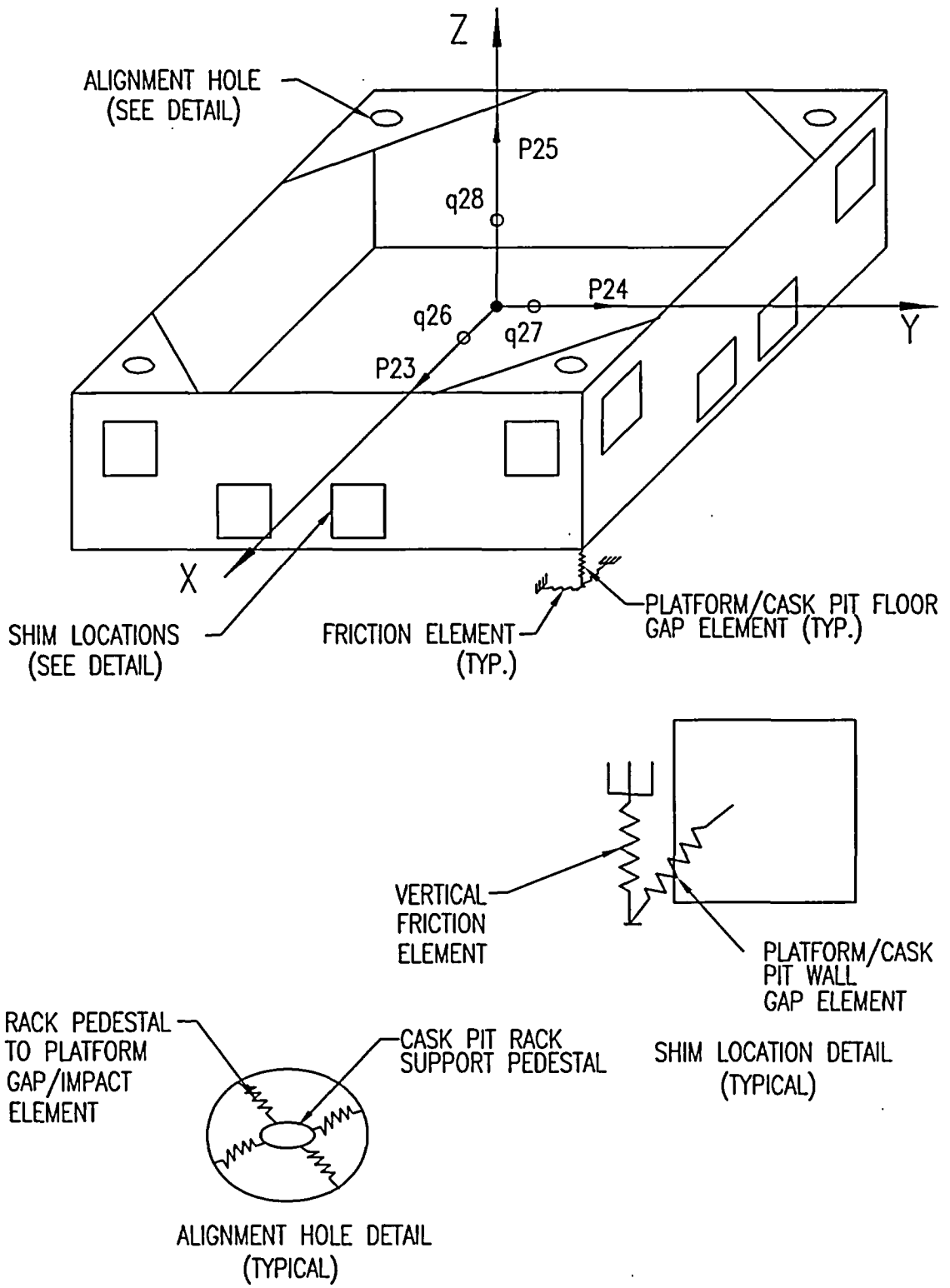

FIGURE 6.5.3; SCHEMATIC OF THE DYNAMIC MODEL OF CASK PIT RACK PLATFORM USED IN DYNARACK

7.0 MECHANICAL ACCIDENTS

7.1 Introduction

The USNRC OT position paper [7.1.1] specifies that the rack design must ensure the functional integrity of the spent fuel racks and the pool under all credible mechanical drop events. This chapter contains synopses of the analyses carried out to demonstrate the regulatory compliance of the proposed racks under postulated accidental drop events germane to the Spent Fuel Pool (SFP) Cask Loading Area (CLA) in Diablo Canyon Power Plant (DCPP), Units 1 and 2.

The proposed change does not alter assumptions or results under the current DCPP licensing basis on the potential fuel damage due to mechanical accidents.

7.2 Description of Mechanical Accidents

Analyses are performed to evaluate the damage to the new cask pit rack, the pool liner, and the concrete slab in the cask pit area subsequent to the impact of a fuel assembly, a rack or a rack platform under various drop scenarios. Four categories of fuel assembly, rack and rack accidental drop events are considered.

In the so-called "shallow" drop event, a fuel assembly, along with the portion of handling tool, which is severable in the case of a single element failure, is assumed to drop vertically and hit the top of a rack cell. Inasmuch as the new racks are of honeycomb construction, the deformation produced by the impact is expected to be confined to the region of collision. However, the "depth" of damage to the affected cell walls must be demonstrated to remain limited to the portion of the cell above the top of the "active fuel region", which is essentially the elevation of the top of the Metamic neutron absorber. Stated in quantitative terms, this criterion implies that the plastic deformation of the cell walls should not extend more than $15^{15}/_{16}$ inches (downwards) from the top. In order to utilize an upper bound of kinetic energy at impact, the impact is assumed to be a fuel assembly and its handling tool (3,000 lbs) and the free-fall height is conservatively assumed to be 3 feet [7.2.1].

It is readily apparent from the description of the rack modules in Section 3 that the impact resistance of a rack at its periphery is considerably less than its interior. Accordingly, the limiting shallow drop scenario, which would produce maximum cell wall deformation, consists of the case where the fuel assembly impacts the peripheral wall of a cell on the periphery of the rack. Figure 7.2.1 depicts the finite element model used to evaluate this scenario.

The second class of drop event postulates that a fuel assembly falls through an empty storage cell impacting the fuel assembly support surface (i.e., rack baseplate) as schematically shown in Fig. 7.2.2. This so-called "deep" drop event threatens the structural integrity of the baseplate. If the baseplate is pierced, and the fuel assembly impacts the rack platform or the liner, then the liner integrity is at risk and water could leak from the pool. The deformed baseplate may also lead to an abnormal condition of the enriched zone of fuel assembly outside the "poisoned" space of the fuel rack. To preclude damage to the pool liner and to avoid the potential of an abnormal fuel storage configuration in the aftermath of a deep drop event, it is required that the baseplate remain unpierced and that the maximum lowering of the baseplate is shown to be acceptable by the criticality evaluations (see Section 4 for further discussion). Note that a dropped fuel assembly may hit the rack baseplate over a supporting pedestal resulting in significant impact on the floor. However, this deep drop scenario is bounded by the rack drop accident as described below in terms of damage to the SFP floor, and therefore is not directly evaluated.

As discussed in Section 3.5, DCPP plan to upgrade the FHB crane to meet single failure proof requirements prior to installation of the new cask pit rack and support platform. Although not required to be postulated as drop accidents, the third and fourth drop events were analyzed for defense-in-depth. The third and fourth classes of drop events assume that a lifted empty rack and a rack platform fall from the top of the SFP water level and impact the floor of the cask pit, respectively. The structural integrity of the SFP liner and the concrete slab in the cask pit area must be demonstrated to be maintained in the rack and rack platform drop events. The acceptance criterion for both the third and fourth drop events is that the pool structure must not be damaged (i.e., develop through-thickness cracks in the concrete slab or punch through the liner and the underlying steel plate) leading to uncontrolled water leakage. Figures 7.2.3 and 7.2.4 depict the rack and platform drop events, respectively.

7.3 Incident Impact Velocity

7.4 Mathematical Model

In the first step of the solution process, the velocity of the dropped object (impactor) is computed for the condition of underwater free fall in the manner of the formulation presented in the above section. Table 7.4.1 contains the computed velocities for the various drop events.

The physical properties of material types undergoing deformation in the postulated impact events are summarized in Table 7.4.2.

7.5 Results

7.5.1 Shallow Drop Event

For the shallow drop event, the dynamic analysis shows that the top of the impacted region undergoes localized plastic deformation. Figure 7.5.1 shows an isometric view of the post-impact geometry of the rack. The maximum depth of plastic deformation is limited to 15.5 inches, which is slightly smaller than the design limit of $15^{15}/_{16}$ inches. It should be pointed out that the weld connection between the inner surface of the impacted cell wall and the adjacent cell is not considered in the model; the actual plastically crushed depth would be significantly smaller than the predicted value if this additional weld connection were considered in the rack model. Therefore, it can be concluded that the damage of the fuel cell due to a shallow drop event does not extend into the active fuel region of any stored fuel.

7.5.2 Deep Drop Events

The deep drop through an interior cell does produce some deformation of the baseplate with local severing of the baseplate/cell wall welds. Figure 7.5.2 shows the deformed baseplate configuration. The fuel assembly support surface is instantaneously lowered by a maximum of 3.55 inches during the impact process. The deformation of the rack baseplate has been determined to be acceptable with respect to lowering the fuel seating position and the resulting criticality consequences, as discussed in Chapter 4.0.

7.5.3 Rack Drop Event

The liner plate experiences a maximum plastic strain of 0.019 in the rack drop accident, as shown in Figure 7.5.3, which is much smaller than the failure strain of the liner material (0.38). The damage to the slab is local and limited to the small area on the concrete surface as demonstrated in Figure 7.5.4, which imposes no structural threat to the cast pit slab. Since the pool floor can maintain its overall integrity and the liner is not breached in the drop event, there will be no abrupt or uncontrollable loss of water from the pool.

7.5.4 Rack Platform Drop Event

The platform drop does not result in through-thickness cracks in the slab as shown in Figure 7.5.5, indicating that the pool floor can maintain its overall integrity. It should be pointed out that the predicted concrete response to the platform impact is very conservative, since the slab reinforcement, which is not considered in the analysis, would significantly suppress the cracks especially at the slab periphery. The liner plate experiences a maximum plastic strain of 0.014 in the rack platform drop accident, as shown in Figure 7.5.6, which is much smaller than the failure strain of the liner material (0.38). Since the liner is not breached in the drop event, there will be no abrupt or uncontrollable loss of water from the pool.

7.6 Conclusion

The drop events postulated for the DCPP SFP were analyzed and found to produce localized damage within the design limits for the racks. The shallow drop event is found to produce some localized plastic deformation in the top of the storage cell, but the region of permanent strain is limited to the portion of the rack structure situated above the top of the active fuel region. The analysis of the deep drop event at cell locations selected to maximize baseplate deformation indicates that the maximum downward displacement of the baseplate is limited to 3.55 inches, which ensures that fuel will remain in a subcritical condition. As previously stated, the consequences of a deep-drop scenario where a fuel assembly enters a cell directly above a rack support pedestal are bounded by the rack drop evaluation. The analyzed rack drop event indicates that the pedestal axial load precludes liner damage and prevents a breach in the integrity of the concrete floor slab. Therefore, there will be no uncontrollable loss of pool water inventory. Similar to the rack drop, the postulated rack platform drop event is also found to be acceptable, since the structural integrity of both the liner plate and concrete slab is not compromised by the accident. In conclusion, the new Holtec spent fuel rack for the DCPP cask pit possess acceptable margins of safety under the postulated mechanical accidents.

7.7 References

[7.1.1] "OT Position for Review and Acceptance of Spent Fuel Storage and Handling Applications," dated April 14, 1978 as amended by the USNRC letter dated 1/18/1979.

[7.2.1] Diablo Canyon Nuclear Plant Specification No. 10029-N-NPG, Rev. 3.

Table 7.4.1

IMPACT EVENT DATA

Case	Impactor Weight (lb)	Impactor Type	Drop Height (in)	Impact Velocity (in/sec)
1. Shallow drop event	3,000	Fuel assembly & handling tool	36	149.3
2. Deep drop event	3,000	Fuel assembly & handling tool	205	282.5
3. Rack drop event	27,200[†]	Empty rack	531	217.6
4. Rack platform drop event	22,825	Rack platform	531	373.0

[†] Bounds maximum empty rack weight of 26,000 lb.

Table 7.4.2

MATERIAL DEFINITION

Material Name	Material Type	Density (pcf)	Elastic Modulus (psi)	Stress		Strain	
				First Yield (psi)	Failure (psi)	Elastic	Failure
Stainless Steel (Rack)	SA240-304L	501	2.787e+07	2.315e+04	6.810e+04	8.306e-04	3.800e-01
Stainless Steel (Liner)	SA240-304	501	2.76e+07	2.500e+04	7.100e+04	9.058e-04	3.800e-01
Stainless Steel	SA564-630	501	2.86e+07	1.092e+05	1.400e+05	3.818e-03	1.400e-01
Carbon Steel	SA-36	490	2.88e+07	3.300e+04	5.800e+04	1.146e-03	2.000e-01
Concrete	f'_c=5,000 psi	140	4.031e+06	--	--	--	--

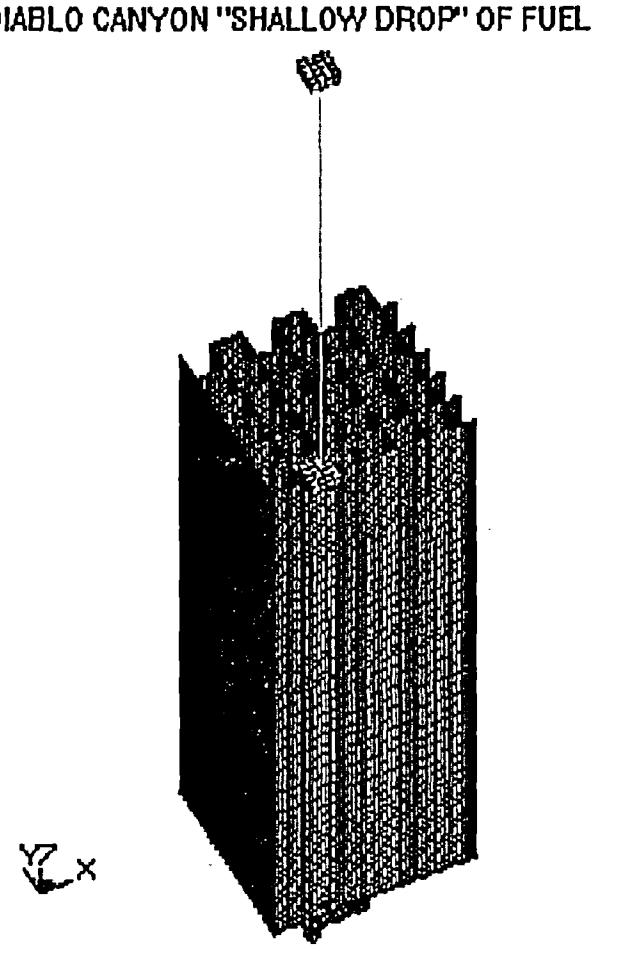

Fig. 7.2.1 Finite Element Model of the "shallow" drop event

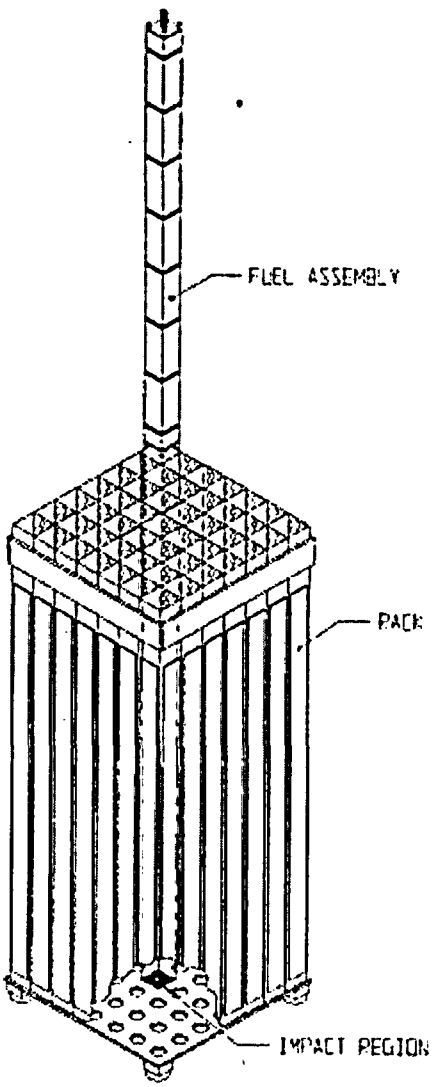

Fig. 7.2.2 Schematics of the "deep" drop scenario

Note: This figure is primarily provided to indicate the impact zone for this scenario. The configuration of the rack is not intended to be accurate.

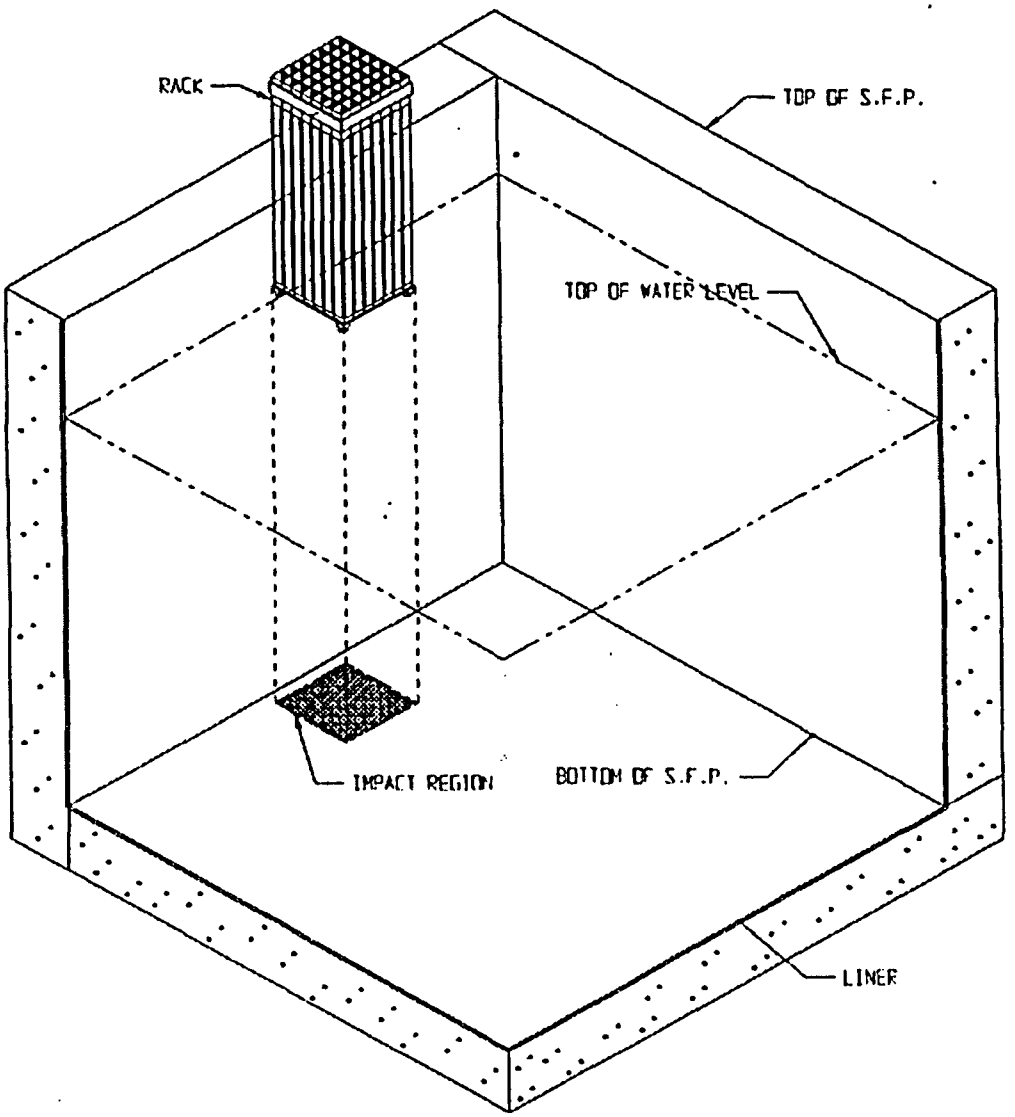

Fig. 7.2.3 Schematics of the rack drop event

Note: This figure is primarily provided to indicate the impact scenario. The configuration of the rack and the SFP is not intended to be accurate.

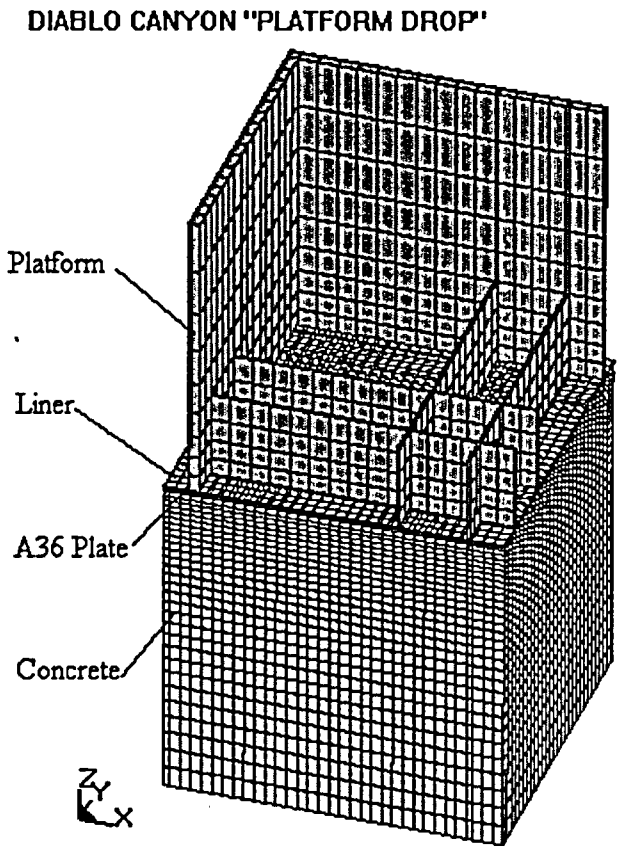

Fig. 7.2.4 Finite element model of the rack platform drop event

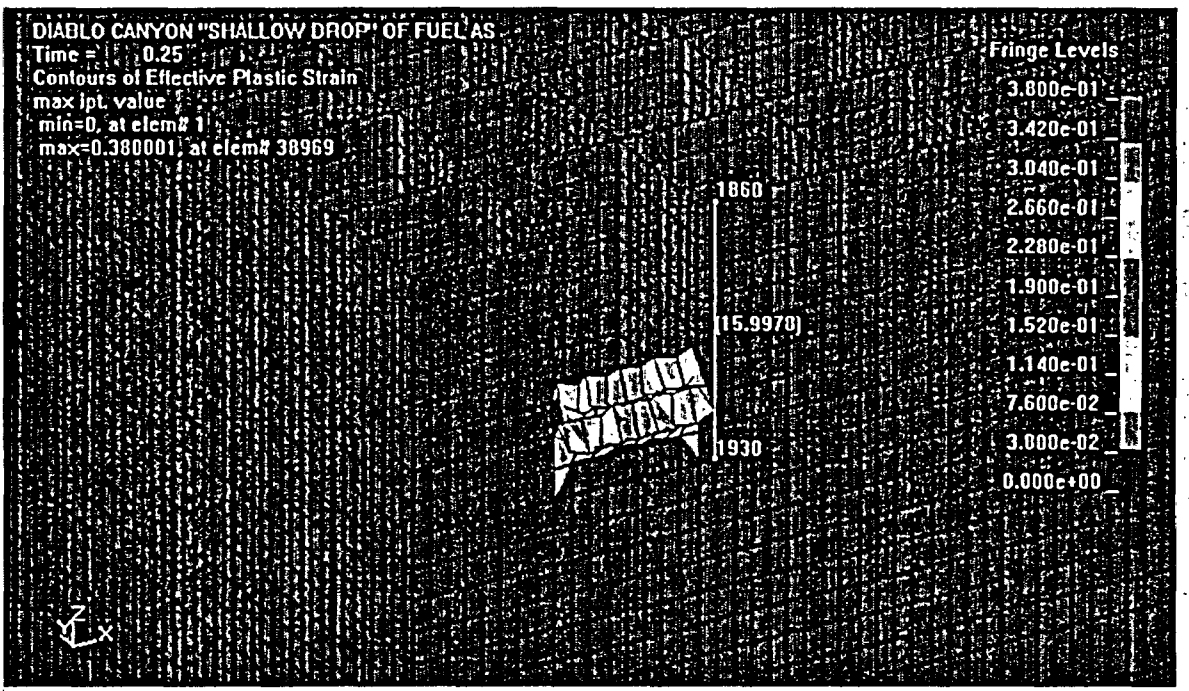

Fig. 7.5.1 "Shallow" Drop: Maximum Plastic Strain

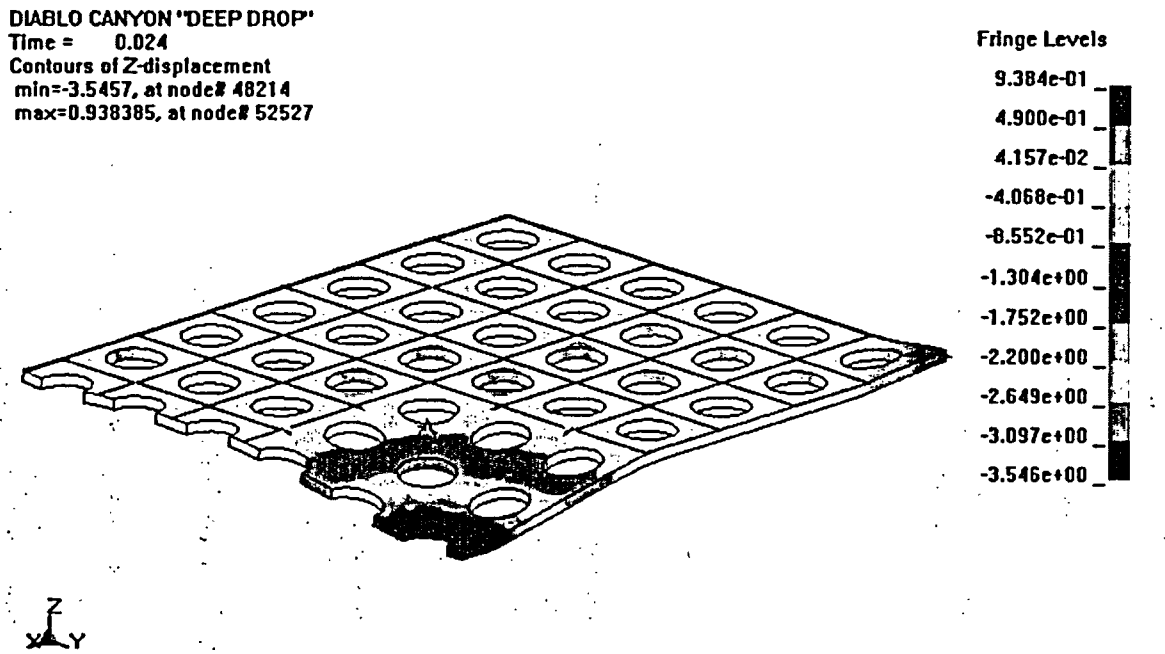

Fig. 7.5.2 "Deep" Drop: Maximum Baseplate Vertical Displacement

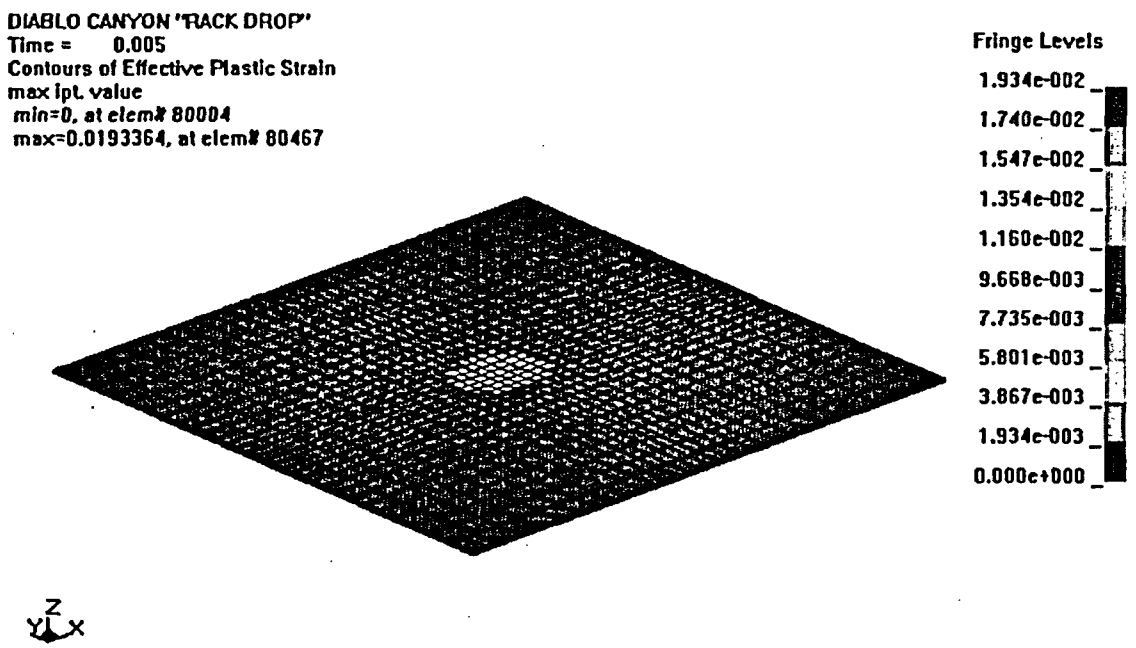

Fig. 7.5.3 Rack Drop: Maximum Plastic Strain – Liner

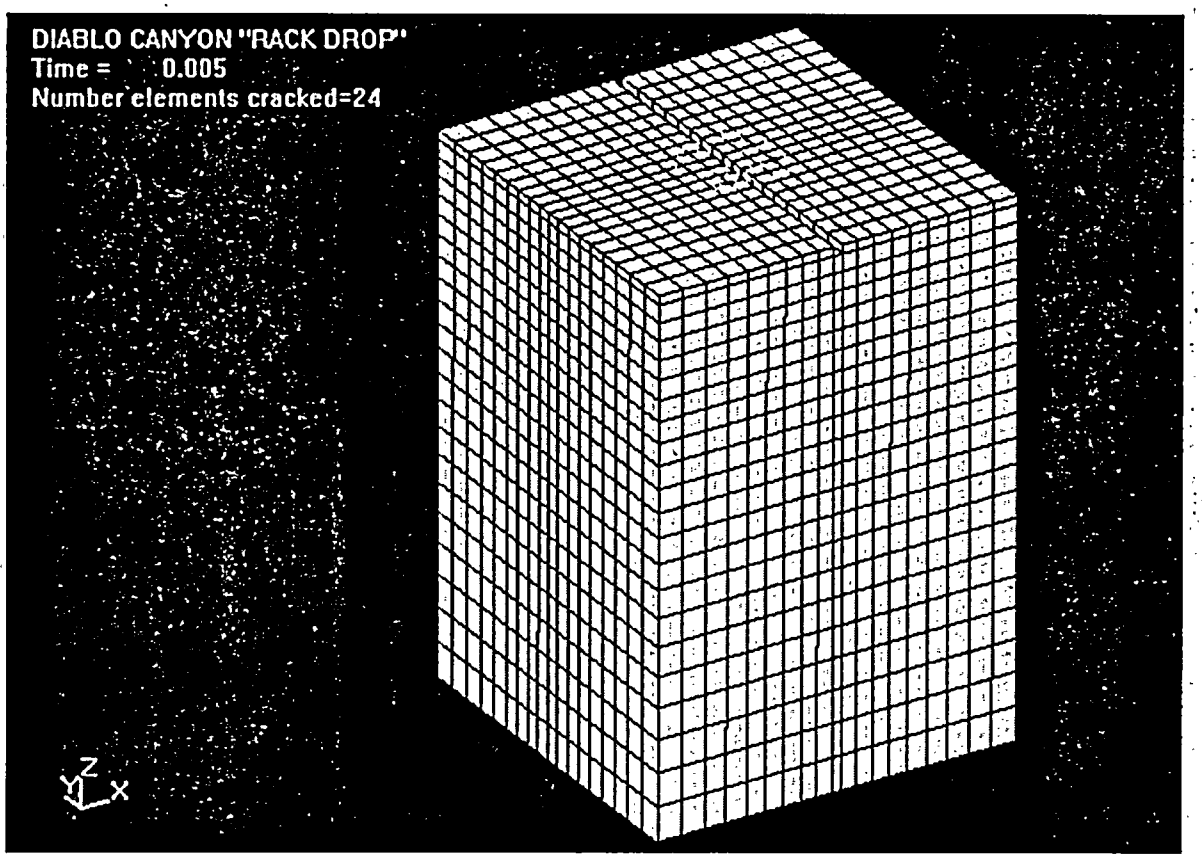

Fig. 7.5.4 Rack Drop: Cracks in the CLA Slab Concrete

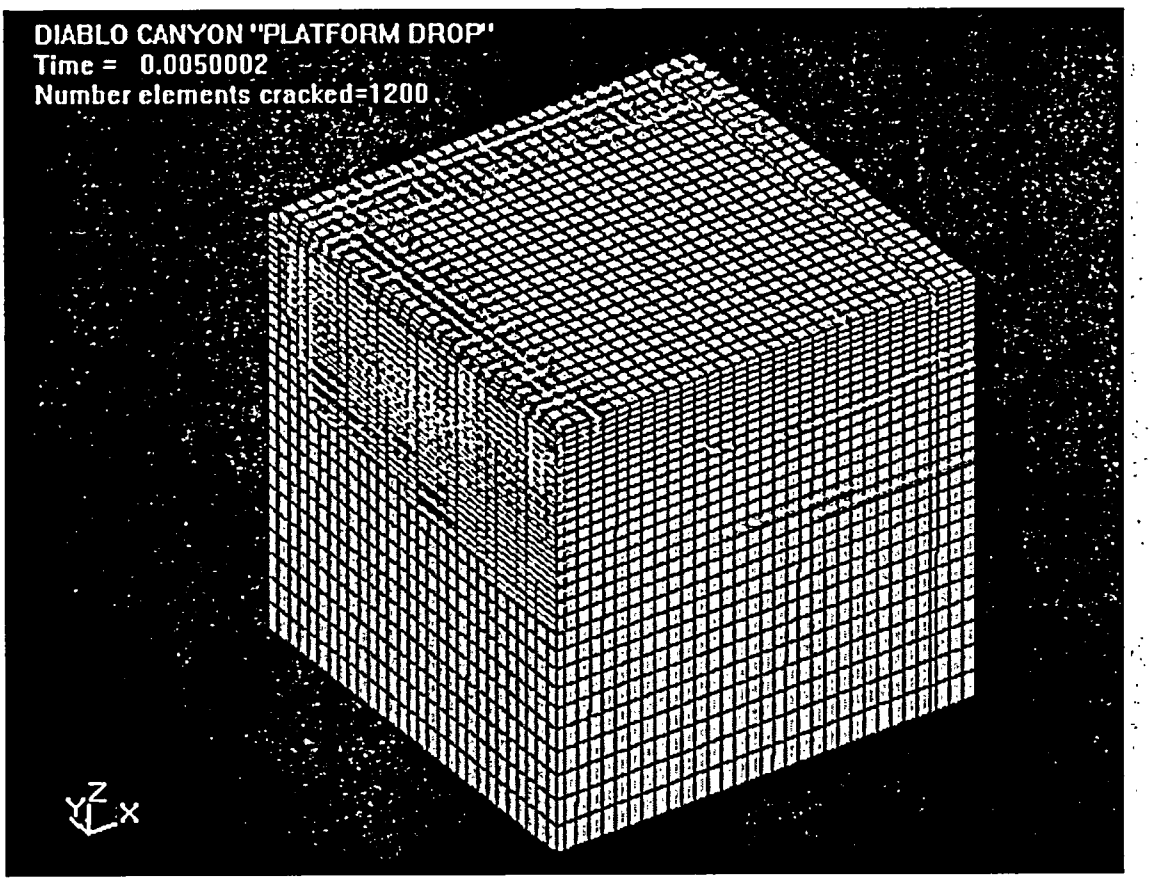

Fig. 7.5.5 Rack Platform Drop: Cracks in the CLA Slab Concrete

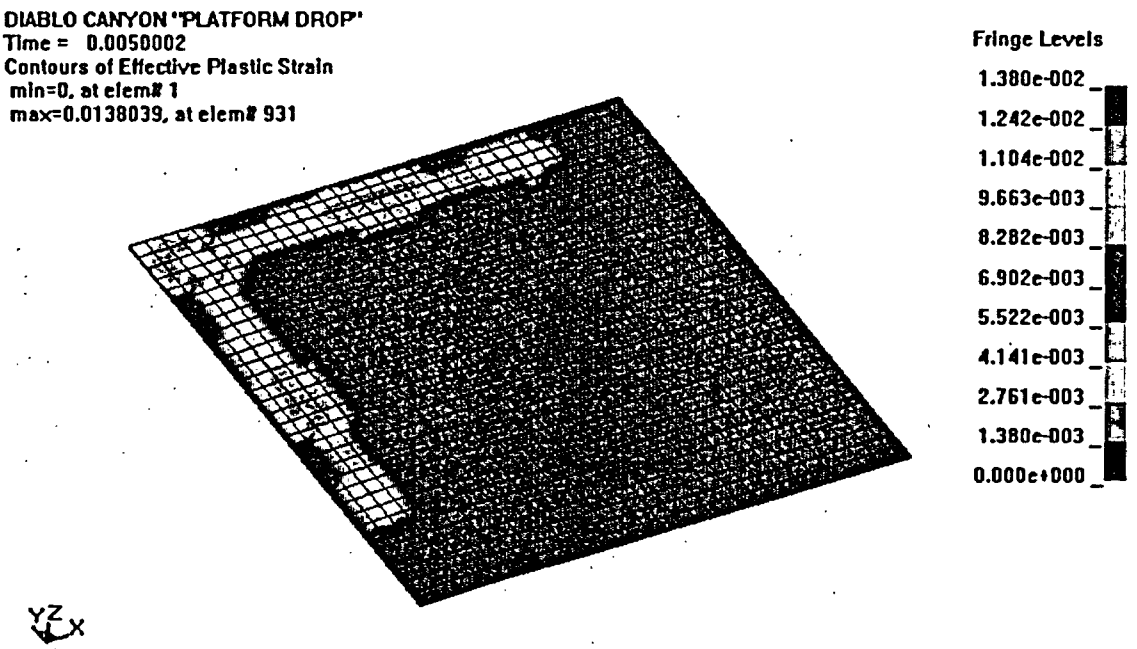

Fig. 7.5.6 Rack Platform Drop: Maximum Plastic Strain – Liner

8.0 POOL STRUCTURE INTEGRITY CONSIDERATIONS

8.1 Introduction

The reinforced concrete spent fuel pool structure serves to withstand all service condition loadings and is designated as a seismic Category I structure in the DCPP FSAR. The consequences of the addition of a fuel storage rack in the cask pit cavity must be evaluated to quantify any increase (or decrease) in the margins of safety available in the presently licensed configuration. This section provides a summary of the evaluations required and performed to support the required structural safety evaluation. The structural loads imposed by the new rack and platform are confined to the floor and walls of the cask pit cavity area. It will be demonstrated that the rack will not be in contact with any portion of the walls of the spent fuel pool at any elevation above the main floor of the pool. Thus, the discussion and evaluation are limited to that portion of the overall pool structure.

8.2 Description of Cask Pit Cavity Structure

The DCPP fuel pool structure is founded on bedrock. In both DCPP units, the cask pit is integral to the fuel pool, occupying a corner of the pool (the southwest corner in Unit One, and northwest corner in Unit 2). The two pools are mirror image of each other. As is typical of many Westinghouse PWRs, the cask pit cavity is deeper than the fuel pool proper: at DCPP, the cask pit is deeper than the main fuel pool by 4'-3". Thus, the bottom 51 inches of the reinforced concrete walls is fully supported from the outside by the hard subgrade.

The entire surface of the cask pit cavity area (floor and walls), is equipped with a ¼" inch thick austenitic stainless steel liner that provides confinement of the pool water and protects the reinforced concrete pool walls and base mat from direct contact with the pool's borated water. The cask pit floor liner plate also has an additional ¾" thick carbon steel backing plate, underlain by a 4'-9" thick reinforced concrete slab founded on bedrock (topped by 5" of concrete cover). Two of the four reinforced concrete walls of the 51 inch deep cavity in the corner of the pool are

merely extensions of the much larger spent fuel pool walls, which are 6'-0" thick. The remaining two 51 inch high walls defining the cask pit depression are 5'-0" thick.

The key data on the reinforced concrete base mat and walls in the cask pit cavity region[†] germane to the structural strength of the pool enclosure is provided in Table 8.2.1 herein.

Table 8.2.1

REINFORCED CONCRETE WALL AND BASEMAT DATA FOR THE CASK PIT CAVITY REGION (Unit One) [††]

	Base Mat	South Wall	West Wall
Total thickness, inch	5'-2"	6'-0"	6'-0"
Concrete Compressive Strength, psi	DE/DDE: 5000 psi Hosgri: 5650 psi LTSP: 0.95(5650)= 5367 psi	DE/DDE: 5000 psi Hosgri:5650 psi LTSP: 0.95(5650)= 5367 psi	DE/DDE: 5000 psi Hosgri: 5650 psi LTSP: 0.95(5650)= 5367 psi
Rebar size and spacing in N-S direction (horizontal for the wall, near water surface)	#11 @ 6"	#11 @ 6"	#11 @ 6"
Rebar size and spacing in E-W direction (vertical for the wall)	#11 @ 6"	#11 @ 7"	#11 @ 7"

8.3 Structural Consequences of the Cask Pit Rack to the Cask Pit Cavity

As discussed in Subsection 2.1, the cask pit rack is designed to be situated on a cask pit platform (CPP), which fits snugly in the 51-inch deep cask pit cavity of the spent fuel pool and is totally confined in the subterranean portion of the cask pit cavity (see Figure 8.3.1). The platform is actually wedged against the sidewalls of the cask pit cavity to eliminate any differential movement between the pool walls and the platform. This ensures that the difference in seismic motion between the cask pit cavity structure and the top of the platform is negligible.

[†] Throughout this document, the term cask pit cavity region refers to the 4'-3" deep subterranean portion of the fuel pool where the cask pit platform is situated.

[††] Unit 2 is identical in all structural attributes, except it is a mirror image of Unit 1.

The rack is mounted on the platform and connected to it through "connector links" (see Subsection 2.1 and Figures 2.1.4 and 2.1.5) that act to restrain the rack in the vertical upward direction. The rack pedestals are inset into recessed holes in the top of the platform (see Figure 2.1.3), which provide lateral rack restraint against sliding and limit lateral motion. Thus, under seismic events, the cask pit rack response produces negligible hydrodynamic forces on the cask pit walls. A free body diagram of the cask pit platform makes it evident that the reaction to the rack and platform inertia forces during an earthquake event will be provided principally by:

- the friction forces between the platform and the cask pit floor liner

and if the friction forces are inadequate to resist the lateral forces on the platform, then by:

- the compressive contact forces between the cask pit walls, and the platform, and
- the friction forces between the platform shims and the cask pit wall liner.

These contact forces act on the 51" tall region of the cask pit walls, which are below grade and thus result in the structural response of the wall that simulates a plate-on-an-elastic foundation. Inasmuch as the structural response of a locally loaded plate-on-elastic foundation produces localized flexure and shear [8.2.1], it follows that the platform-to-cask pit wall reaction forces will produce local moments and shear in the loaded region of the cask pit cavity.

In contrast to the earthquake-induced loading of the reinforced concrete structure by the cask pit racks, the high-density racks, licensed and installed in the 1980s, exert impact loads as well as substantial hydrodynamic loads on the pool walls. These loads, however, act at locations on the reinforced concrete walls that are far removed and structurally apart from the region loaded by the cask pit racks. Thus, the response of the reinforced concrete structure of the plant to the loadings from the existing racks do not interact, i.e., they are completely uncoupled. The moments and shears on the reinforced concrete structure from the loadings due to the cask pit rack can, therefore, be analyzed independently from the loadings produced by the existing array of racks (which do not exert any loads on the cask pit cavity region). Therefore, the addition of

the temporary rack and its support platform in the cask pit area will not have an adverse effect on the overall structural integrity of the spent fuel pool

8.4 Load Cases and Combinations

The DCPP reinforced concrete pool structure was designed using ACI 318-63 Code. The applicable load combinations are taken from reference [8.3.1].

8.4.1 Normal Load Conditions

For the normal load conditions the pool structure was evaluated using the Working Stress Design (WSD) method with the following numbered load case combinations.

(1) $C = D + L + DE + T_o + R_o$

(2) $C = D + L + W + T_o + R_o$

where:

C= Required Load Capacity of the Section

D= Dead Weight

L= Live Load

DE= Design Earthquake

W= Normal Wind

T_o= Normal Thermal Loads

R_o= Normal Pipe Reactions

8.4.2 Abnormal Load Conditions

For the abnormal load conditions the pool structure was evaluated using the Ultimate Stress Design (USD) method with the following numbered load case combinations.

(3) $U = D + L + T_A + R_A + 1.5\,P_A$

(4) $U = D + L + T_A + R_A + 1.25\,P_A + 1.0(Y_J + Y_M + Y_R) + 1.25\,DE$

(5) $U = D + L + T_A + R_A + 1.0\,P_A + 1.0(Y_J + Y_M + Y_R) + DDE$

(6) $U = D + L + T_A + R_A + 1.0\,P_A + 1.0(Y_J + Y_M + Y_R) + HE$

(7) $U = D + L + T_A + R_A + 1.0\,P_A + 1.0(Y_J + Y_M + Y_R) + LTSP$

where:

U = Required Load Capacity of the Section

T_A= Abnormal Thermal Loads

R_A= Abnormal Pipe Reactions

P_A= Abnormal Pressure Loads

Y_J= Jet Impingement Loads

Y_M= Missile Impact Loads

Y_R= rupture restraint Reactions

DDE= Double Design Earthquake

HE= Hosgri Earthquake

LTSP= Long Term Seismic Program Earthquake

Obviously, many of the load cases listed above, such as wind and piping loads, do not apply to the cask pit cavity design.

8.4.3 Affected Load Cases

The following load conditions are commonly evaluated for pool structures where racks are being installed or removed. Each condition is assessed below to address any potential influence from the addition of the new cask pit rack and associated support platform.

a. Dead Load: The cask pit cavity's base mat is subjected to the dead load of the loaded cask pit rack and its platform. This load is applied as a bearing pressure on the platform/cavity liner contact surface.

b. Hydrostatic Load: This load, exerted by the column of water (43 feet nominal height) acts on the cask pit cavity liner as well as the walls. This considered as a dead load and is not a consequence of the introduction of the cask pit racks.

c. Thermal Load: Thermal-hydraulic calculations presented in Section 5 of this report show that the bulk pool temperature of the water mass in the pool will remain below the existing licensed limit. However, there will be normal forces at shim locations on the cask pit walls due to thermal expansion of the platform.

d. Seismic Loads: Any of the four earthquake events described in Section 6 will, if sufficiently strong, produce lateral reaction between the platform and the cask pit cavity walls. The base mat will also experience increased transient loads.

It is concluded from the above that only an earthquake in combination with thermal and the rack dead weight would produce additional loadings on the reinforced concrete structure and that the remaining loading (hydrostatic) remains unchanged.

Further, the effect of the seismic loading on the cask pit cavity is to produce local bending and shear in contrast to the global bending and shear produced by other loads in the aboveground portion of the pool structure. Therefore, the structural assessment of the consequences of adding the cask pit rack resolves to evaluating the local moment and shear in the cask pit cavity base mat and walls and comparing them against the available corresponding capacities. Therefore, the addition of the temporary rack and its support platform in the cask pit area will not have an adverse effect on the overall structural integrity of the spent fuel pool.

8.5 Strength Evaluation

The cask pit cavity walls, basemat, and liner plate and anchorages are evaluated using the maximum reaction loads obtained from the cask pit rack/platform dynamic analyses, which are discussed in Section 6. Local bearing and shear stresses in the reinforced concrete walls and basemat are compared with the appropriate ACI Code stress limits. Finite element calculations are performed to determine the strain levels in the cask pit liner due to friction loads.

The Cask Pit floor and wall liners, and liner anchorage computed safety factors are provided in Table 8.5.1.

Table 8.5.1
Safety Factors for the Liner and Liner Anchorage

Considered Load Combinations [†]	Cask Pit Floor		Cask Pit Wall	
	Liner	Anchor	Liner	Anchor
1 and 4	1.8	1.7	1.4	1.1
5 through 7	2.8	2.0	3.3	2.3

Safety factors against punching shear, diagonal edge shear, and bearing on the Cask Pit concrete wall and floor are summarized in Table 8.5.2.

[†] Note that the reported safety factors are the bounding values from the listed load case combinations.

Table 8.5.2 Safety Factors for the Cask Pit Concrete Wall and Floor					
Considered Load Combinations †	Cask Pit Wall		Cask Pit Floor		Diagonal Edge Shear
	Punching Shear	Bearing	Punching Shear	Bearing	
1 and 4	9.5	1.2	23.8	6.8	1.3
5 through 7	10.5	2.0	13.4	5.5	1.5

8.6 Conclusion

It is concluded from the results presented in this report that the available structural capacity in the loaded region of the cask pit is incomparably greater than the stress resultants arising from the applied loads. Therefore, the spent fuel pool structure is adequate to withstand the additional loads imposed by the addition of the cask pit rack and associated support platform.

The auxiliary building, which includes the Spent Fuel Pool structures, has been seismically qualified using the criteria outlined in Chapter 3 of the Diablo Canyon FSAR update. As described in FSAR Section 3.7.2.1.7.1, the seismic inertia loads were obtained using time-history analyses of spring and lumped mass models (two horizontal and one vertical) of the auxiliary building. A detailed analytical static model of the auxiliary building was then used to distribute seismic inertia forces and moments to various walls, diaphragms, and columns, as described in FSAR Section 3.8.2.4. The effect of the change in weight on the seismic models due to the cask pit rack is considered to be insignificant, since the increase in global mass is determined to be less than 1.5%. Therefore, there is no change in the seismic responses and forces reported in the FSAR.

8.7 References

[8.2.1] Timoshenko and Goodier, Theory of Elasticity, Section §139, 3rd Edition, McGraw Hill.

[8.3.1] Diablo Canyon Power Plant Units 1 & 2, Design Criteria Memorandum No. T-2, Auxiliary Building, dated January 6, 2000.

[8.3.2] DCPP Adminstrative Work Procedure E-015, Rev. 0 "Application of the Long-Term Seismic Program to Diablo Canyon Power Plant Additions and Modifications".

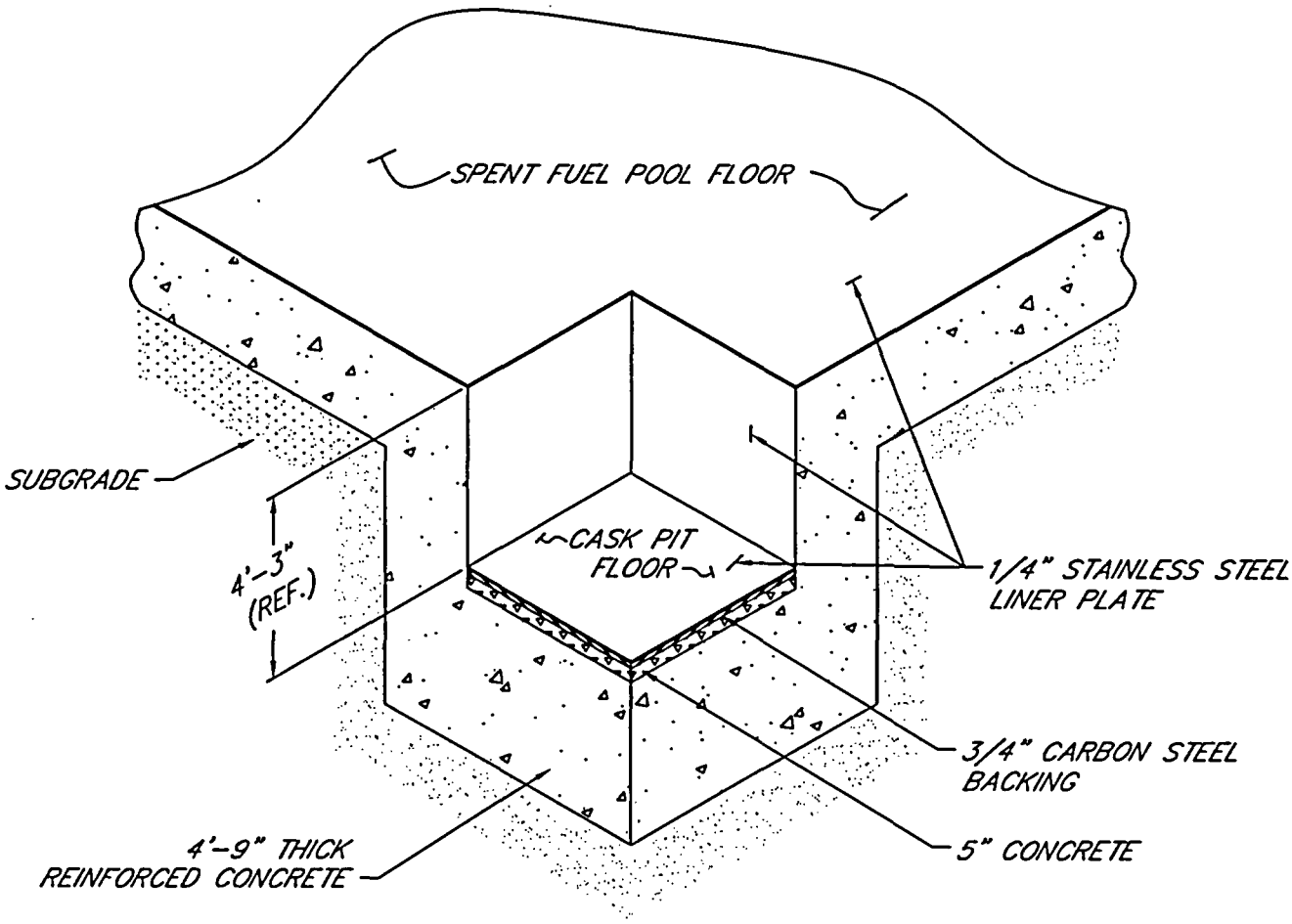

FIGURE 8.3.1 CASK PIT CAVITY ISOMETRIC

NOTE: FULL HEIGHT NEAR POOL WALLS NOT SHOWN FOR CLARITY.

9.0 RADIOLOGICAL AND SHIELDING CONSIDERATIONS

This Section will address the dose exposure consequences associated with the installation of temporary cask pit racks and supporting platforms at the Diablo Canyon Power Plant (DCPP).

9.1 Fuel Handling Accident

The installation and removal of the temporary cask pit racks and support platforms will not result in a change in the consequences of a fuel handling accident (FHA) previously analyzed in DCPP FSAR Update Section 15.5. The temporary cask pit rack and support platform will be installed at the same water depth as the existing SFP racks, providing the same iodine decontamination factors assumed in the FHA analysis. Furthermore, the fuel stored in the temporary cask pit rack will have at least a 10-year decay time. Thus, the radioactivity source term for the fuel that will be stored in the temporary cask pit rack is much less than the conservative assumption made in the existing DCPP FSAR Update Section 15.5 analysis (freshly discharged fuel). Hence, the existing DCPP FSAR Update Section 15.5 FHA analysis is bounding.

9.2 Solid Radwaste

The only time that the number of fuel assemblies stored in either SFP will exceed the current licensing basis will be during the 14th and 15th refueling outages when the core is fully offloaded or in the unlikely event a full core offload is required outside of a refueling outage. For each Unit, this amounts to a total of approximately 2 months. The necessity for resin replacement is determined primarily by the requirement for water clarity, and the resin is normally changed about once a year. Because of the small time frame over which the number of fuel assemblies stored in the SFP will exceed the existing licensing basis, no significant increase in the volume of resin generated solid radioactive waste from either unit is expected to result from the addition of the temporary racks.

Once removed from the spent fuel pools, the temporary cask pit racks may be shipped to a vendor for volume disposal, disposed of as radioactive waste, stored for temporary use, or stored until decommissioning. The disposal of the used temporary rack will result in a one-time incremental increase in solid waste. Since the temporary cask pit rack will be packaged, transported, and disposed of in a manner consistent with NRC regulations, there will be no significant radiological impact on the environment. Because ongoing volume reduction efforts have effectively minimized the amount of waste generated, the incremental increase from disposal of the temporary cask pit racks is bounded by the plant's original licensing basis described in the Final Environmental Statement and therefore, is acceptable.

9.3 Gaseous Releases

The storage of additional spent fuel assemblies in the spent fuel pool (SFP) during the 14th and 15th refueling outages is not expected to significantly affect the releases of radioactive gases from the SFP. Gaseous fission products such as krypton-85 and iodine-131 are produced by the fuel in the reactor core during reactor operation. Tritium is routinely produced in an operating reactor core through neutron capture by deuterium present in the reactor coolant. Small amounts of krypton-85 and iodine-131 fission gases are released to the reactor coolant from the small number of fuel assemblies that develop leaks during reactor operation. During refueling operations, some of these gaseous fission products enter the SFP and are subsequently released into the air. There will not be an increase in the amounts of gaseous fission products released to the atmosphere as a result of the temporary increase in SFP storage capacity because the frequency of refueling and the number of freshly off-loaded spent fuel assemblies stored in the SFP, at any one time, will not increase. The dominant source of the tritium inventory in the SFP at DCPP originates from the Reactor Cooling System (RCS). Normally, DCPP recycles RCS waste and recovers the boron and the high purity water. This water contains moderate concentrations of tritium from the RCS. This water is used to replenish SFP water inventory losses due to evaporation, and is the major source of tritium in the SFP. The contribution of tritium produced from neutron capture in the boron-10 of the storage racks is insignificant to the total inventory. Therefore, the additional racks will have a negligible effect on the overall tritium level in the SFP.

Normally, the contributions from the fuel storage areas are negligible compared to the other sources of gaseous releases and no significant increases are expected in either unit as a result of the expanded storage capacity.

9.4 Liquid Radiological Releases

The release of radioactive liquids will not be affected directly as a result of the temporary rack installation. The SFP ion exchanger resins remove soluble radioactive materials from the SFP water. When the resins are changed out, the small amount of resin sluice water is processed by the radioactive waste system before release to the environment. The frequency of resin change out may increase slightly during the installation and removal of the temporary rack and installation of the support platform. However, the amount of liquid effluents released to the environment as a result of the temporary rack and support platform is expected to be negligible.

9.5 Personnel Exposures

Personnel exposures in the vicinity of the SFP at each unit result principally from radionuclides in the pool water and from fuel in transit underwater. The radionuclides in the water derive generally from: 1) the mixing of primary system water with the pool water and 2) the spalling of crud deposits from the spent fuel assemblies as they are moved in the storage pool during refueling operations. Although the overall storage capacity of each pool is temporarily being increased, the movement of fuel during refueling is independent of storage capacity. Similarly, the dose rate from fuel in transit does not increase with increased storage capacity. The use of the temporary cask pit rack will require fuel transits paths in the vicinity of the southwest corner of the Unit 1 SFP and the northwest corner of the Unit 2 SFP, similar to transit paths that would be used during cask loading. These transit paths will not increase the dose rate beyond that already experienced at these locations during placement of fuel into racks adjacent to the Cask Pit. Similarly, the dose rate from fuel stored in the temporary cask pit racks is expected to be comparable to the dose rate from fuel stored in the existing spent fuel pool racks adjacent to the Cask Pit, because the exterior wall thickness surrounding the Cask Pit is the same as the wall thickness surrounding the pool.

An evaluation has been performed to demonstrate that although the water gap between the temporary cask pit racks and the cask pit pool wall is slightly smaller than the gap between the existing racks and the spent fuel pool wall, there will be no change in the previously analyzed dose rates at the exterior wall surface. This is attributed to a source term strength reduction due to a minimum cooling time restriction of 10 years for all assemblies stored in the temporary cask pit racks.

Operating experience has shown that there have been negligible concentrations of airborne radioactivity during normal operations, and no increases are expected as a result of the expanded storage capacities or during the temporary cask pit rack installation or removal. However, continuous air monitors are used in the immediate vicinity of the spent fuel pools during periods of underwater activities.

No significant increase in radiation exposure to operating personnel of either unit is expected as a result of adding a temporary cask pit rack; therefore, neither the current health physics programs nor the area monitoring systems need to be modified.

9.6 Anticipated Exposure During Rack Installation

All operations involved in installing a temporary cask pit rack in each unit will utilize detailed procedures prepared with full consideration of As Low As Reasonably Achievable (ALARA) principles. Similar operations have been performed in a number of facilities in the past, and experience indicates that the relatively simple task of installing these cask pit racks and support platforms in locations not previously occupied by other racks can be accomplished with minimum radiation exposure to personnel. Diving operations are not required based on a physical survey of the existing spent fuel pool configuration and the design of the temporary cask pit racks and support platforms, which allow remote installation.

The combined occupational exposure for installing a rack in each unit is estimated to be a total of approximately 0.3 person-rem. This estimated dose is based on the following.

OPERATION	MANHOURS PER UNIT	ESTIMATED PERSON-REM EXPOSURE PER UNIT
Clean and Vacuum Cask Pit Area	20	0.050
Install Support Platform	30	0.075
Install Platform Shims (16 per Unit)	16	0.040
Install Cask Pit Rack	30	0.075
Install Connector Links (8 per Unit)	20	0.050

Typical dose rates above the SFPs during normal operations are approximately 2.5 mrem or less.

The existing radiation protection programs at DCPP are adequate for the rack installation and removal operations. Radiation Work Permits (RWPs) will govern activities, and personnel monitoring equipment will be issued to each individual. As a minimum, this will include thermoluminescent dosimeters (TLDs) and self-reading dosimeters (SRDs), which are normally personnel electronic dosimeters. All work in the SFP will be directly monitored and controlled by a radiation protection technician and exposures maintained ALARA.

9.7 Rack Removal and Storage Prior to Cask Handling Operations

Based on the projected storage capacity of DCPP, PG&E does not expect to remove the temporary racks until 2010 for Unit 1 and 2011 for Unit 2. In preparation for dry cask loading operations, the spent fuel assemblies must be removed from the temporary cask pit racks followed by removal of the cask pit racks from the SFP. The support platforms will remain in place for cask loading activities. Thereafter, the temporary racks may be shipped to a vendor for volume reduction, disposed of as radioactive waste, stored for temporary use, or permanently stored until decommissioning.

Based on Holtec experience with rack module removal and decontamination projects, the removal and storage process will not create significant radiological waste or personnel exposure. The removal and decontamination process should not result in more than 0.2 person-rem exposure based on a pool surface dose rate of 2.5 mrem/hr, an estimated rack contact surface dose rate of 20 mrem/hr, and a job estimate of 80 man-hours. Typically, the surfaces of a rack module as well as the cell interiors can be decontaminated to lower the dose and contamination levels of the rack. During all handling operations, appropriate radiological controls will be in place for all rack handling and storage activities.

During the installation and removal of the racks, exposures will be maintained ALARA consistent with the requirements of 10CFR20 and DCPP's existing ALARA program. The radiation protection section will prepare one or more radiation work permits (RWPs) for various in-pool and out-of-pool activities. The RWPs and supporting documentation will establish requirements in the following areas:

- Frequency of radiation, contamination, and airborne surveys.
- Individual monitoring devices, typically a TLD and SRD.
- Protective clothing
- Access and work controls
- Contamination controls including controls for radioactive materials that could involve significant shallow dose equivalent and effective dose equivalent exposures.

- Contamination and radiation limits at various steps requiring the evaluation of further controls or activities. (e.g., results of monitoring the rack as it breaks the water may "trigger" additional underwater efforts including pressure washing.

Radiation protection technicians will be involved in the movement, decontamination, packaging, and storage of the temporary racks. Constant coverage by a radiation protection technician will be required for all activities involving work in the SFP including the removal of items from the spent fuel pools. In addition to work activities in the SFP, additional periods of continuous coverage by the technicians will be as specified in the RWPs covering the work activities. During SFP activities and periods of work with high levels of contamination, a portable continuous air monitor with alarming capability will be used to provide warning in the event of increasing airborne radioactivity in the immediate work areas. Respiratory protection may be used if shown to be TEDE ALARA consistent with the requirements of 10CFR20 and plant procedures.

The DCPP radiation protection section will perform the following actions prior to and during rack removal:

- Vacuuming of the Cask Pit area prior to rack installation.
- Underwater survey of accessible areas of the rack.
- Underwater pressure wash or rinse as appropriate.
- Monitoring and rinsing of the rack as it breaks the water surface as appropriate.
- Survey of the rack prior to wrapping in plastic or bagging.

Once wrapped or bagged, the rack will either be stored on site protected from the elements or placed into an approved shipping container for shipment to a vendor for volume reduction and/or disposal.

All items or tools used in areas posted as contaminated will either be surveyed and released if free of contamination or treated as radioactive material and handled in accordance with DCPP procedures.

Each member of the project team will receive radiation protection training consistent with the requirements of 10CFR19. Project specific information such as the potential for extremity doses when removing and decontaminating items from the spent fuel pool and operating experience with spent fuel pool activities will be discussed in pre-job briefings. Radiation protection technicians, involved in the project, will participate in pre-job briefings involving their activities associated with the work.

10.0 INSTALLATION

10.1 Introduction

The installation phase of the Diablo Canyon cask pit rack project will be executed by Holtec International's Field Services Division. Holtec, serving as the installer, is also responsible for performance of specialized services. All installation work at Diablo Canyon is performed in compliance with NUREG-0612 (refer to Section 3.0), Holtec Quality Assurance Procedure 19.2, Diablo Canyon project specific procedures, and applicable Diablo Canyon procedures.

Crane and fuel bridge operators are trained in the operation of overhead cranes per the requirements of ANSI/ASME B30.2, and the plant's specific training program. Consistent with the installer's past practices, a videotape aided training session is presented to the installation team, all of whom are required to successfully complete a written examination prior to the commencement of work. Fuel handling bridge operations are performed by Diablo Canyon personnel, who are trained in accordance with Diablo Canyon procedures.

Rack lifting rigs are required for installation of the cask pit platform and the rack. These two lifting rigs are almost identical and are designed to remotely engage and disengage on lift points at the bottom of each component. The lifting rigs comply with the provisions of ANSI N14.6-1978 and NUREG-0612, including compliance with the design stress criteria, load testing at a multiplier of maximum working load, and nondestructive examination of critical welds.

A surveillance and inspection program shall be implemented as part of the installation of the cask pit rack and platform. A set of inspection points, which have been proven to be effective in producing high quality work in previous rack projects, is implemented by the installer.

Due to the design of the cask pit rack and associated platform, underwater diving operations are not required for this project.

Holtec International developed procedures, to be used in conjunction with the Diablo Canyon procedures, which cover the scope of activities for the installation effort. Similar procedures have been utilized and successfully implemented by Holtec on previous rack installation projects. These procedures are written to include ALARA practices and provide requirements to assure equipment, personnel, and plant safety. These procedures are reviewed and approved in accordance with Diablo Canyon administrative procedures prior to use on site. The following is a list of the Holtec procedures, used in addition to the Diablo Canyon procedures to implement the installation phase of the project.

A. Installation/Handling Procedure:

This procedure provides direction for the handling/installation of the rack platforms and new storage rack modules in the Cask Pit. This procedure delineates the steps necessary to receive the rack on site, the proper method for unloading and uprighting the rack, staging the rack prior to installation, and installation of the platforms and racks. The cask pit platform has a cross section that closely matches the rack but a shorter height and lower weight. The process for placement of the cask pit platforms is similar to that for the racks. The procedure provides for the installation of cask pit platform, positioning and leveling of the cask pit platform, if necessary to compensate for any Cask Pit floor uneveness, and installation of the wedges. This procedure also provides for the installation of the rack onto the platform, including the leveling of the rack, installation of the connector links between the rack and the platform, and verification of the as-built field configuration to ensure compliance with design documents.

B. Receipt Inspection Procedure:

This procedure delineates the steps necessary to perform a thorough receipt inspection of the rack modules and cask pit platforms after their arrival on site. The receipt inspection includes dimensional measurements, cleanliness inspection, visual weld examination, and verticality measurements.

C. Cleaning Procedure:

This procedure provides for the cleaning of rack module and cask pit platform, if required. The components are to meet the requirements of ANSI N45.2.1, Level B, prior to placement in the Cask Pit. Methods and limitations on cleaning materials to be utilized are provided.

D. Pre- and Post-Installation Drag Test Procedure:

These two procedures stipulate the requirements for performing a functional test on the rack module prior to and following installation. The procedures provide direction for inserting and withdrawing an insertion gage or dummy fuel assembly into designated cell locations, and establishes an acceptance criteria in terms of maximum drag force.

E. ALARA Procedure:

Consistent with Holtec International's ALARA Program, this procedure provides guidance to minimize the total man-rem received during the rack installation project, by accounting for time, distance, and shielding. This procedure will be used in conjunction with the Diablo Canyon ALARA program.

F. Liner Inspection Procedure:

In the event that a visual inspection of any submerged portion of the pool liner is deemed necessary, this procedure describes the method to perform such an inspection using an underwater camera and describes the requirements for documenting any observations.

G. Leak Detection Procedure:

This procedure describes the method to test the pool liner for potential leakage using a vacuum box. This procedure may be applied to any suspect area of the liner.

H. Liner Repair and Underwater Welding Procedure:

In the event of a positive leak test result, underwater welding procedures may be implemented which provide for a weld repair, or placement of a stainless steel repair patch, over the area in question. The procedures contain appropriate qualification records documenting relevant variables, parameters, and limiting conditions. The weld procedure is qualified in accordance with ASME Section XI , or may be qualified to an alternate code accepted by Pacific Gas & Electric and Holtec International.

10.2 Rack Arrangement

The rack installation process will not directly require any fuel shuffling. During refueling outages prior to the rack installation, final placements of fuel assemblies within the spent fuel pool will maximize the open storage locations adjacent to the Cask Pit. The final rack arrangement allows for a 12 by 13 cell Region II style rack to be installed in both the Unit 1 and Unit 2 Cask Pit Areas. Schematic plan views depicting Cask Pit Area storage rack configurations are shown in Figures 1.0.1 and 1.0.2.

10.3 Rack Interferences

A survey was conducted to identify any objects which would interfere with cask pit rack and platform installation or prevent usage of any storage locations. Prior to installation of the platform, PG&E will remove two lighting brackets from each of the spent fuel pools in the vicinity of the Cask Pits and will perform a minor modification to the corner bracket of the Cask Restraint to provide clearance for the rack/platform installation. Any existing miscellaneous equipment that is temporarily stored within the Cask Pit will be removed followed by vacuuming prior to installation of the cask pit rack and platform.

10.4 SFP Cooling

The pool cooling system shall be operated in order to maintain the pool water temperature at an acceptable level. It is anticipated that activities, such as platform placement, may require the temporary shutdown of the Spent Fuel Pool cooling system.

Prior to any shutdown of the Spent Fuel Pool cooling system, the estimated time after shutdown to increase the pool bulk coolant temperature to a selected value of ≤120 °F will be determined. A temperature of ≤ 120 °F is chosen with enough margin such that cooling may be restored to ensure the pool bulk temperature will not exceed 150 °F.

10.5 Installation of Cask Pit Rack

Installation of the cask pit rack, supplied by Holtec International, involves the following activities. The rack is delivered in the horizontal position. The new rack module is removed from the shipping trailer using a suitably rated crane, while maintaining the horizontal configuration. The rack is placed on the up-ender and secured. Using two independent overhead hooks, or a single overhead hook and a spreader beam, the rack is up-righted into a vertical position.

The cask pit rack lifting rig is engaged in the lift points at the bottom of the rack. The rack is then transported to a pre-leveled surface where, after leveling the rack, the appropriate quality control receipt inspection is performed (See 10.1B & D). The cask pit rack is lifted with the 125-ton Fuel Handling Building (FHB) Crane and transported along the pre-established safe load paths. The cask pit platform is handled in a similar fashion and staged for installation into the Cask Pit.

The Cask Pit Area floor is inspected and any debris, which may inhibit the installation of the cask pit platform, is removed. The floor elevations in the Cask Pit have been carefully measured and leveling shims are installed, if necessary, at the cask pit platform load bearing points.

The cask pit platform is lifted via the lifting rig and lowered by the FHB Crane into position slightly above the Cask Pit floor. Following a final check of positioning, the cask pit platform is lowered into position. The platform is equipped with adjustable removable wedge shims which secure it in the Cask Pit cavity. The wedge shims are installed using long handled tools from above the SFP surface. Elevation readings are taken to confirm that the platform is level and to pre-set the extensions on the rack pedestals prior to rack installation. In addition, platform-to-wall offset distances are also measured. Adjustments are made as necessary to ensure compliance with design documents. The lifting rig is disconnected from the cask pit platform and removed.

The rack module is carefully lowered into the Cask Pit Area and positioned slightly above the cask pit platform. After final positioning, the rack is lowered onto the cask pit platform. The rack pedestals are then adjusted using the remote adjustment tool, if necessary, to ensure that the final position is level and upright.

A set of connector links are installed in the rack using long-handled tools to secure the rack to the platform. The connector links are an "I" shaped key (see Figure 2.1.5), which when rotated 90 degrees, engages the bottom against small tabs attached to the platform. Continued turning allows the threaded end on the connector link to tighten against the stops in the platform.

The lifting rig is then disengaged and removed from the Cask Pit Area under Health Physics direction. As directed by procedure, post-installation free path verification is performed on all rack cells using a dummy fuel assembly.

10.6 Safety, Health Physics, and ALARA Methods

10.6.1 Safety

During the installation phase of the cask pit rack project, personnel safety is of paramount importance. All work shall be carried out in compliance with applicable approved procedures.

10.6.2 Health Physics

Health Physics is carried out per the requirements of the Diablo Canyon Radiation Protection Program.

10.6.3 ALARA

The key factors in maintaining project dose As Low As Reasonably Achievable (ALARA) are time, distance, and shielding. These factors are addressed by utilizing many mechanisms with respect to project planning and execution.

Time

Each member of the project team is trained and provided appropriate education and understanding of critical evolutions. Additionally, daily pre-job briefings are employed to acquaint each team member with the scope of work to be performed and the proper means of executing such tasks. Such pre-planning devices reduce worker time within the radiological controlled area and, therefore, project dose.

Distance

Remote tooling such as lift fixtures, pneumatic grippers, support leveling device, connector link installation tool, and a lift rod disengagement device have been developed to execute numerous activities from the SFP surface, where dose rates are relatively low.

Shielding

During the course of the cask pit rack project, primary shielding is provided by the water in the Spent Fuel Pool. The amount of water between an individual at the surface and an irradiated fuel assembly is an essential shield that reduces dose. Additionally, other shielding may be employed to mitigate dose when work is performed around high dose rate sources. If necessary, additional shielding may be utilized to meet ALARA principles.

10.7 Radwaste Material Control

Radioactive waste generated from the rack installation will be controlled in accordance with established Diablo Canyon procedures.

11.0 ENVIRONMENTAL AND ECONOMIC CONSIDERATIONS

Article V of the USNRC OT Position Paper [11.1] specifies environmental and economic considerations as essential predicates for a fuel storage capacity enhancement. This section provides justification for selecting installation of an additional rack in each of the DCPP cask pits as fulfilling the directive of the OT Position Paper.

11.1 Need for Temporary Spent Fuel Storage Capacity

PG&E is currently undertaking a project to construct an Independent Spent Fuel Storage Installation (ISFSI) at DCPP. It is planned for the ISFSI facility to be in operation in early 2007 to maintain a Full Core Offload Capability (FCOC) for both Units at DCPP. However, to avoid the potential for the loss of FCOC due to any ISFSI Project delays, PG&E intends to temporarily expand the spent fuel storage capacity by adding an additional fuel storage rack within the Cask Pit of each Unit. Based on the current inventory of fuel assemblies stored in the spent fuel pools (SFPs) and the anticipated future discharges of spent fuel, Unit 1 will lose full core reserve capacity in 2007 and Unit 2 will lose full core reserve capacity in 2008.

The proposed temporary cask pit rack and support platform would be installed in Units 1 and 2 for Cycles 14 through 16. The temporary cask pit rack would allow the temporary storage of an additional 154 spent fuel assemblies per unit. The total spent fuel pool storage capacity per unit would be increased to 1478 spent fuel assemblies for Cycles 14 through 16.

11.2 Environmental Considerations

The proposed temporary increase in SFP storage capacity described and analyzed in this report, will not result in a significant impact to the environment as described below.

i. Thermal Impact

Thermal effects on the environment due to adding a temporary cask pit rack to each unit will be negligible. Any additional heat load attributed to the installation of a cask pit rack only occurs during relatively short periods of time during an outage when the reactor core is offloaded. During non-outage periods, the maximum number of spent fuel assemblies stored in the SFP will not exceed the existing licensing basis, resulting in no additional heat load imposed on the environment.

The most significant contributor to the SFP decay heat load is from the number of assemblies discharged during a reactor offload to the SFP. Since the size of planned refueling discharges are unchanged, there will be no significant increase in SFP heat load. A small temporary heat load will be imposed on the SFP cooling system from the oldest spent fuel that is allowed to remain in the SFP longer due to the additional storage capacity provided by the temporary cask pit rack. However, this additional decay heat load will be a small fraction of the existing SFP heat load and insignificant when compared to the total heat rejected to the environment by the plant.

ii. Consumption of Raw Materials

It is estimated conservatively that the manufacturing of the two cask pit racks and support platforms will require the following raw material resources:

Stainless Steel:	80,000 lbs
Aluminum:	5,000 lbs
Boron Carbide:	4,000 lbs
Stainless Steel Weld Wire and Flux:	500 lbs
Argon Gas (for welding):	1,000 SCF

The annual worldwide consumption of each of the above materials is at least 100,000 times as much as the quantities needed for the cask pit rack project implementation. Therefore, it is readily concluded that this project will have a negligible effect on the world's production and availability of the above-mentioned raw materials.

iii. Generation of Radioactive Waste

The radioactivity and impurities in the SFP water are not expected to increase as a result of the addition of the temporary cask pit storage rack and support platform. Replacement of filters or demineralizers would offset any anticipated increase of the radioactivity and impurity level of the water. The temporary increase in spent fuel storage capacity during fueling outages is not expected to result in a significant change in long-term generation of solid radioactive waste.

Prior to installing the cask pit racks and support platforms, equipment temporarily stored in the cask pit will be removed and the pit floor will be cleaned using an underwater vacuum. These activities are expected to generate a small volume of low-level solid radwaste that will be captured underwater in vacuum filter cartridges and properly disposed of using DCPP radwaste handling procedures.

Storing and removing fuel assemblies from the cask pit racks is not expected to generate any additional solid or gaseous radwaste from either unit compared to the current practice of storing fuel assemblies in the SFP. Because each cask pit rack must eventually be removed for cask handling operations, rack contamination will be minimized by a fuel loading process that will preferentially select non-failed fuel for storage in this rack.

The disposal of the used temporary rack will result in a one-time incremental increase in solid waste. Because ongoing volume reduction efforts have effectively minimized the amount of waste generated, this incremental increase is bounded by the plant's original licensing basis described in the Final Environmental Statement and therefore, is acceptable.

iv. Gaseous Emissions and Liquid Discharges

As discussed in Section 9, the temporary storage of additional spent fuel assemblies in the SFP during Cycles 14-16 is not expected to significantly affect the releases of radioactive gases from the SFP.

The release of radioactive liquids will not be affected as a result of the temporary rack installation. The SFP ion exchanger resins remove soluble radioactive materials from the SFP water. When the resins are changed out, the small amount of resin sluice water is processed by the radioactive waste system before release to the environment. The frequency of resin change out may increase slightly during the installation and removal of the temporary rack and installation of the support platform. However, the amount of liquid effluents released to the environment as a result of the temporary rack and platform is expected to be negligible.

v. Hazardous Human Activity

Manufacturing and installation of fuel racks in fuel pools is a routine and commonplace human activity. Thousands of racks have been manufactured and installed world-wide. As discussed in Section 9, there is no significant increase in occupational radiation exposure. There is no scientific evidence (or assertion by any group) that the manufacture or use of fuel racks entails any human risk factors.

vi. Transport of Hazardous Materials

The temporary use of the cask pit racks does not involve off-site movement of spent nuclear fuel or any other radiologically significant cargo. It is therefore concluded that the proposed temporary rack installation is environmentally benign in all respects.

11.3 Project Alternatives

Alternatives to the proposed action will be discussed in detail in PG&E's license amendment request. As previously discussed, the installation of the temporary rack is to provide interim storage during Cycles 14 through 16 while outstanding issues are being resolved to provide dry cask storage for long-term spent fuel storage.

11.4 Design Basis Events

This Licensing Report has addressed both the safety and environmental aspects of a fuel handling accident, an event which bounds the potential adverse consequences of accidents attributable to operation of a spent fuel pool with high-density racks. A fuel handling accident is a design basis event that the pool and its associated structures, systems and components are designed and constructed to prevent and mitigate. The environmental impacts of this accident were found to be bounded by the previous licensing basis in the DCPP FSAR Update Section 15.5.

11.5 Summary

The installation of the temporary cask pit rack and support platform, temporary storage of spent fuel in the rack, and the removal of the rack will not significantly increase the probability or consequences of accidents. There are no significant changes in the types or significant increase in the quantities of effluents that may be released offsite and there is no significant increase in occupational or public radiation exposure.

11.6 References

[11.1] OT Position Paper for Review and Acceptance of Spent Fuel Storage and Handling Applications, USNRC (April 1978).

[11.2] Electric Power Research Institute, Report No. NF-3580, May 1984.

[11.3] "Spent Fuel Storage Options: A Critical Appraisal", by K.P. Singh, Power Generation Technology, Sterling Publishers, pp. 137-140, U.K. (November 1990).

[11.4] USNRC, "Environmental Assessment and Finding of No Significant Impact Related to the Construction and Operation of the Diablo Canyon Independent Spent Fuel Storage Installation", October 24, 2003.